Durham E-Theses

Small x physics.

Askew, Adrian John

UNIVERSITY OF DURHAM
Centre for Particle Theory

Small x Physics.

A thesis presented for the degree of

Doctor of Philosophy

by

Adrian John Askew,

July 1995.

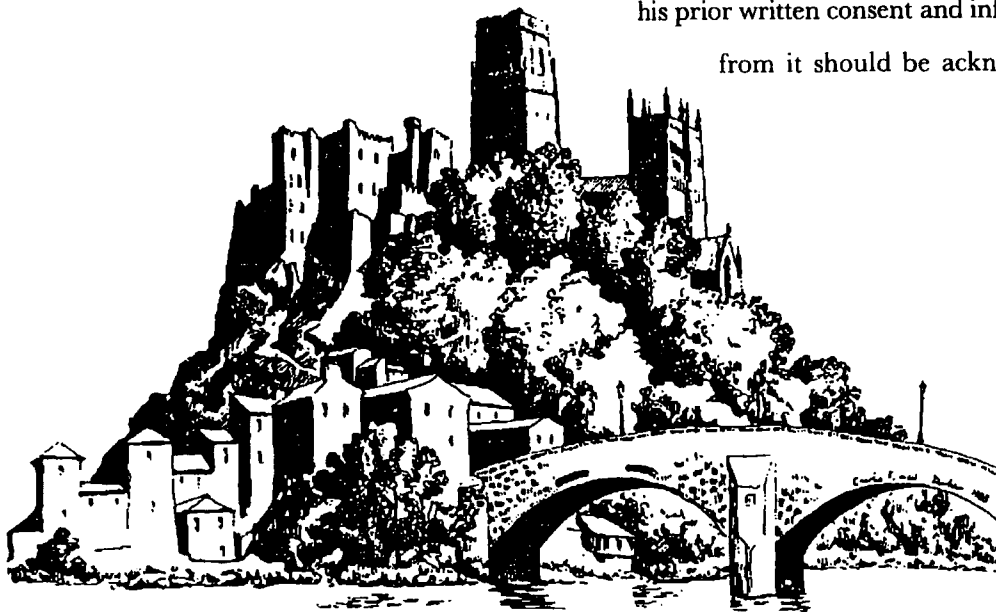# Abstract

We study the small-x limit of the structure functions for deep inelastic scattering in Quantum Chromodynamics. The standard approach to this process, based on the DGLAP equations, runs into difficulties in the small-x region due to the higher order corrections becoming large. As an attempt to overcome these obstacles we reinterpret the small-x limit in terms of high energy asymptotics. The relevant high energy formalism is developed in terms of Reggeon Field Theory, which leads to the BFKL equation for the scattering amplitude. These results are reviewed fully, for completeness.

We then apply the resulting formalism to structure functions at small-x to determine the phenomenological implications of this high energy resummation. The DESY electron-proton collider HERA is presently exploring the region of the structure functions for $x \lesssim 10^{-3}$, $Q^2 \sim 10$ GeV^2, and the results of these experiments are compared with our theoretical analysis.

The structure functions are a very inclusive measurement; so in order to try and focus on some cleaner indication of the BFKL behaviour we then turn to an analysis of dijet production in deep inelastic scattering. The results of the BFKL formalism are compared with standard analysis in terms of the DGLAP equations.

Declaration

I declare that no material in this thesis has previously been submitted for a degree at this or any other University.

All the research work in this thesis has been carried out in collaboration with Professors A.D. Martin and J. Kwieciński, together with contributions from Drs P.J. Sutton, K. Golec-Biernat, and D. Graudenz. Chapters 1 and 2 consist mainly of a review of known results, and are not claimed to be fully original. The material in chapters 3 and 4 is based heavily on the work which was first published in the following articles:

A.J. Askew, J. Kwieciński, A.D. Martin, P.J. Sutton:

Physical Review **D47** (1993) 3775

A.J. Askew, J. Kwieciński, A.D. Martin, P.J. Sutton:

Modern Physics Letters **A8** (1993) 3813

A.J. Askew, J. Kwieciński, A.D. Martin, P.J. Sutton:

Physical Review **D49** (1994) 4402

A.J. Askew, K. Golec-Biernat, J. Kwieciński, A.D. Martin, P.J. Sutton:

Physics Letters **B325** (1994) 212

A.J. Askew, D. Graudenz, J. Kwieciński, A.D. Martin:

Physics Letters **B338** (1994) 92

Acknowledgements

As a child I felt myself to be alone, and I am still, for I know things and must hint at things which others apparently know nothing of, and for the most part do not want to know. Loneliness does not come from having no people about one, but from being unable to communicate the things that seem important to oneself, or from holding certain views which others find inadmissible.

Carl Jung

Contents.

2.6: The model for small-x processes. 61

Chapter 3: Implications of the BFKL formalism for structure functions.

3.1: Introduction 71

3.2: The photon-gluon impact factor. 79

3.3: Analytic properties of the BFKL formalism. . . . 85

3.4: Numerical predictions (I). 101

3.5: Numerical predictions (II). 109

Chapter 4: Dijet production at HERA as a probe of BFKL dynamics.

Chapter 5: Summary and conclusions.

1

Deep Inelastic Scattering.

1.1: Introduction.

Our modern theory of hadronic structure is based upon the concept of a nonabelian gauge theory of quarks and gluons — Quantum Chromodynamics (QCD) — which has scored notable experimental successes in predicting and explaining hadronic phenomena. The outstanding property of QCD, on which the validity of its perturbative analysis relies, is that the theory is 'asymptotically free': that is, at asymptotically small distance scales the fundamental field quanta behave as quasi-free particles. At larger distance scales the effective interaction strength grows stronger and stronger, and so offers a plausible mechanism for the formation of the experimentally observed hadrons, which in this picture are composites of quarks and gluons. Let us briefly review some of the observations which pointed towards QCD as a theory of hadronic structure [1, 2]:

Quarks : From the time of the fifties onwards, the particle accelerators of the day were regularly producing 'new' hadrons and hadronic resonances. As the number of these hadronic 'particles' grew, so also did the conviction that they could not all be fundamental. As the experiments collected data on the properties and quantum numbers of these resonances, it became clear that many of the hadrons could be arranged into families of particles with similar properties. It was noted by Gell-Man and Zweig [3] that the quantum numbers within these families followed naturally from the assumption that hadrons were composites of *quarks*, fractionally charged particles with spin-$\frac{1}{2}$. Initially these quarks were used as simply a book-keeping device, since the experiments showed no sign of free quarks existing outside of hadrons.

Colour : The first indication that quarks may carry an extra quantum number over

and above the hypercharge, isospin and strangeness that they were introduced with came from the Δ^{++} resonance. This has spin $\frac{3}{2}$, angular momentum zero, and is made of three u quarks. This means, that if the quarks are regarded as particles then they seem to violate the usual Fermi exclusion principle, since the above state is symmetric in spin, space and flavour. One way around this problem is to postulate that the quarks carry an extra quantum number — colour — taking three values. The Δ^{++} state can then maintain the exclusion principle by being antisymmetric in its colour wavefunction. Hadrons in this scheme are 'colourless' — singlets under the colour symmetry group.

Further evidence for colour comes from the ratio of hadronic final states to electromagnetic final states in the e^+e^- annihilation processes: here there is clear evidence for a threefold multiplicity of quarks of each flavour.

Asymptotic Freedom : Following on in the tradition of the Rutherford experiment which discovered the nucleus, experimenters at SLAC during the sixties performed high energy electron-proton scattering, smashing the proton into pieces in an attempt to see what it was made from. They measured the cross section for the inclusive process

$$\text{Electron } (k) \;+\; \text{Proton } (p) \;\rightarrow\; \text{Electron } (k') \;+\; \text{Anything}$$

as a function of the electron variables, namely the momentum transfer $Q^2 = -(k-k')^2$ and energy loss in the lab frame $\nu = k_0 - k'_0$. Their data for this process showed the intriguing property of *scaling*: instead of depending on Q^2 and ν alone, to a good approximation their data depended only on the combination of these given by the scaling variable $x = \frac{Q^2}{2M_p\nu}$. It was pointed out by Feynman that this observation arises very naturally in a simple model in which the proton is considered as a conglomerate of free, pointlike particles he dubbed *partons*. Ultimately, these partons became identified with the quarks and gluons of QCD, and the approximate scaling is interpreted as a consequence of asymptotic freedom.

1.2: Deep Inelastic scattering in QCD.

1.2.1: Introduction.

Historically, the inelastic scattering of leptons off hadrons was one of the first processes to which a perturbative analysis was applied. The following figure sets out the kinematics

and event topology of this process.
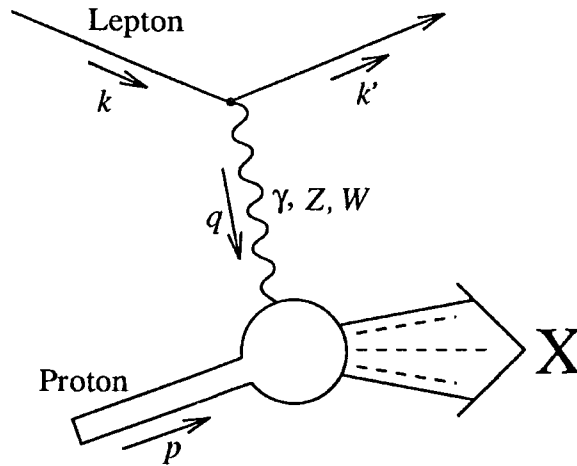
Figure 1.1: The kinematics of the process $lp \to l'X$, where X stands for any hadronic final state.

This thesis will be concerned only with neutral current processes at moderate values of Q^2, for which we can to good accuracy ignore the exchange of the electroweak Z boson and simply work within the framework of QED. To lowest order in the electromagnetic coupling the cross section can be calculated from the graph shown in figure 1.2, in which we have introduced a 'cut' notation whereby we represent, on the same diagram, the amplitude and its complex conjugate.
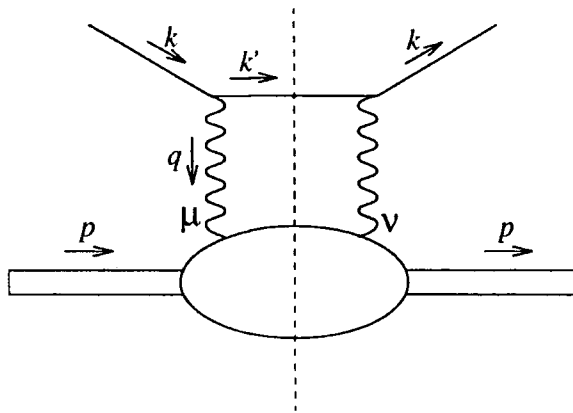
Figure 1.2: The Feynman graph from which the deep inelastic scattering cross section may be calculated, to lowest order in α_{em}.

For the spin-averaged inelastic cross section we arrange our normalisation of the various

3

factors such that[4]

$$d\sigma = \frac{1}{4p.k} \frac{1}{2} \sum_{\lambda_e,\lambda_e'} \frac{1}{2} \sum_{\lambda_p} \sum_X \int d\Phi_X |A(ep \to e'X)|^2 \frac{d^3k'}{(2\pi)^3 2k_0'}$$

$$\equiv \frac{2}{p.k} \left(\frac{\alpha_{em}}{q^2}\right)^2 L^{\mu\nu} W_{\mu\nu} \frac{d^3k'}{2k_0'}$$

(1.1)

with $L^{\mu\nu}$ given as the polarisation factor from the Lepton vertex,

$$L^{\mu\nu} = \frac{1}{4}Tr[(\not{k}+m_e)\gamma^\mu(\not{k}'+m_e)\gamma^\nu] = k'^\mu k^\nu + k^\mu k'^\nu + \left(\frac{q^2}{2}\right)g^{\mu\nu}$$

and $W_{\mu\nu}$ given by

$$W_{\mu\nu}(p,q) = \frac{1}{4\pi} \sum_{X,\lambda_p} \langle p|\hat{j}_\mu(0)|X\rangle\langle X|\hat{j}_\nu(0)|p\rangle \, (2\pi)^4\delta^{(4)}(p_X^\mu - p^\mu - q^\mu)$$

(1.2)

$$= \frac{1}{2\pi} \int d^4y e^{iq\cdot y} \frac{1}{2} \sum_{\lambda_p} \langle p|\hat{j}_\mu(y)\hat{j}_\nu(0)|p\rangle,$$

(1.3)

and illustrated diagrammatically in figure 1.3.

Figure 1.3: Diagrammatic representation of the hadronic tensor $W_{\mu\nu}(p,q)$ governing the cross section for spin averaged deep inelastic scattering.

The tensor $W_{\mu\nu}$ contains all the information about the hadronic side of the process: the rest is purely from QED. From Lorentz invariance, the tensor $W_{\mu\nu}$ depends only on the scalar products which can be made from the four momenta p, q. Traditionally, the independent

variables are taken as the momentum transfer $Q^2 \equiv -q^2$ and the Bjorken scaling variable

$$x \equiv \frac{Q^2}{2p.q},$$

which in the basic parton model has a neat interpretation as the fraction of the proton's longitudinal momentum carried by the struck parton in that frame in which the momentum of the proton is very large [5].

It is useful to decompose the tensor $W_{\mu\nu}$ in terms of a set of basis tensors which respect the current conservation and symmetries of QED. These requirements reduce the number of independent functions in $W_{\mu\nu}$ down to just two, which we define here to be the transverse (F_T) and longitudinal (F_L) structure functions. That is, we expand

$$W_{\mu\nu}(p,q) = \left[\frac{p_\mu q_\nu + q_\mu p_\nu}{p.q} - \frac{q_\mu q_\nu}{q^2} - \frac{p_\mu p_\nu q^2}{(p.q)^2} \right] \frac{F_L(x,Q^2)}{x}$$
$$+ \left[-g_{\mu\nu} - \frac{p_\mu p_\nu q^2}{(p.q)^2} + \frac{p_\mu q_\nu + q_\mu p_\nu}{p.q} \right] \frac{F_T(x,Q^2)}{x}. \tag{1.4}$$

So far we have made no assumptions about the hadronic structure: the analysis has simply involved QED. Let us now proceed to show how this process is analysed within QCD. Firstly, we note that the classic kinematic régime for which QCD has been applied to deep inelastic scattering is that region where both Q^2 and the mass of the hadronic final state, $W^2 = (p+q)^2$, tend to infinity in such a way that $W^2/Q^2 \sim 1$, so that no large logarithms $\log(W^2/Q^2)$ can develop. This limits the analysis in the first instance to that region of x neither too large nor too small, thus

$$\log(1/x) \sim \log(1/(1-x)) \sim 1.$$

At small x, we will find in fact that large logarithms $\log(W^2/Q^2)$ will develop and spoil our analysis; but we will ignore that for the present in order to introduce the standard formulation of the problem.

1.2.2: The operator product expansion.

Equation (1.3) can be rewritten

$$W_{\mu\nu} = \frac{1}{2\pi} \int d^4 y \, e^{iq\cdot y} \frac{1}{2} \sum_{\lambda_p} \langle p | [\hat{j}_\mu(y), \hat{j}_\nu(0)] | p \rangle, \tag{1.5}$$

since it is possible to show that the extra term in the commutator does not contribute to the process[4]. If we examine which regions of integration are important in the above formula, we find that the integrand vanishes for $y^2 < 0$ through microcausality and is dominated by the region $y^2 \sim 0$. Generally speaking the product of two operators in quantum field theory tends to be singular as their spacetime separation $y^2 \to 0$; a simple example would be the singular form of the Feynman propagator of a scalar field ϕ,

$$-i\langle 0 | T \hat{\phi}(y)\hat{\phi}(0) | 0 \rangle = \Delta_F(y) = \int \frac{d^4 k}{(2\pi)^4} \frac{e^{-ik\cdot y}}{k^2 - m^2 + i\epsilon}$$
$$\sim \frac{i}{4\pi^2(y^2 - i\epsilon)} + O(m^2 y^2) \text{ as } y^2 \to 0. \tag{1.6}$$

To pick out the dominant behaviour in the limit $Q^2 \to \infty$ we need only to determine the most singular terms as $y^2 \to 0$ of the current commutator appearing in (1.5): the less singular pieces are suppressed by a power of Q^2. In order to perform this task we appeal to the operator product expansion (OPE). Firstly we can rewrite the current commutator in terms of a bilocal operator as [4, 6]

$$\left[\hat{j}_\mu(z), \hat{j}_\nu(z') \right] = \left(\partial_\mu \partial'_\nu - g_{\mu\nu} \partial . \partial' \right) \hat{O}_L(z, z')$$
$$+ \left(g_{\mu\lambda} \partial_\rho \partial'_\nu + g_{\rho\nu} \partial_\mu \partial'_\lambda - g_{\mu\lambda} g_{\rho\nu} \partial . \partial' - g_{\mu\nu} \partial_\lambda \partial'_\rho \right) \hat{O}_2^{\lambda\rho}(z, z') + \cdots \tag{1.7}$$

where we have dropped terms which are antisymmetric under the interchange $\mu \leftrightarrow \nu$, which do not contribute to the unpolarised structure functions. This equation is essentially the expression of (1.4) in coordinate space, after introducing a new structure function $F_2 = F_T + F_L$. We can then make the general expansion of these bilocal operators, writing

$$\hat{O}_L(z, z') = \sum_{i,n} C_{L,n}^i(y^2) y^{\mu_1} \cdots y^{\mu_n} \hat{O}_{L\,\mu_1\cdots\mu_n}^{[i]} \left(\frac{z + z'}{2} \right),$$
$$\hat{O}_2^{\lambda\rho}(z, z') = \sum_{i,n} C_{2,n}^i(y^2) y^{\mu_1} \cdots y^{\mu_n} \hat{O}_{2\,\mu_1\cdots\mu_n}^{[i]\lambda\rho} \left(\frac{z + z'}{2} \right) \tag{1.8}$$

where $y = z - z'$ and the sum is over all the local operators of the theory, their products, and their derivatives. Equation (1.8) basically states that any quantum state can be generated through some combination of the local operators. The coefficient functions C_n contain all the singularities for $y^2 \to 0$. Let us arrange our operators as a series of definite spin, where a spin-n operator $\hat{O}^{i,n}$ is symmetric and traceless in all its n Lorentz indices. In the deep inelastic limit, for a given spin we keep only those terms with the most singular coefficient functions $C_{i,n}$ as $y^2 \to 0$. For a free field theory, the strength of the singularity of $C_{i,n}$ can be estimated simply on the basis of dimensional arguments: if $d_{i,n}$ and d_j are the naive mass dimensions of the operators $\hat{O}^{i,n}$ and $\hat{j}$ then we have from (1.7) and (1.8) that

$$C_{i,n} \sim (\sqrt{y^2})^{d_{i,n} - n - 2d_j} \quad \text{[Modulo logarithms]}$$

for $y^2 \to 0$. The leading behaviour therefore comes from those operators of the lowest value of '*twist*' τ, where

$$\tau_{i,n} \equiv d_{i,n} - n. \tag{1.9}$$

In QCD, the fermion fields $\psi, \bar{\psi}$ and also the gauge field $\mathcal{F}^a_{\mu\nu}$ all have twist one, while a derivative $\mathcal{D}_\mu$ has twist zero; thus the leading twist operators which contribute to deep inelastic scattering are those with the minimum number of fundamental fields, subject to the constraint that the overall quantum numbers of the operator coincide with those of the product $j_\mu(x) j_\nu(0)$. So the leading twist operators have $\tau = 2$ and are given by

$$
\begin{aligned}
\hat{O}^{t_i,n}_{\mu_1\mu_2\cdots\mu_n} &= i^{n-1}\, \mathcal{S}\, \bar{\psi}\gamma_{\mu_1}\mathcal{D}_{\mu_2}\cdots\mathcal{D}_{\mu_n} t^i \psi, \\
\hat{O}^{F,n}_{\mu_1\mu_2\cdots\mu_n} &= i^{n-1}\, \mathcal{S}\, \bar{\psi}\gamma_{\mu_1}\mathcal{D}_{\mu_2}\cdots\mathcal{D}_{\mu_n}\psi, \\
\hat{O}^{A,n}_{\mu_1\mu_2\cdots\mu_n} &= 2i^{n-2}\, \mathcal{S}\, \mathcal{F}_{\mu_1\nu}\mathcal{D}_{\mu_2}\cdots\mathcal{D}_{\mu_{n-1}}\mathcal{F}^\nu_{\mu_n}.
\end{aligned}
\tag{1.10}
$$

The operator $\mathcal{S}$ denotes symmetrisation in the lorentz indices $\mu_1 \cdots \mu_n$.

Within an interacting, renormalisable theory, the dimension of these operators recieve a correction to their canonical free field values — the anomalous dimension. These corrections, and similarly those to the coefficient functions, are computable in perturbation theory and are responsible for scaling violations in structure functions. Let us consider the

contribution of a non-singlet operator given by

$$\hat{O}_{t^i,n} \sim i^{n-1} \, \mathcal{S} \, \bar{\psi} \, t^i \gamma_{\mu_1} \mathcal{D}_{\mu_2} \cdots \mathcal{D}_{\mu_n} \psi. \tag{1.11}$$

From (1.8) its coefficient function is then of the form,

$$\tilde{C}_n^i(y) = C_n^i(y^2) y^{\mu_1} \cdots y^{\mu_n}. \tag{1.12}$$

The matrix element of (1.11) between proton states after averaging over spin can only take the form,

$$\frac{1}{2} \sum_{\lambda_p} \langle p | \mathcal{S} \, \bar{\psi} \, t^i \gamma_{\mu_1} \mathcal{D}_{\mu_2} \cdots \mathcal{D}_{\mu_n} \psi | p \rangle = A_n^i(\mu^2) p_{\mu_1} p_{\mu_2} \cdots p_{\mu_n}, \tag{1.13}$$

plus terms proportional to $p^2 g_{\mu_i \mu_j}$ and suchlike; we neglect these under the assumption that $p^2 = M_p^2 \ll p.q$. However, there have been recent calculations attempting to generate parton distributions in the proton by starting from a valence-like input at a very small scale $Q_0^2 \sim \Lambda^2$ and then evolving, simply using the usual renormalisation group equations to next-to-leading order [7]. Quite apart from the fact that the perturbative expansion is liable to be badly behaved, these calculations neglect the target mass corrections associated with the terms proportional to M_p^2 above. At scales $Q_0^2 < M_p^2$, these mass terms alter the entire structure of the formalism, so it seems impossible to take such calculations seriously.

The contribution of the operator $\hat{O}_{i,n}$ to a structure function F_n is given by, after the fourier integral in (1.5),

$$\bar{F}_n^i(x, Q^2) \equiv x^{-n} F_n^i(Q^2) = \left(\frac{2p.q}{Q^2} \right)^n C_n^i(Q^2/\mu^2) A_n^i(\mu^2). \tag{1.14}$$

This particular contribution to $F^i(x, Q^2)$ can be isolated by appealing to a dispersion relation in x; the outcome of this being the result

$$F_n^i(Q^2) = \int_0^1 \frac{dx}{x} x^{n-1} F^i(x, Q^2) \tag{1.15}$$

In (1.14) we have assumed that the scale μ^2 introduced in regularising and renormalising the theory is the only mass scale in the Lagrangian, and we neglect possible fermion masses.

8

1.2.3: The renormalisation group analysis.

We have arrived at the following representation for the moments of structure functions in QCD,

$$F_n(Q^2) = \sum_i A_{i,n}(\mu^2) C_{i,n}\left(Q^2/\mu^2, g^2(\mu^2)\right) \tag{1.16}$$

The apparent dependence upon μ^2 must cancel between the two terms on the right hand side, since F_n is an observable. As a result of this we can derive the renormalisation group equation for the coefficient function [4, 6], which for a nonsinglet contribution takes the form

$$\left[\mu\frac{\partial}{\partial\mu} + \beta(g)\frac{\partial}{\partial g} - \gamma_{i,n}\right] C_{i,n}(Q^2/\mu^2, g^2(\mu^2)) = 0. \tag{1.17}$$

The resulting solution to this equation as we change Q^2 gives

$$C_{i,n}(Q^2/\mu^2, g^2(\mu^2)) = \exp\left[-\int_{g(\mu^2)}^{\bar{g}(Q^2)} \frac{dg'}{\beta(g')}\gamma_{i,n}(g'^2)\right] \times C_{i,n}(Q^2/\mu^2 = 1, \bar{g}^2(Q^2)) \tag{1.18}$$

with $\bar{g}$ being the solution to

$$\mu\frac{d\bar{g}}{d\mu} = \beta(\bar{g}). \tag{1.19}$$

For Q^2 large we can expand[1]

$$\beta(\bar{g}) = -\beta_0\bar{g}^3 - \beta_1\bar{g}^5 - \cdots$$

from which we can integrate equation (1.19) to give $\bar{g}^2(Q^2)$ as the implicit solution to

$$\frac{1}{\bar{g}^2} + \frac{\beta_1}{\beta_0}\log\left(\frac{\beta_0\bar{g}^2}{1 + \frac{\beta_1}{\beta_0}\bar{g}^2}\right) = \beta_0\log(Q^2/\Lambda^2).$$

This equation is conventionally expanded in powers of $1/\log Q^2$ to give (with a slight

---

[1] We use the conventions of reference [4].

change in definition of $\Lambda \simeq \Lambda'$)

$$
\begin{aligned}
\bar{g}_{NL}^2(Q^2) &\simeq \frac{1}{\beta_0 \log(Q^2/\Lambda'^2)} \left[1 - \frac{\beta_1}{\beta_0^2} \frac{\log\left(\log(Q^2/\Lambda'^2)\right)}{\log(Q^2/\Lambda'^2)} \right] \\
&= \bar{g}_{LL}^2(Q^2) \left[1 - \frac{\beta_1}{\beta_0} \bar{g}_{LL}^2(Q^2) \log\left(\log(Q^2/\Lambda'^2)\right) \right].
\end{aligned}
\tag{1.20}
$$

Function $\bar{g}_{LL}^2(Q^2)$ is the leading order expression for the coupling,

$$
\bar{g}_{LL}^2(Q^2) = \frac{1}{\beta_0 \log(Q^2/\Lambda'^2)},
\tag{1.21}
$$

and the term in square brackets represents the NLO correction.

Equation (1.18) gives for $F_{i,n}$,

$$
F_{i,n}(Q^2) = \tilde{A}_{i,n} \exp\left[-\int^{\bar{g}(Q^2)} \frac{dg'}{\beta(g')} \gamma_{i,n}(g') \right] \times C_{i,n}(1, \bar{g}^2(Q^2)).
\tag{1.22}
$$

The leading log formula for $F_{i,n}$ then comes from expanding (1.22) to leading order in $1/\log(Q^2/\Lambda^2)$, thus if we denote the expansions of anomalous dimension and coefficient functions as

$$
\begin{aligned}
\gamma_{i,n} &= \gamma_{i,n}^{(0)} g^2 + \gamma_{i,n}^{(1)} g^4 + \cdots \\
C_{i,n} &= C_{i,n}^{(0)} + C_{i,n}^{(1)} g^2 + \cdots
\end{aligned}
\tag{1.23}
$$

then to leading logarithmic order we get

$$
F_{i,n}^{LL}(Q^2) = \tilde{A}_{i,n} C_{i,n}^{(0)} \left(g^2(Q^2) \right)^{\frac{\gamma_{i,n}^{(0)}}{2\beta_0}} = \tilde{A}_{i,n} C_{i,n}^{(0)} \left(\beta_0 \log(Q^2/\Lambda^2) \right)^{-\frac{\gamma_{i,n}^{(0)}}{2\beta_0}}.
\tag{1.24}
$$

This exhibits two free parameters: the constant $\tilde{A}_{i,n}$ characterises the nonperturbative structure of the proton; and we have traded off the parameters g, μ^2 of the QCD Lagrangian for a single dimensionful parameter Λ. These parameters can be fixed by experiment, if we measure the structure function F_n at two large values of $Q^2 = Q_1^2, Q_2^2$. Thus

$$
F_n^{LL}(Q^2) = F_n(Q_1^2) \times \left(\frac{\log(Q^2/\Lambda^2)}{\log(Q_1^2/\Lambda^2)} \right)^{-\frac{\gamma_{i,n}^{(0)}}{2\beta_0}}.
\tag{1.25}
$$

If we only need to know the structure function in a limited region of Q^2, we can expand

10

(1.25) as

$$F_n^{LL}(Q^2) \simeq F_n(Q_1^2) \left[1 - \frac{\gamma_{i,n}^{(0)}}{2\beta_0} \log \left[\frac{\log(Q^2/\Lambda^2)}{\log(Q_1^2/\Lambda^2)} \right] + \cdots \right]$$

$$\simeq F_n(Q_1^2) \left[1 - \frac{\gamma_{i,n}^{(0)}}{2} \bar{g}_{LL}^2(Q_1^2) \log(Q^2/Q_1^2) + \cdots \right] \qquad (1.26)$$

which will be a good approximation provided the evolution length is small, $\log(Q^2/Q_1^2) \ll \log(Q_1^2/\Lambda^2)$; however equation (1.25) as it stands is accurate for arbitrarily large values of $Q^2 > Q_1^2$.

The next-to-leading log results come from expanding (1.18) to keep further terms of order $1/\log(Q^2/\Lambda^2)$ relative to (1.24), giving [4]

$$F_{i,n}^{NL}(Q^2) = \tilde{A}_{i,n} \left[\beta_0 \log(Q^2/\Lambda^2) \right]^{\frac{-\gamma_{i,n}^{(0)}}{2\beta_0}} \left[C_{i,n}^{(0)} + (\beta_0 \log(Q^2/\Lambda^2))^{-1} \times \right.$$

$$\left. \left\{ C_{i,n}^{(1)} + \frac{C_{i,n}^{(0)}\beta_1}{2\beta_0} \left(\frac{\gamma_{i,n}^{(1)}}{\beta_1} - \frac{\gamma_{i,n}^{(0)}}{\beta_0} \right) - C_{i,n}^{(0)}\frac{\beta_1\gamma_{i,n}^{(0)}}{2\beta_0^2} \log\log(Q^2/\Lambda^2) \right\} + \cdots \right]. \qquad (1.27)$$

The explicit next to leading log calculations of $C^{(1)}$ and $\gamma^{(1)}$ are to be found in [8].

The above formal expressions in moment space can be expressed in more physical terms if we interpret (1.15) as a Mellin transform in $x \to n$. This integral transform has the standard inversion

$$F_2^i(x, Q^2) = \int_{\sigma-i\infty}^{\sigma+i\infty} \frac{dn}{2\pi i} x^{1-n} F_2^{i,n}(Q^2) \qquad (1.28)$$

where the contour integral is along a line parallel to the imaginary axis in the n plane, to the right of all the singularities of F_n. We can write the general non-singlet structure function as a sum over contributions from definite quark flavour, q, thus [6]

$$F_n^{NS}(Q^2) = \sum_q \delta_q^{NS} A_n^q \exp\left[-\int^{\bar{g}(Q^2)} \frac{dg'}{\beta(g')} \gamma_n^{NS}(g') \right] C_{q,n}^{NS}\left(Q^2/\mu^2 = 1, \bar{g}^2(Q^2) \right) \qquad (1.29)$$

with the δ_q^{NS} some known coefficient. Defining an effective quark density f_q^{NS} by

$$f_q^{NS}(n, Q^2) = A_n^q \exp\left[-\int^{\bar{g}(Q^2)} \frac{dg'}{\beta(g')}\gamma_n^{NS}(g')\right] \qquad (1.30)$$

then the factorisation in (1.29) becomes

$$F_2^{NS,n}(Q^2) = \sum_q \delta_q^{NS} f_q^{NS}(n, Q^2) C_{q,n}^{NS}(\bar{g}^2(Q^2))$$

which in x-space is, from (1.28),

$$F_2^{NS}(x, Q^2) = \sum_q \delta_q^{NS} x \int_x^1 \frac{dx'}{x'} C_q^{NS}(x/x', \bar{g}^2(Q^2)) f_q^{NS}(x', Q^2). \qquad (1.31)$$

In particular, to lowest order $C_{q,n}$ is constant, thus $C_q(z) \sim e_q^2 \delta(1-z)$, and we have simply

$$F_2^{NS}(x, Q^2) = \sum_q \delta_q^{NS} x\, e_q^2\, f_q^{NS}(x, Q^2)$$

which has the same form as the simple parton model expression for the structure functions, but with Q^2 dependent parton distributions. Indeed, the evolution equations can be derived in terms of this partonic language [9, 10, 11, 12], and this allows the parton-like factorisation to be extended to other processes, such as Drell-Yan production of lepton pairs in hadron-hadron scattering.

1.3: The small-x region.

Within the standard application of the factorisation theorem, presented above, it is assumed to be valid to calculate γ_n, C_n to just one- or two- loop order. This is a valid line of approach provided that the higher order terms which are neglected are of much lesser significance than the first terms. For moderate x (corresponding to $n > 1$ but not *too* large) this is acceptable since the coefficients in the perturbative expansion, $C_n^{(m)}, \gamma_n^{(m)} \sim 1$ and so the naive expectation that the extra powers of $\bar{g}^2$ makes these terms subdominant is reasonable.

However, in the region of small-x (or equivalently $n \to 1$), this need not be the case. Explicit calculation of the one-loop singlet splitting functions for $z \to 0$ gives [13]

$$P_{gg}^{(0)}(z) \sim \frac{C_A}{z}, \tag{1.32}$$

$$P_{gq}^{(0)}(z) \sim \frac{C_F}{z}, \tag{1.33}$$

$$P_{qq}^{(0)}(z) \sim \text{Constant}, \tag{1.34}$$

$$P_{qg}^{(0)}(z) \sim \text{Constant for } z \to 0. \tag{1.35}$$

The $1/z$ singularities translate through to poles $\sim 1/(n-1)$ in moment space. The splitting function calculation can be carried through to higher order, when one encounters now the complication that beyond the leading order there is no longer an unambigous definition of the coefficient functions and anomalous dimensions, but rather that there is some freedom in defining these quantities. Therefore, beyond leading order one has to fix some *factorisation convention*, that is, some separation of the coefficient and anomalous dimension terms. Two such schemes are frequently used: firstly, there is the *DIS scheme*, in which the quark distribution is defined in such a way that the naive parton model result for the structure functions is still valid, that is

$$F_2(x, Q^2) \equiv \sum_q e_q^2 \, x f_q(x, Q^2) \bigg|_{DIS}.$$

A disadvantage of this scheme is that it is geared very much towards F_2 in deep inelastic scattering, and it turns out that the coefficient functions for other hard subprocesses become quite complex.

The second, and most common, factorisation scheme is that given by the so-called $\overline{MS}$ *scheme*. This has the advantage of being more easily 'portable' from one hard subprocess to another. Within the $\overline{MS}$ scheme, the leading behaviour of the NLO contribution to the singlet splitting functions in the region $z \to 0$ are given as [13]

$$P_{qq}^{(1)}(z) \sim \frac{40 C_F N_F T_R}{9z} + \cdots \tag{1.36}$$

$$P_{qg}^{(1)}(z) \sim \frac{40 C_A N_F T_R}{9z} + \cdots \tag{1.37}$$

$$P_{gq}^{(1)}(z) \sim \frac{9C_A C_F - 40 C_F N_F T_R}{9z} + \cdots \tag{1.38}$$

$$P_{gg}^{(1)}(z) \sim \frac{12 C_F N_F T_R - 46 C_A N_F T_R}{9z} + \cdots \tag{1.39}$$

and on comparison with the leading order splitting functions we see in particular that for P_{qq} and P_{gq} the higher order term $P^{(1)}$ will actually dominate for sufficiently small $z \ll \alpha_s$. In even higher orders, we find in fact that the leading behaviour of $P^{(n)}$ can be as high as

$$P^{(n)}(z) \sim \frac{\log^{n-1}(1/z)}{z}$$

in which case the higher order corrections are becoming more and more important as z becomes small.

In fact it may be remarked that the result given in (1.27) is not exactly the expression which is presently used for NLO phenomenology of structure functions. Rather, the analysis takes (1.31) as the starting point, fixing the parton distribution $f_i(x, Q^2)$ at some $Q^2 = Q_0^2 \sim 4 \text{GeV}^2$, and then evolving this distribution using the equation

$$\frac{\partial f_i(x, \mu^2)}{\partial \log \mu^2} = \sum_j \int_x^1 \frac{dx'}{x'} P_{ij}(x/x', \bar{g}^2(\mu^2)) f_j(x, \mu^2)$$

with $P(x/x')$ being the anomalous dimension γ_n transformed through to x space, to next-to-leading order accuracy, thus

$$P(x/x') = \bar{g}_{NL}^2(\mu^2) P^{(0)}(x/x') + \bar{g}_{NL}^4(\mu^2) P^{(1)}(x/x').$$

One problem with this approach however is that the NLO anomalous dimension $\gamma_n^{(1)}$ is in principle entirely arbitrary — we can shift terms between $\gamma_n^{(1)}$ and $C_n^{(1)}$ by a different convention for the factorisation scheme. This will lead to a factorisation scheme dependence of the structure functions. Explicitly, this prescription corresponds in moment space to the representation for a nonsinglet structure function

$$F_n^{NS}(Q^2) = \sum_q \delta_q^{NS} f_q^{NS}(n, Q_0^2) \exp \left[\int_{Q_0^2}^{Q^2} \frac{dQ'^2}{Q'^2} \bar{g}_{NL}^2(Q'^2) \left[\gamma_{NS,n}^{(0)} + \bar{g}_{NL}^2(Q'^2) \gamma_{NS,n}^{(1)} \right] \right]$$

$$\times \left(C_{q,n}^{(0)} + g_{NL}^2(Q^2) C_{q,n}^{(1)} \right) \tag{1.40}$$

and since the anomalous dimension piece is exponentiated, this gives rise to terms which are arbitrarily far down in inverse powers of $\log Q^2$ by comparison with (1.27). This is not to

say that the formula is any less accurate, in the sense that the corrections to (1.27) beyond NLO are arbitrary anyway, and if they are unimportant in (1.27) then they ought to be unimportant in (1.40) too. However, for $n \to 1$ we know that the higher order corrections to the (singlet) structure functions will be enhanced, by powers of $1/(n-1)$, so to be consistent it may be important to keep track of exactly which terms are being summed. The analysis of the following chapter can be thought of as an all-orders resummation of the singlet anomalous dimension and coefficient function [14], summing all the leading singular terms of the form

$$\gamma_n, C_n \sim \sum_{m=0}^{\infty} A_n^{(m)} \left(\frac{\alpha_s}{n-1} \right)^{m+1}. \tag{1.41}$$

This resummation is carried out by the BFKL equation, which takes the form of an integral equation for the scattering amplitude.

There is a further, serious problem which will crop up as $x \to 0$. The fact is, that the factorisation theorem we write down for F_2 in terms of coefficient functions and distribution functions is valid only to leading order in $1/Q^2$. We have truncated the sum over operators which appears in the OPE to keep only the lowest twist operators, which are those whose coefficient functions are would seem to be most singular on the light cone, by naive dimensional counting. However, we know that within an interacting field theory an operator in general receives a deviation from its naive scaling dimension owing to quantum effects (the anomalous dimension). It can in principle happen that the anomalous dimension becomes sufficiently large to overcome the intrinsic $1/Q^2$ suppression and make the higher-twist contributions as important as the lowest twist. Such an occurence happens in deep inelastic scattering in fact, at the extreme edges of phase space. For $x \to 1$, the anomalous dimension of the leading twist operator becomes sufficient to suppress the leading twist contribution to F_2 so that for any fixed Q^2 there is some value of $x \sim 1$ for which the higher twist contributions become important [15].

Similarly, on taking $x \to 0$ at fixed Q^2 one ultimately faces up to the problem that the anomalous dimension of higher twist operators can become so large that they compete on an even footing with the lowest twist. In more physical language this means that the virtual photon no longer interacts with each parton incoherently, and that there may be multiple scattering off several partons. An estimate of the probability of any one gluon to

15

interact with a neighbour would be [16]

$$W \sim \alpha_s(Q^2) \frac{\delta A}{A} xg(x, Q^2)$$

with $\delta A \sim 1/Q^2$ being roughly the parton transverse size and $A \sim \pi R_P^2$ the transverse area of the proton, thus

$$W \sim \frac{\alpha_s(Q^2)}{Q^2} \frac{xg(x, Q^2)}{\pi R_p^2}.$$

We shall find that at small-x we expect the gluon distribution to become very large; so W can become appreciable, in which case parton-parton interactions (higher twist operators) can no longer be ignored. This means that ultimately the small-x region may become strongly non-perturbative, requiring arbitrarily high twist operators to be taken into account; however we should be able to analyse the transition region — between perturbative and strongly nonperturbative régimes — through perturbative techniques.

References.

[1] I.J.R. Aitchison and A.J.G. Hey, *Gauge Theories in Particle Physics*, Institute of Physics publishing, 1989

[2] A.D. Martin, University of Durham preprint DTP/95/44

[3] M. Gell-Mann, Phys. Lett. **8**, 214 (1964);
    G. Zweig, CERN preprints 8182/TH.401, 8419/TH.412 (1964)

[4] T. Muta, *Foundations of Quantum Chromodynamics*, World Scientific, 1987

[5] R.P. Feynman, *Photon-hadron interactions*, Benjamin, 1972

[6] F.J. Ynduráin, *The Theory of Quark and Gluon Interactions*, Springer-Verlag 1993

[7] M. Glück, R.M. Godbole and E. Reya, Z. Phys. C **41** 667 (1989); M. Glück, E. Reya and A. Vogt, Z. Phys. C48 475 (1990); Z. Phys. C53 127 (1992); Dortmund Univ. preprint DO-TH-92-19.

[8] G. Curci, W. Furmanski and R. Petronzio, Nucl. Phys.**B175** , 27 (1980);
    E.G. Floratos, D.A. Ross and C.T. Sachrajda, Nucl. Phys. **B129**,66 (1977);
    E.G. Floratos, R. Lacaze and C. Kounnas, Phys. Lett. **B98**, 89 (1981);
    W. Furmanski and R. Petronzio, Phys. Lett. **B97**, 437 (1980)

[9] Yu.L. Dokshitzer, D.I. Dyakonov and S.I. Troyan, Phys. Rep. **58**, 269 (1980)

[10] G. Altarelli, Phys. Rep. **81**, 1 (1982)

[11] A useful selection of Physics Reports articles, including those of references [9, 10] is to be found in the book *Perturbative Quantum Chromodynamics*, edited by M. Jacob, North-Holland publishing, 1982

[12] J.C. Collins, D.E. Soper and G. Sterman, in *Perturbative Quantum Chromodynamics*, edited by A.H. Mueller, World Scientific 1989

[13] J. Blümlein, in *Problems of High Energy Physics*, the proceedings of the International Winter School on Theoretical High Energy Physics, St Petersburg Nuclear Physics Institute, 1993.

[14] S. Catani, M. Ciafaloni and F. Hautmann, Phys. Lett. **B242** ,91 (1990); Nucl. Phys. **B366**,135 (1991); S. Catani, M. Ciafaloni and F. Hautmann, Proc. of the Workshop "Physics at HERA", DESY, Hamburg, Germany, October 1992, eds. W. Buchmüller and G. Ingelman, Vol. 2 (1992) p690

[15] M.R. Pennington, Rep. Prog. Phys. **46**, 393 (1983)

[16] L.V. Gribov, E.M. Levin and M.G. Ryskin, Phys. Rep. **100**, 1 (1983)

2

The high energy limit of QCD.

We should take care not to make the intellect our God;

it has, of course, powerful muscles, but no personality.

Albert Einstein

2.1: Preamble.

We have seen that at small-x the standard approach to QCD faces difficulties due to large higher order corrections and higher twist effects. In the present chapter we would like to look at the subject from a slightly different viewpoint, in order to gain some insight into the physical situation at small-x.

Our starting point is to recast the small-x limit of DIS in terms of high energy asymptotics. The invariant mass of the hadronic final state in DIS is given by

$$W^2 \equiv (p+q)^2 = \frac{Q^2}{x}(1-x) + M_P^2 \simeq \frac{Q^2}{x} \qquad (2.1)$$

for small x. We are thus led to the conclusion that structure functions in the limit $x \to 0$ for fixed Q^2 give simply the *high-energy limit* of the total cross section for a proton interacting with a photon of fixed virtuality. Back in the days prior to QCD, when it was not clear that hadronic interactions might be amenable to a perturbative analysis, a great deal of work in particle physics focussed on exactly this topic of high energy asymptotics. Powerful machinery was developed in order to try to understand this subject through non-perturbative methods based on very general principles like unitarity, Lorentz invariance, analyticity and such like. In particular, the concept of an analytic continuation in angular

momentum, which forms the basis of Regge theory, was especially fruitful. It is in terms of these esoteric formalisms that the results of QCD perturbation theory in the high energy limit have their simplest representation and interpretation.

In fact there are now alternative derivations of the BFKL equation which do not require the arcane knowledge of Regge theory [1,2], however the original logic is quite elegant and sufficient for this thesis, which focusses on quite inclusive quantities. For less inclusive quantities such as the associated distributions and multiplicities it may be necessary to account more carefully for coherence effects within the parton cascade [3].

2.2: General results in the high energy limit.

As our starting point we consider the simplified situation of the scattering of two spinless particles of mass m. The scattering amplitude is a function of the Lorentz scalars

$$
\begin{aligned}
s &= (p_1 + p_2)^2, \\
t &= (p_1 - p_3)^2, \\
u &= (p_1 - p_4)^2.
\end{aligned}
\tag{2.2}
$$

Only two of these quantities are independent, which we generally take to be s and t; u is then fixed by the relation

$$
s + t + u = 4m^2.
\tag{2.3}
$$

In a very abbreviated style we now list some of the key properties which we would expect this scattering amplitude to possess [4, 5]:

• **Analyticity** : We regard the variables s, t, u as complex, and the scattering amplitude $A(s, t, u)$ as a real analytic function of its arguments, with only such singularities as are required by unitarity. Generally speaking, the amplitude function $A(s, t)$ will be discontinous across the real axis; so in the s-channel physical region we define the physical amplitude as the limit as we approach from above the real axis

$$
A_{\text{phys}}(s, t) = \lim_{\epsilon \to 0^+} A(s + i\epsilon, t).
\tag{2.4}
$$

• **Crossing** : The same function $A(s, t, u)$ describes the amplitude for all processes $1 + 2 \to 3 + 4$, $1 + \bar{3} \to \bar{2} + 4$, $1 + \bar{4} \to \bar{2} + 3$ and suchlike, analytically continued to the

appropriate physical region of the variables. The s-channel physical region, that is the region in which the process $1 + 2 \to 3 + 4$ can genuinely occur with physical momenta, is given by

$$s \geq 4m^2, 4m^2 - s < t < 0, u = 4m^2 - s - t. \tag{2.5}$$

and similar relationships hold for the other physical regions.

• **Unitarity** : We assume that the S-matrix conserves probability and so is *unitary*, that is $\hat{S}^\dagger \hat{S} = 1$. This translates through to a nonlinear restriction on the scattering amplitude, which gives us some information about its singularity structure. If we write $\hat{S} = 1 + i\hat{T}$, we have

$$\hat{S}^\dagger \hat{S} = 1 \Rightarrow \hat{T} - \hat{T}^\dagger = i \hat{T}^\dagger \hat{T}. \tag{2.6}$$

Sandwiching this relation between $2 \to 2$ particle scattering states we get

$$\langle f|\hat{T}|i\rangle - \langle f|\hat{T}^\dagger|i\rangle = i \sum_n \int d\Phi_n \, \langle f|\hat{T}^\dagger|n\rangle \langle n|\hat{T}|i\rangle \tag{2.7}$$

where the n-particle intermediate states contain physical, on-shell particles, and the integral $d\Phi_n$ is over the full phase space of this intermediate state subject to momentum conservation. Denoting $A(s,t) = \langle f|\hat{T}|i\rangle$ and suchlike this equation gives

$$D_s(s,t) = i \sum_n \int d\Phi_n A^\dagger(n \to f) A(i \to n) \tag{2.8}$$

where the function $D_s(s,t)$ — the discontinuity of the scattering amplitude — is defined here as

$$D_s(s,t) = \text{Disc}_s A(s,t) = A(s,t) - A^\dagger(s,t) = \lim_{\epsilon \to 0^+} \left(A(s + i\epsilon, t) - A(s - i\epsilon, t) \right). \tag{2.9}$$

Expression (2.8) shows that unitarity *requires* the scattering amplitude to have cut singularities along the real axis, with the endpoints of these cuts being the threshold momenta for n-particle production, $s_{th} = (2m)^2.(3m)^2, (4m)^2 \cdots$. The discontinuity across each of these cuts is given in terms of n-particle production amplitudes by (2.8).

These properties of the scattering amplitude we take for granted for the rest of the thesis.

2.2.1: Partial Wave expansions.

The s-channel centre of mass scattering angle is given by

$$z_s \equiv \cos \theta_s = 1 + \frac{2t}{(s - 4m^2)}. \tag{2.10}$$

In the standard way we can decompose the amplitude in terms of s-channel angular momentum; this can be useful, since angular momentum is a conserved quantum number. Thus we write,

$$A(s,t) = \sum_{l=0}^{\infty} (2l + 1)A_l(s) \, P_l(z_s), \tag{2.11}$$

with

$$A_l(s) = \frac{1}{2} \int_{-1}^{1} dz_s P_l(z_s) A\big(s, t(s, z_s)\big). \tag{2.12}$$

For small energies s, this representation is extremely useful since only a small number of angular momenta contribute to the right hand side of (2.11). However we are really more interested in the asymptotic Regge limit, for which

$$\frac{s}{t} \to \infty, \qquad \qquad t \sim m^2 \quad \text{kept fixed.} \tag{2.13}$$

In this kinematical region, a great many angular momenta can contribute, and representation (2.11) is of less obvious value.

The key observation though is that we still have $t \sim m^2$; so we may be able to find a more manageable representation of $A(s,t)$ on the basis of t channel partial waves. This idea is one of the central elements of Regge theory. In the t channel physical region then we expand

$$A(s,t) = \sum_{l=0}^{\infty} (2l + 1)A_l(t)P_l(z_t) \tag{2.14}$$

with A_l, z_t given similarly to (2.12) and (2.10) but with $s \leftrightarrow t$. We need some means of analytically continuing the expansion in (2.14) into the s-channel physical region: as it stands, this expression diverges long before we reach the Regge limit in which we are interested.

21

Firstly then we rewrite $A(s,t)$ in terms of its singularities through a dispersion integral; the procedure is sketched in the following figure.
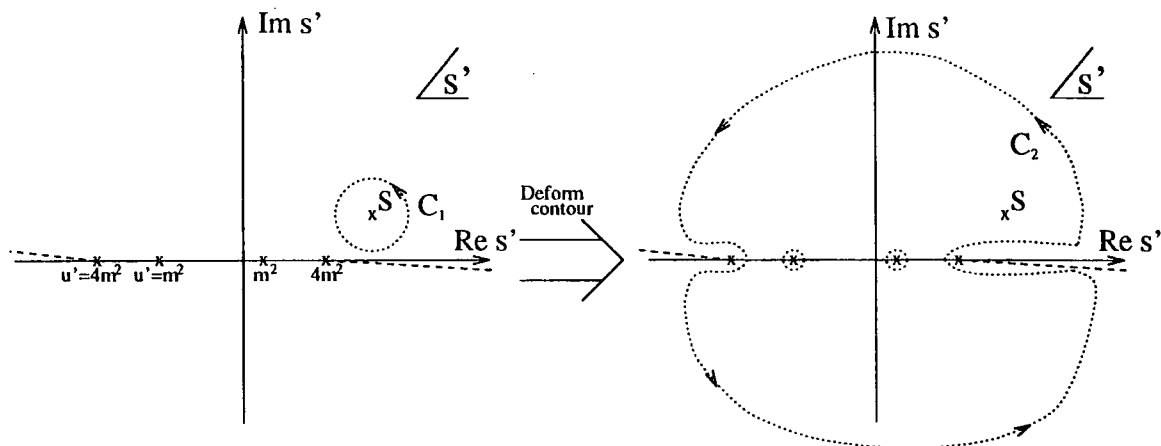
Figure 2.1: The contour integral from which the dispersion integral is derived. The crosses denote *pole* singularitites of the scattering amplitude at s' (resp. u')= m^2 and the endpoints of *cut* singularities at s' (resp. u') $= 4m^2$. (With u' defined by $u' \equiv 4m^2 - s' - t$).

By Cauchy's theorem, if $A(s,t)$ is analytic within the region enclosed by C_1, then

$$A(s,t) = \frac{1}{2\pi i} \oint_{C_1} \frac{ds'}{s'-s} A(s',t)$$

and provided that the behaviour at infinity is sufficiently tame we can open up this contour into that given by C_2, thus

$$
\begin{aligned}
A(s,t) &= \frac{1}{2\pi i} \oint_{C_2} \frac{ds'}{s'-s} A(s',t) + \frac{G_s(t)}{m^2-s} + \frac{G_u(t)}{m^2-u} \\
&= \frac{G_s(t)}{m^2-s} + \frac{G_u(t)}{m^2-u} \\
&\quad + \frac{1}{2\pi i} \int_{4m^2}^{\infty} \frac{ds'}{s'-s} D_s(s',t) + \frac{1}{2\pi i} \int_{4m^2}^{\infty} \frac{du'}{u'-u} D_u(u',t)
\end{aligned}
\tag{2.15}
$$

where the functions $D_s(s,t)$ and $D_u(u,t)$ represent the discontinuity of the scattering amplitude across its right and left hand cuts in the s-plane, defined similarly to (2.9). If the scattering amplitude does not vanish sufficiently fast as $s \to \infty$ we may need to introduce subtractions into this dispersion integral, but the basic reasoning remains the same [4,6]. Equation (2.15) can be rewritten as an integral over the t channel scattering

angle as (dropping the pole terms for simplicity)

$$A(s,t) = \frac{1}{2\pi i}\int_{z_R}^{\infty}\frac{dz'}{z'-z_t}D_s\big(s'(z',t),t\big) + \frac{1}{2\pi i}\int_{-z_L}^{-\infty}\frac{dz'}{z'-z_t}D_u\big(u'(z',t),t\big), \qquad (2.16)$$

with $z_R \equiv z_t(s = 4m^2, t), -z_L \equiv z_t(u = 4m^2, t)$.

If we insert this representation into the analogous expression to equation (2.12) we get the Froissart-Gribov projection,

$$A_l(t) = \frac{1}{2\pi i}\int_{z_R}^{\infty} dz'\, D_s\big(s'(z',t),t\big) Q_l(z') + \frac{1}{2\pi i}\int_{-z_L}^{-\infty} dz'\, D_u\big(u'(z',t),t\big) Q_l(z') \qquad (2.17)$$

where the Legendre function of the second kind $Q_l(z)$ is defined for positive integral vales of l through the Neumann relation

$$Q_l(z) = -\frac{1}{2}\int_{-1}^{1} dz'\frac{P_l(z')}{z'-z}. \qquad (2.18)$$

For these integral values of l, $Q_l(-z) = (-1)^{l+1}Q_l(z)$ so we can rewrite equation (2.17) as

$$A_l(t) = \frac{1}{2\pi i}\int_{z_{min}}^{\infty} dz'\left[D_s\big(s'(z',t),t\big) + (-1)^l D_u\big(u'(-z',t),t\big)\right] Q_l(z') \qquad (2.19)$$

where $z_{min} \equiv min[z_L, z_R]$.

For technical reasons [4,6] it is necessary to introduce signatured amplitudes in order to analytically continue the scattering amplitude to complex l. These amplitudes are defined by

$$A^{\pm} \equiv A(z_t, t) \pm A(-z_t, t) \qquad (2.20)$$

and the physical amplitude $A(s,t)$ can be written in terms of these amplitudes by

$$A(s,t) = \frac{1}{2}\Big(A^+(z_t,t) + A^+(-z_t,t)\Big) + \frac{1}{2}\Big(A^-(z_t,t) - A^-(-z_t,t)\Big). \qquad (2.21)$$

The analogous equation to (2.19) for these functions is

$$A_l^{\pm}(t) = \frac{1}{2\pi i}\int_{z_{min}}^{\infty} dz'\left[D_s\big(s'(z',t),t\big) \pm D_u\big(u'(-z',t),t\big)\right] Q_l(z'). \qquad (2.22)$$

We can take the equation (2.22) as defining $A_l^{\pm}(t)$ for arbitrary (complex) values of l. The analogous inversion of the partial wave expansion to (2.11) can, now that we are

thinking of l as complex, be converted to a contour integral through the Sommerfeld-Watson transform,

$$A^{\pm}(s,t) = \frac{-1}{2i} \oint_{C_1} dl\, \frac{(2l+1)P_l(-z_t)A_l^{\pm}(t)}{\sin(\pi l)} \tag{2.23}$$

where the contour of integration is shown on diagram (a) of the following figure.
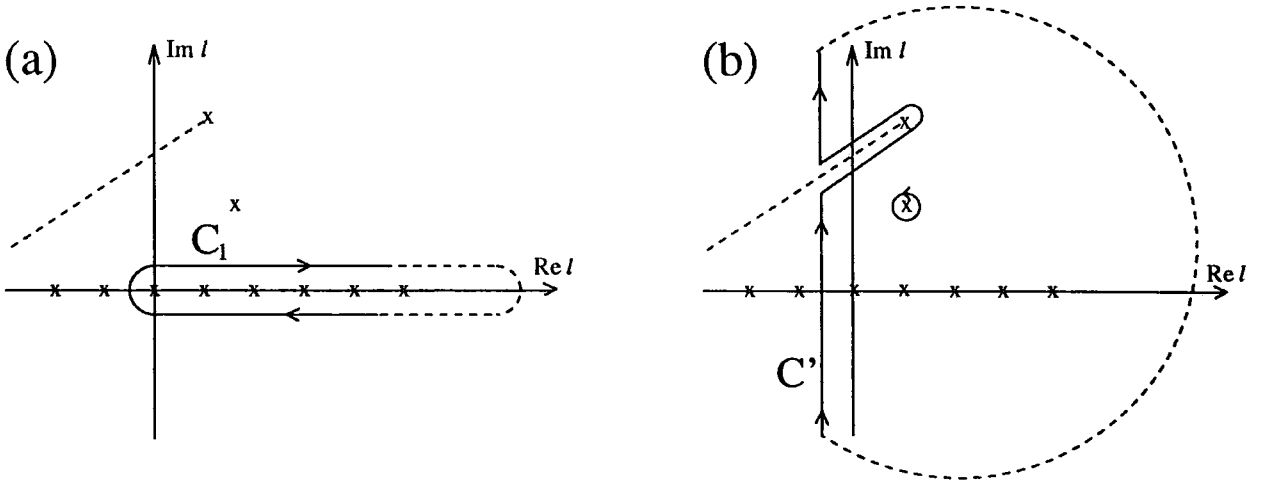
Figure 2.2: The contour of integration in the inversion of the Sommerfeld-Watson transform. Crosses denote singularities (poles, and the endpoint of a cut) of the integrand.

If we make the hypothesis that $A_l^{\pm}(t)$ has only isolated singularities in the complex l plane, then we can deform the contour of integration to that shown in diagram 2.2(b).

Say one of the signatured partial wave amplitudes $A_l^{\pm}(t)$ has just a single isolated pole in the region $Re\, l > -\frac{1}{2}$, that is

$$A_l^{\pm}(t) \simeq \frac{\beta(t)}{l - \alpha(t)}, \tag{2.24}$$

then we can see that the contour integral in figure 2.2(b) is, explicitly,

$$A_R^{\pm}(s,t) = \frac{-1}{2i} \oint_{C'} dl\, (2l+1)\, A_l^{\pm}(t)\frac{P_l(-z_t)}{\sin(\pi l)} - \pi(2\alpha(t)+1)\beta(t)\frac{P_{\alpha(t)}(-z_t)}{\sin\left(\pi\alpha(t)\right)}. \tag{2.25}$$

The $\int_{C'}$ (the 'background integral') is taken along the line $Re\, l = -\frac{1}{2}$ in the l-plane. In the Regge asymptotic limit, we can generally throw away this contribution as being insignificant compared to the pole term.

From (2.21), the corresponding pole contribution to the physical scattering amplitude is

$$
A_R(s,t) = -\pi(2\alpha(t) + 1)\beta(t)\frac{\left[P_{\alpha(t)}(-z_t) \pm P_{\alpha(t)}(z_t)\right]}{2\sin\left(\pi\alpha(t)\right)}
$$
$$
\simeq -\frac{\pi}{2}(2\alpha(t) + 1)\beta(t)\zeta^{\pm}_{\alpha(t)}P_{\alpha(t)}(-z_t)
$$

(2.26)

where the *signature factor* $\zeta^{\pm}_{\alpha(t)}$ is given by

$$
\zeta^{\pm}_{\alpha(t)} = \frac{1 \pm e^{-i\pi\alpha(t)}}{\sin\pi\alpha(t)}
$$

and controls the phase of the amplitude.

Equation (2.26) is the famous Regge pole form of a scattering amplitude; if we take into account that $z_t \simeq 2s/t$ and that the leading term of $P_l(z_t) \sim z^l$ we see that (2.26) gives the characteristic Regge pole behaviour,

$$
A(s,t) \sim \left(2\alpha(t) + 1\right)\beta_{12\to34}(t)\zeta^{\pm}_{\alpha(t)}s^{\alpha(t)}
$$

(2.27)

for $s/t \to \infty$. Moreover, we can show that the residue function must factorise, that is

$$
\beta_{12\to34}(t) = \beta_{13}(t)\,\beta_{24}(t)
$$

where β_{13} depends only on particles $1,3$; and similarly function β_{24} depends only on particles $2,4$.

2.2.2: Reggeon Calculus.

Originally it was hoped that the only singularities of $A_l(t)$ would be the simple poles (Regge poles) of the previous section. This is the case in potential scattering for a wide class of potentials; however it was soon realised that a relativistic field theory amplitude could have a much more complex singularity structure. Thus, for example, there is no reason in principle why a Reggeon should not be exchanged more than once in the same amplitude, as in the following diagram.
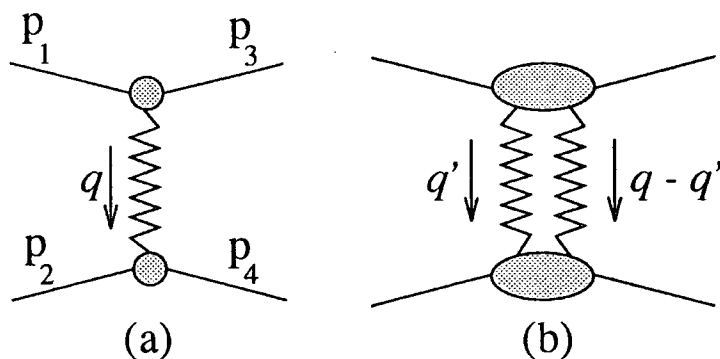
Figure 2.3: Contributions to the scattering amplitude from

(a) One-Reggeon exchange,

(b) Two-Reggeon exchange.

The jagged line denotes the exchange of a simple Regge pole with trajectory $\alpha(t = -\vec{q}^{\,2}) = \alpha_0 - \alpha'\vec{q}^{\,2}$, which we might think of as a phenomenologically motivated model for the soft pomeron [7]. Thus the diagram in figure 2.3(a) gives a contribution to the amplitude of

$$A_1^1(s,t) \sim \beta_1(\vec{q})s^{\alpha_0-\alpha'\vec{q}^{\,2}}\beta_1(\vec{q}). \tag{2.28}$$

where we have explicitly shown the factorised form of the residue function and have introduced a notation in which we make explicit the number of pomerons coupling to particles A and B. The importance of additional pomeron exchange now depends upon the value of α_0, the pomeron intercept. The total cross section is related by the optical theorem to the forward scattering amplitude, such that

$$\sigma_{TOT} = \frac{1}{2s}Im\,A(s+i\epsilon, t=0) \sim s^{\alpha_0-1}$$

so we see that the pomeron intercept is the crucial factor in the behaviour of the total cross section for $s \to \infty$: for $\alpha_0 < 1$ all cross sections must vanish asymptotically as a power of energy. It is also the crucial factor in determining whether multiple pomeron exchange will be important asymptotically. This we can see from the diagram in figure 2.3(b), which has the asymptotic behaviour

$$A_2^2 \sim s^{2\alpha_0-1}\int d^2\vec{q}'\,\beta_2(\vec{q},\vec{q}')s^{-\alpha'\vec{q}'^2-\alpha'(\vec{q}'-\vec{q})^2}\beta_2(\vec{q},\vec{q}'). \tag{2.29}$$

If we Mellin transform this, then we get a *cut* singularity in the j plane with its branch

26

point at $j = \alpha_0 + (\alpha_0 - 1)$ and extending back towards $j \sim -\infty$. If $\alpha_0 < 1$, then this singularity lies to the left of the one-pomeron amplitude and is suppressed relative to it; however as $\alpha_0 \to 1$ the two terms can be of comparable importance. In fact the point $\alpha_0 = 1$ is something of a specialty and is given a special name — the *critical* pomeron — since at this point all the cuts corresponding to multiple pomeron exchange converge around the point $j = 1$. This is in analogy to mass singularities as $m \to 0$, where all the multi-particle threshold singularities in the scattering amplitude pile up at $s = 0$.

We must further allow for the possibility of the Reggeons interacting with each other, as well as coupling to the external particles. These multiple exchanges of Reggeons can be accounted for through the Regge calculus.[1] The basic idea is to set up an effective field theory in which these Reggeons are the fundamental units, with couplings to each other and to external states. The theory is formulated as a 2+1 dimensional nonrelativistic field theory; two transverse dimensions plus a third ('time') dimension parameterised by the Mellin transform variable j. It turns out that the results of the leading log calculations of the remainder of the chapter have a very direct correspondence with this old fashioned Reggeon Field Theory (RFT).

---

[1] A review of the subject is given in [8]; and for a selection of reprints of important articles in this area see [9].

2.3: Preliminaries to the QCD analysis.

Some of the key early papers on this subject date back to the mid-70's and were written by Balitsky, Fadin, Kuraev and Lipatov; hence the results we describe are generally attributed to them [10, 11, 12, 13]. In particular the final integral equation for the scattering amplitude is known as the *BFKL equation*, named after these authors. The following treatment of it draws upon a mixture of sources, using ideas from the original Feynman gauge analysis mixed with later work carried out in the Coulomb gauge, in which certain results can be derived much more simply. We consider gluon-gluon scattering in the limit $s \gg t$. The important Feynman rules which are necessary for our calculation are shown in the following figure [14].

$$\mu \xrightarrow{k} \nu \; = \; \delta^{ab} \frac{P_{\mu\nu}(k)}{k^2 + i\varepsilon}$$

$$= [if_{abc}] \; g \; g^{\mu\rho} \; (p+p')^\nu$$

Figure 2.4: The Feynman rules which are needed in the calculation of $gg \to gg$ scattering in the multi-Regge limit. The polarisation sum $P_{\mu\nu}(k)$ depends upon the gauge; for example, in the Feynman gauge we have $P_{\mu\nu} = g_{\mu\nu}$. It is useful to calculate the colour factor and spacetime factor seperately for each diagram, so let us define $[if_{abc}]$ as the appropriate colour factor for the vertex and the rest as the spacetime factor.

These Feynman rules must be supplemented by the integration measure

$$\int \frac{d^4k}{(2\pi)^4 i}$$

for each closed loop.

The gluon momenta, polarisation vectors and colour indices are labelled as p_i, μ_i, and a_i respectively with $i = 1 \cdots 4$ and the labelling is as shown in figure 2.5.
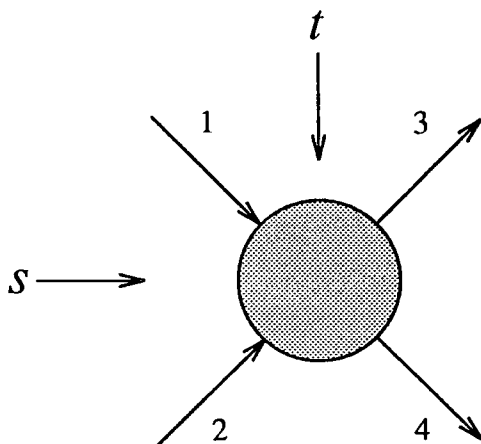
Figure 2.5: Labelling of particles for the scattering process $gg \to gg$.

We need to decompose the scattering amplitude in terms of the t-channel quantum number exchange, that is

$$\mathcal{A}^{\{a_i, \lambda_i\}}(s, t) = \Gamma_0^{\{a_i\}} A_0^{\{\lambda_i\}}(s, t) + \Gamma_{\bar{8}}^{\{a_i\}} A_{\bar{8}}^{\{\lambda_i\}}(s, t) + \text{higher colour spins...} \qquad (2.30)$$

where Γ_i are colour tensors of different colour spin in the t-channel. Explicitly, these are given for the colour singlet and colour octet channels (0 and $\bar{8}$ respectively) as

$$\Gamma_0^{\{a_i\}} = \delta_{a_1 a_3} \delta_{a_2 a_4} \qquad (2.31)$$

$$\Gamma_{\bar{8}}^{\{a_i\}} = (i f_{a_1 c a_3})(i f_{a_2 a_4 c}) \qquad (2.32)$$

with f_{abc} the structure constants for $SU(3)$. We shall find that the scattering amplitude displays markedly different behaviour between the two different channels 0 and $\bar{8}$. In particular, the behaviour of $A_{\bar{8}}$ is quite simple, while that for the vacuum (colour singlet) channel A_0 will be very much more complex.

Some general properties of the two amplitudes A_0 and $A_{\bar{8}}$ come from the requirement that the full amplitude $\mathcal{A}(s, t)$ be symmetric under the interchange of particles $1 \leftrightarrow 2$. In particular this consideration shows that $A_{\bar{8}}(s, t) = -A_{\bar{8}}(u, t)$ (odd signature in octet channel) and $A_0(s, t) = +A_0(u, t)$ (even signature in singlet channel). In the Regge asymptotic regime $u \simeq -s$ so A_0 and $A_{\bar{8}}$ are effectively odd and even in s.

29

2: The high energy limit of QCD.

Let us work in the centre-of-momentum frame of the two incoming gluons, and define their momenta as lying along the z-axis. It is useful to decompose four-momenta in a light-cone basis. For the following chapter we will do this in two ways, depending on whichever is most convenient at the time. Firstly we have the typical decomposition,

$$q^\mu = q_+^\mu + q_-^\mu + q_\perp^\mu$$

where q_+^μ (q_-^μ) is a lightlike vector along the incident momentum of particle 1 (2), and $q_\perp^\mu$ is a two-dimensional spacelike vector in the x, y plane transverse to the incoming momenta. Choosing $q_\pm = \frac{1}{\sqrt{2}}(q_0 \pm q_3)$ we normalise the scalar product such that

$$q^\mu . q'_\mu = q_+ q'_- + q_- q'_+ + q_\perp^\mu . q'_{\perp\mu} \equiv q_+ q'_- + q_- q'_+ - \vec{q} . \vec{q}'$$

where from here on we define vectors $\vec{q}, \vec{q}'$ transverse to the incoming momenta and such that they have a *positive* inner product rather than the negative one appropriate for space-like vectors; thus $\vec{q}^{\,2} \equiv -q_\perp^\mu . q_{\perp\mu}$ and such like.

Alternatively we may scale the vectors q_+, q_- to be explicitly proportional to the incident particle momenta, thus

$$q^\mu = \alpha p_1^\mu \pm \beta p_2^\mu + q_\perp^\mu .$$

A general scalar product of two of these momenta is then given by

$$q^\mu . q'_\mu = \pm(\alpha\beta' + \beta\alpha')p_1 . p_2 + q_\perp^\mu . q'_{\perp\mu}$$

and the Jacobian for the change of variables is

$$d^4 q^\mu \Rightarrow |p_1 . p_2| \, d\alpha \, d\beta \, d^2 q_\perp .$$

2.4: The colour octet amplitude.

To order g^2, we have the following diagrams for the $gg \rightarrow gg$ amplitude.

(i)   (ii)   (iii)   (iv)
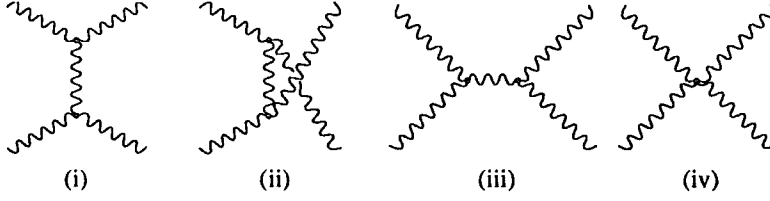
Figure 2.6: Feynman graphs contributing to the process $gg \rightarrow gg$ at tree level.

The dominant diagram in Regge kinematics is that of t-channel gluon exchange, diagram (i) of the set above. The other contributions are suppressed by a power of s relative to this one and are not important. Thus we have that for gluon-gluon scattering at Born level in the leading approximation and the Feynman gauge

$$A_{\bar{8}}^{\{\lambda_i\}}(s,t) = g^2 \, \Gamma^{\mu_1 \nu \mu_3}(p_1, -q, -p_3) \, D_\nu^{\nu'}(q) \, \Gamma_{\nu' \mu_2 \mu_4}(p_2, -p_4, q) \, \epsilon_{\mu_1}^{\lambda_1} \epsilon_{\mu_2}^{\lambda_2} \epsilon_{\mu_3}^{\lambda_3 *} \epsilon_{\mu_4}^{\lambda_4 *},$$
$$A_0^{\{\lambda_i\}}(s,t) = 0.$$

Again to the leading power of energy, we can approximate the 3-gluon vertices as

$$\Gamma^{\mu_1 \nu \mu_3}(p_1, -q, -p_3) \simeq g^{\mu_1 \mu_3} \, 2p_1^\nu$$
$$\Gamma_{\nu' \mu_2 \mu_4}(p_1, -q, -p_3) \simeq g_{\mu_2 \mu_4} \, (-2p_2)^{\nu'} \tag{2.33}$$

which gives rise to the suppression of helicity-flip amplitudes at high energies, since we get the factor

$$\epsilon_{\mu_3}^{\lambda_3 *} g^{\mu_1 \mu_3} \epsilon_{\mu_1}^{\lambda_1} \simeq -\delta_{\lambda_1 \lambda_3} \left[1 + \mathcal{O}\left(\frac{t}{s}\right) \right] \tag{2.34}$$

and a similar factor from the lower vertex. Bearing this in mind we drop the λ indices on A_0 and $A_{\bar{8}}$ from now on. So finally, to order g^2, we have:

$$A_{\bar{8}}^{[2]}(s,t) \simeq g^2 \, \frac{-2s}{t} \, (-\delta_{\lambda_1 \lambda_3})(-\delta_{\lambda_2 \lambda_4}) \tag{2.35}$$

$$A_0^{[2]}(s,t) = 0. \tag{2.36}$$

Consider now the one-loop corrections of the type shown in figure 2.7:
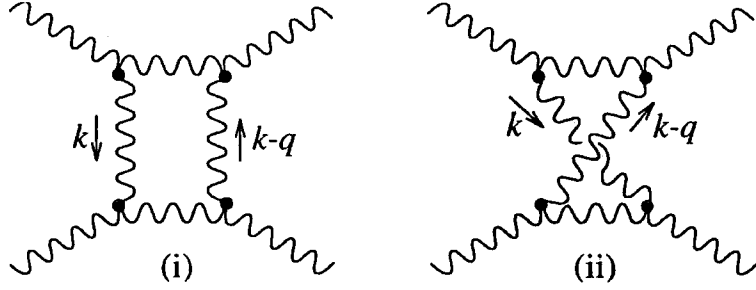
Figure 2.7: Two graphs for $gg \to gg$ at one loop, giving logarithms in the Feynman gauge but not the Coulomb gauge.

The amplitude corresponding to graph (i) above is, in the Feynman gauge,

$$
\mathcal{M} \simeq \int \frac{d^4 k}{i(2\pi)^4} \frac{(2p_1 - k)_\alpha g_{\mu_1 \nu_1} g_{\nu_1 \mu_3} (2p_1 - k - q)_\beta \, (2p_2 + k)^\alpha g_{\mu_2 \nu_2} g_{\nu_2 \mu_4} (2p_2 + k + q)^\beta}{k^2 (p_1 - k)^2 (p_2 + k)^2 (k - q)^2}
$$
$$
\times \, \epsilon^{\lambda_1}_{\mu_1} \epsilon^{\lambda_2}_{\mu_2} \epsilon^{\lambda_3}_{\mu_3}{}^* \epsilon^{\lambda_4}_{\mu_4}{}^* (g)^4 \times [\text{Colour Structure}]
$$
$$
\simeq (-\delta_{\lambda_1 \lambda_3})(-\delta_{\lambda_2 \lambda_4}) \frac{g^4}{i} (4p_1 \cdot p_2)^2 \, \frac{s}{2} \int \frac{d\alpha \, d\beta \, d^2 k_\perp}{(2\pi)^4} \frac{1}{k^2 (p_1 - k)^2 (p_2 + k)^2 (k - q)^2}
$$
$$
\times \, [\text{Colour Structure}]
$$

$$(2.37)$$

where we have approximated the vertices to the leading power in energy as before, for which the tensor structure simplifies dramatically. We have also changed to an integration over the Sudakov variables, expanding $k = \alpha p_1 - \beta p_2 + k_\perp$. The Jacobian for this change of variables is $s/2$. The crucial region of integration has both $\alpha, \beta \ll 1$ and this has been taken into account to allow the numerator to be simplified. The various propagators become, in terms of the Sudakov variables,

$$
(p_2 + k)^2 = \alpha(1 - \beta)s - \vec{k}^2
$$
$$
(p_1 - k)^2 + i\epsilon = (1 - \alpha)\beta s - \vec{k}^2 + i\epsilon
$$

We now perform the integral over β by circling around the pole in the $(p_1 - k)^2 + i\epsilon$

propagator, thus giving

$$\mathcal{M} \simeq (-\delta_{\lambda_1\lambda_3})(-\delta_{\lambda_2\lambda_4})\frac{g^4}{i}(2s)^2\,\frac{s}{2}\frac{-2\pi i}{s}\int\frac{d\alpha\,d^2k_\perp}{(2\pi)^4}\frac{1}{k^2(\alpha s - \vec{k}^2)(k-q)^2} \qquad (2.38)$$
$$\times\,[\text{Colour Structure}].$$

The logarithm comes from the integral over α in that region for which $k^2/s \ll \alpha \ll 1$ for which the t–channel propagators are essentially transverse, so that ultimately we have for the first graph in figure 2.7,

$$\mathcal{M} \simeq \left(g^2\frac{-2s}{t}(-\delta_{\lambda_1\lambda_3})(-\delta_{\lambda_2\lambda_4})\right)\left(\frac{g^2t}{(2\pi)^3}\int\frac{d^{2+\epsilon}\vec{k}}{\vec{k}^2(\vec{k}-\vec{q})^2}\right)(\log s) \qquad (2.39)$$
$$\times\,[\text{Colour Structure}].$$

Notice that we have here introduced dimensional regularisation to tame the infrared divergence in the transverse momentum integration. The most systematic procedure would be to generate masses for the gluon through the Higgs mechanism, and later to take the limit as this mass goes to zero if desired. This, indeed, was the method used by the original BFKL authors [10, 11, 12]. For the purposes of the present discussion though the use of dimensional regularisation seems adequate, and simpler. We know, too, that the integral equation for the vacuum amplitude which will be the end result of our analysis is infrared finite, at least when coupled to colourless bound states like hadrons [13, 15].

It is very simple to get the corresponding amplitude for graph (ii) of the above pair. It is basically the same, except for a relative minus sign owing to the lower propagator becoming here spacelike rather than timelike, and the different colour structure. The appropriate colour algebra is most easily carried out by diagrammatic methods making use of the Jacobi identity, a diagrammatic representation of which is portrayed in figure 2.8[16]. The fact that the overall colour structure is dependent only upon the Jacobi identity makes it clear that all scattering processes ($gg \to gg$, $gq \to gq$, $qq \to qq\ldots$) pick up the same overall factor relative to the Born term on calculating the one-loop correction. This is a crucial requirement for the Reggeisation of the t-channel gluon.
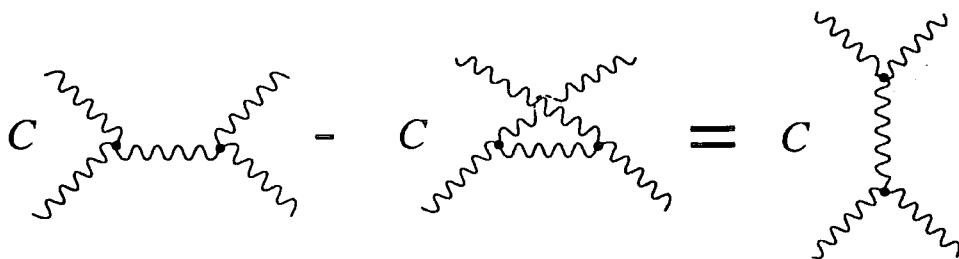
Figure 2.8: A diagrammatic representation of the Jacobi identity, which relates the colour structure of different diagrams. The C by each diagram means that the Feynman rules associated with each vertex are only those corresponding to the colour degrees of freedom, that is the colour factors if_{abc} of $SU(3)$.

Having carried out the colour algebra one picks up a factor $N_c/2$ times the colour octet tensor defined in (2.32). Thus the full order g^4 contibution to the colour-octet amplitude to $LL(s)$ is,

$$A_{\bar{8}}^{[4]} \simeq A_{\bar{8}}^{[2]} \cdot \left(\frac{g^2 N_c t}{2(2\pi)^3} \int \frac{d^{2+\epsilon}\vec{k}}{\vec{k}^2(\vec{k}-\vec{q})^2} \right) \log s \qquad (2.40)$$

$$= A_{\bar{8}}^{[2]} \omega(t) \log s, \qquad (2.41)$$

with

$$\omega(t) = \frac{g^2 N_c t}{2(2\pi)^3} \int \frac{d^{2+\epsilon}\vec{k}}{\vec{k}^2(\vec{k}-\vec{q})^2}. \qquad (2.42)$$

We stress again that equations (2.41) and (2.42) are independent of the particular particles (gluons or quarks) which undergo the scattering process.

The above calculation was performed in the Feynman gauge. The scattering amplitude, of course, should not depend on our gauge fixing condition; however, experience with the derivation of the DGLAP evolution equations from within perturbative QCD has shown that a careful choice of gauge can simplify the classes of diagrams which contribute to a given process to leading logarithmic accuracy. It turns out that a similar simplification occurs in the analysis of the Regge limit scattering amplitude, if one is content to dispense with explicit Lorentz invariance by introducing the noncovariant Coulomb gauge. The

advantage of this gauge over the fully Lorentz covariant gauges lies in the structure of the graphs which give logarithms in higher orders of perturbation theory. In particular, for the colour octet channel these noncovariant gauges allow for a very simple analysis [17, 18].

The Coulomb gauge corresponds to the classical gauge fixing condition,

$$\nabla.\mathbf{A}^a = 0,$$

or in a different notation,

$$\partial_\mu A_a^\mu - (N_\mu \partial^\mu)(N_\mu A_a^\mu) = 0$$

where $N_\mu = (1,0,0,0)$ and $a = 1 \dots N_c^2 - 1$. This gives rise to the propagator,

$$D_{\mu\nu}^{ab}(k) = \frac{P_{\mu\nu}(k)\delta^{ab}}{k^2 + i\epsilon} = \frac{\delta^{ab}}{k^2 + i\epsilon}\left[g_{\mu\nu} - \frac{k.N(k_\mu N_\nu + k_\nu N_\mu) - k_\mu k_\nu}{(k.N)^2 - k^2}\right]. \qquad (2.43)$$

From here we can see how our desired simplification can arise. If we consider the exchange of a gluon across a large rapidity gap such that the polarisation sum of the exchanged gluon is dominated by its $+-$ component simple algebra shows that the relevant propagator (2.43) is well approximated by

$$D_{-+}(k) \simeq \frac{1}{(N.k)^2 - k^2},$$

corresponding to an instantaneous Coulomb exchange across the rapidity gap. A large flow of $+$ momentum down such a line will now be suppressed relative to similar cases in the Feynman gauge, since

$$D_{-+} \sim \frac{1}{(k^+)^2} \qquad \text{in Coulomb gauge}$$

which is reduced by a power of k^+ over

$$D_{-+} \sim \frac{1}{(2k^+k^- - \vec{k}^2)} \qquad \text{in Feynman gauge.}$$

Thus the logarithm which appears in the graphs in figure 2.7 for the Feynman gauge will be absent here because a large flow of $+$ momentum down line k and back up line $k - q$ makes these propagators 'hard' and kills the logarithmic integral over α.

We know that the amplitude does not depend on the choice of gauge, so the logarithms in the Coulomb gauge must show up in some other form of graph. The relevant graphs are vertex corrections, an example of which is given in figure 2.9:
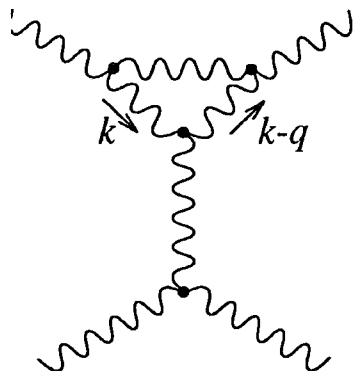
Figure 2.9: A vertex correction type of graph which contributes a leading logarithm in the Coulomb gauge, but not the Feynman gauge.

In a covariant gauge this could not give a logarithm of s, since it could only depend on scalar products of momenta at the top vertex which are all of order t; but here it can also be a function of $p_1.N$, with N the timelike vector used in defining the Coulomb gauge. Consequently the graph in figure 2.9 gives a contribution

$$\Delta A^{[4]} \simeq g^4 \int \frac{dk^+ dk^- d^2 k_\perp}{(2\pi)^4 i} (2p_1 - k)_\alpha g_{\mu_1 \mu'} \frac{P_{\mu' \mu''}(p_1 - k)}{(p_1 - k)^2 + i\epsilon} g_{\mu'' \mu_3} (2p_1 - k - q)_\beta$$

$$\times \frac{P_{\beta' \beta}(k - q)}{(k - q)^2 + i\epsilon} g^{\alpha' \beta'} \frac{P_{\alpha \alpha'}(k)}{k^2 + i\epsilon} (2k - q)^\nu \frac{P_{\nu \nu'}(q)}{q^2} (-2p_2 - q)^{\nu'} \epsilon_{\mu_1}^{\lambda_1} \epsilon_{\mu_2}^{\lambda_2} \epsilon_{\mu_3}^{\lambda_3 \, *} \epsilon_{\mu_4}^{\lambda_4 \, *} .$$

$$\times \, [\text{Colour Structure}]$$

The colour algebra is again easily performed through use of the Jacobi identity and again gives $N_c/2$ times the colour tensor (2.32). Then, using

$$2p_1^\alpha P_{\alpha \alpha'}(k) g^{\alpha' \beta'} P_{\beta' \beta}(k - q) 2p_1^\beta \simeq 4 \left(\frac{p_1^+}{k^+} \right)^2 k.(k - q)$$

this becomes

$$\Delta A_{\bar{8}}^{[4]} \simeq \frac{g^4}{i} (-\delta_{\lambda_1 \lambda_3}) (-\delta_{\lambda_2 \lambda_4}) \frac{N_c}{2}$$

$$\times \int \frac{dk^+ dk^- d^2 k_\perp}{(2\pi)^4} 4 \left(\frac{p_1^+}{k^+} \right)^2 \frac{k.(k - q)}{k^2 (k - q)^2} \frac{1}{(p_1 - k)^2 + i\epsilon} \frac{(-4k^+ p_2^-)}{q^2} .$$

36

We do the integral over k^- by picking up the pole from the propagator

$$(p_1 - k)^2 = -2p_1^+ \left(k^- - \frac{k^2 + i\epsilon}{2p_1^+} \right)$$

to give

$$\Delta A_{\bar{8}}^{[4]} \simeq \left[g^2 \frac{-4p_1^+ p_2^-}{t} (-\delta_{\lambda_1 \lambda_3})(-\delta_{\lambda_2 \lambda_4}) \right] \times \frac{N_c}{2} 2g^2 \int_\mu^{p_1^+} \frac{dk^+}{k^+} \int \frac{d^{2+\epsilon}\vec{k}}{(2\pi)^3} \frac{\vec{k}.(\vec{k} - \vec{q})}{\vec{k}^2(\vec{k} - \vec{q})^2} \quad (2.44)$$

with μ some lower limit to the integral over k^+. The apparent ultraviolet divergence in (2.44) from the transverse momentum integration cancels out when we account for the other vertex correction and external wavefunction renormalisation graphs. For the present we can simply assume the standard rule in dimensional regularisation that

$$\int \frac{d^{2+\epsilon}k}{\vec{k}^p} = 0$$

and throw away the divergent term. On changing variables from $\vec{k} \to \vec{k}' = \vec{k} - \vec{q}/2$ the remaining transverse integral then becomes

$$-\int \frac{d^{2+\epsilon}\vec{k}'}{(2\pi)^3} \frac{(\vec{k}' + \vec{q}/2).\vec{q}}{(\vec{k}' - \vec{q}/2)^2(\vec{k}' + \vec{q}/2)^2} = \frac{-\vec{q}^2}{2} \int \frac{d^{2+\epsilon}\vec{k}}{(2\pi)^3} \frac{1}{\vec{k}^2(\vec{k} - \vec{q})^2}$$

so that finally we have

$$\Delta A_{\bar{8}}^{[4]} \simeq A_{\bar{8}}^{[2]} \times \omega(t) \log \left(\frac{p_1^+}{\mu} \right). \quad (2.45)$$

Lorentz covariance is preserved once the relevant contribution from the $p_2 - p_2' - q$ vertex correction is included, since this gives $A_{\bar{8}} \sim \log(p_1^+) + \log(p_2^-) \sim \log(s)$.

Generally speaking then, multiple gluon exchange across a large rapidity gap does not generate logarithms, in the Coulomb gauge [17, 18]. Therefore the general leading diagram in Coulomb gauge is as shown in figure 2.10 in which the blobs represent full vertices calculated to all orders at leading logarithmic accuracy, and also include wavefunction renormalisation factors for the external legs.

37
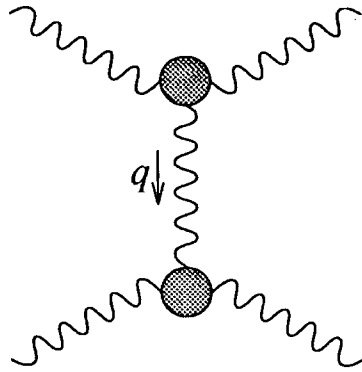
Figure 2.10: The general leading diagram for the colour-octet amplitude in the Coulomb gauge. The blobs represent full vertices calculated to leading logarithmic accuracy.

It is now very easy to show that the full vertices must exponentiate. We can simply apply the requirement of Lorentz invariance of the full scattering amplitude [17]. Taking into account helicity conservation of the scattered gluons we can write the leading logarithmic $p_1 - q - p_3$ vertex as

$$\Gamma^{\mu_1 \nu \mu_3}(\zeta, q) = g^{\mu_1 \mu_3} \, 2p_1^\nu \, \gamma_1(\zeta, q)$$

where $\zeta = \log\left(\frac{p_1^+}{\mu}\right)$. Similarly, the $p_2 - p_4 - q$ vertex we can write as

$$\Gamma^{\mu_2 \mu_4 \nu'}(\eta, q) = g^{\mu_2 \mu_4} \, (-2p_2)^\nu \, \gamma_2(\eta, q)$$

with $\eta = \log\left(\frac{p_2^-}{\mu}\right)$. The amplitude in figure 2.10 is then

$$A_{\bar{8}}^{[LL]} = g^2 \frac{-2s}{t} \, (-\delta_{\lambda_1 \lambda_3})(-\delta_{\lambda_2 \lambda_4}) \, \gamma_1(\zeta, q)\gamma_2(\eta, q). \tag{2.46}$$

From Lorentz invariance under a boost in the z-direction, we know that the amplitude cannot depend upon ζ and η independently, but only in the combination $\zeta + \eta = \log s$. That is,

$$\gamma_1(\zeta, q)\gamma_2(\eta, q) = F(\zeta + \eta, q)$$

hence the vertex factors γ necessarily exponentiate,

$$\gamma_1(\zeta, q) = A(q) \exp\left(\omega(q)\zeta\right),$$
$$\gamma_2(\eta, q) = B(q) \exp\left(\omega(q)\eta\right).$$

With the convention adopted for our definition of the vertex factors, a comparison with

the Born term shows that $A(q) = B(q) = 1$ and so finally

$$A_{\bar{8}}^{[LL]} \sim A_{\bar{8}}^{[2]} \left(\frac{s}{\mu^2} \right)^{\omega(t)} . \tag{2.47}$$

If we apply a Mellin transform to this amplitude, defining

$$F(j,t) = \frac{1}{\mu^2} \int_{\mu^2}^{\infty} \frac{ds'}{s'} \left(\frac{s'}{\mu^2} \right)^{-j} A_{\bar{8}}^{[LL]}(s',t) \tag{2.48}$$

then we get

$$F(j,t) = \frac{f(t)}{j - 1 - \omega(t)}$$

which, in the language of Regge theory, means that the colour octet amplitude is described by a *simple Regge pole* with a trajectory given by $\alpha(t) = 1 + \omega(t)$. It merely remains to calculate the trajectory function $\omega(t)$, which can be found very simply from a one-loop calculation. In fact from our Feynman gauge considerations we already know the trajectory function, from (2.42).

2.5: The vacuum channel.

We shall find that the behaviour in the vacuum channel is not nearly so straightforward as for the colour octet case. In fact the amplitude A_0 will not turn out to be a simple Regge pole, but rather a fixed cut in the angular momentum plane corresponding to the exchange of a 'bound state' of two interacting reggeised gluons. We shall attack the problem along the following chain of logic, as used by the BFKL authors and Bartels [11, 12, 15]:

- We use the results on the reggeisation of the gluon plus general principles of analyticity of the S-matrix to write down the $2 \to (2+n)$ amplitudes to all orders, at leading logarithmic accuracy.

- These amplitudes are inserted into the unitarity equations in order to calculate the absorptive part of the scattering amplitude in the vacuum channel, $\mathrm{Disc}_s A_0(s,t)$.

- Owing to the fact that the absorptive part of A_0 is dominated to our accuracy by diagrams with only two reggeons in the t-channel a recurrence relation can be written down which links n gluon emission with $(n-1)$ gluon emission. This recurrence relation takes the form of an integral equation for the scattering amplitude: the BFKL equation itself.

- In principle, a dispersion integral can be written to get the full amplitude from its absorptive part. Here, however, we are really more interested in the absorptive part itself, so will not carry the analysis through to its conclusion. In fact, the real part of the vacuum amplitude coming from the dispersion integral is formally nonleading, being down by a power of $\log s$ relative to the imaginary (absorptive) part. This is shown easily by expanding the general $\log^n s$ term of the expansion for the vacuum amplitude, $-s\log^n(-s) - u\log^n(-u) \simeq i\pi n\log^{n-1}(s) + \cdots$. Here as always we interpret $\log(-s) = \log s - i\pi$ when we approach physical s from above the real axis.

2.5.1: The phase space for extra gluon emission.

As we set out above, our analysis of the vacuum channel will require the amplitude for $2 \to (2 + n)$ gluons to leading logarithmic accuracy. It may seem perverse to look at the $2 \to (2 + n)$ amplitudes when one is in fact interested in just the $2 \to 2$ scattering amplitude in the vacuum channel; however, this approach is actually a simplification in that the $2 \to (2 + n)$ amplitude to leading accuracy can be written down purely in terms of colour octet exchanges, which are relatively simple. The appropriate starting point is to introduce the variables by which a production amplitude is described. These are defined in the figure 2.11.
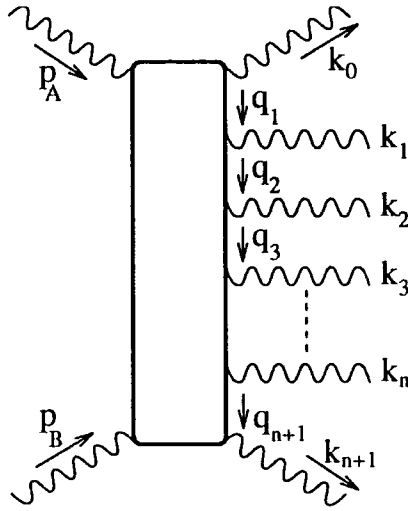
Figure 2.11: The definitions of external particle momenta and momentum transfers for the $2g \to (2 + n)g$ production process.

The $(2 + n)$-particle phase space is, as usual,

$$d\Phi_{2+n} = \prod_{i=0}^{n} \frac{d^4 k_i}{(2\pi)^4} \prod_{j=0}^{n+1} 2\pi \delta(k_j^2) \Theta(k_j^0),$$

or equivalently

$$d\Phi_{2+n} = \prod_{i=1}^{n+1} \frac{d^4 q_i}{(2\pi)^4} \prod_{j=0}^{n+1} 2\pi \delta(k_j^2) \Theta(k_j^0).$$

It is useful to decompose the various momentum transfers q_i in terms of Sudakov param-

eters,

$$q_i^\mu = \alpha_i p_A^\mu - \beta_i p_B^\mu + q_{i\perp}^\mu.$$

The phase space then becomes

$$d\Phi_{2+n} = 2\pi \, s^{n+1} \prod_{i=1}^{n+1} \frac{d\alpha_i d\beta_i d^2 \vec{q}_{i\perp}}{2(2\pi)^3} \prod_{j=0}^{n+1} \delta((\alpha_j - \alpha_{j+1})(\beta_{j+1} - \beta_j)s - k_{j\perp}^2),$$

with the definitions $\alpha_0 = \beta_{n+2} = 1$. To avoid double counting, we choose a specific labelling of the final state particles such that they are ordered in rapidity y, where y is defined as

$$y = \frac{1}{2} \log\left(\frac{\beta}{\alpha}\right), \tag{2.49}$$

and so we number the momenta such that

$$y_{n+1} > y_n > \cdots > y_2 > y_1. \tag{2.50}$$

With this understanding, we need no symmetry factor to account for the identical particles in the final state since we have prevented any double counting from the outset.

The variables α and β are limited from above by 1 and from below by something of the order of μ^2/s with μ^2 some scale (much less than s) at which the transverse momentum integrals are dominated, typically $\mu^2 \sim |q_i^2| \sim m^2$ in the Regge limit of a massive theory. Thus rapidity y varies roughly from

$$-\frac{\zeta}{2} = -\frac{1}{2} \log\left(\frac{s}{\mu^2}\right) \lesssim y \lesssim +\frac{1}{2} \log\left(\frac{s}{\mu^2}\right) = +\frac{\zeta}{2}.$$

and integrals over rapidity give rise to logarithms of energy owing to the large area of phase space which is available. To leading logarithmic accuracy, we can make a stronger statement than (2.50) and assume that the gluons are distributed in the so-called *multi-Regge* kinematics, so that in fact

$$y_{n+1} \gg y_n \gg \cdots \gg y_2 \gg y_1. \tag{2.51}$$

In doing this we understand that our resulting amplitude will be a poor approximation for any configuration for which two gluons are closer in rapidity than some fixed interval

42

$\Delta y = \epsilon$ say; however, this is irrelevant to a leading log calculation, since

$$\int_{\frac{-\zeta}{2}}^{\frac{\zeta}{2}} dy_n \int_{\frac{-\zeta}{2}}^{y_n - \epsilon} dy_{n-1} \cdots \int_{\frac{-\zeta}{2}}^{y_2 - \epsilon} dy_1 = \frac{\zeta^n}{n!} \left[1 + \mathcal{O}\left(\frac{\epsilon}{\zeta} \right) + \cdots \right]$$

so to leading log we can set $\epsilon = 0$. In terms of the α and β variables the strong ordering in rapidity means that

$$\begin{aligned}
1 \gg \alpha_1 \gg \alpha_2 \gg \cdots \gg \alpha_{n+1} &\simeq \frac{q_{n+1}^2}{s}, \\
1 \gg \beta_{n+1} \gg \beta_n \gg \cdots \gg \beta_1 &\simeq \frac{q_1^2}{s}.
\end{aligned} \tag{2.51}$$

With our strong ordering approximation then, and after using the δ functions to fix each β_i and also α_{n+1}, (from which we get the lower bounds on α and β used above) we find our phase space measure to be [11]

$$d\Phi_{2+n} = \frac{2\pi}{s} \prod_{i=1}^{n} \frac{d\alpha_i}{\alpha_i} \prod_{j=1}^{n+1} \frac{d^2 \vec{q}_{i\perp}}{2(2\pi)^3}. \tag{2.52}$$

Equivalently, we can change variables to rapidity,

$$dy_i = \frac{d\alpha_i}{\alpha_i}$$

so that

$$d\Phi_{2+n} = \frac{2\pi}{s} \prod_{i=1}^{n} dy_i \prod_{j=1}^{n+1} \frac{d^2 \vec{q}_{i\perp}}{2(2\pi)^3}. \tag{2.53}$$

2.5.2: 2 to 3 amplitude at tree level.

Let us consider first of all the production of just one extra gluon, and at tree level only. The appropriate graphs which contribute to leading power of energy in the Feynman gauge are as shown in figure 2.12.
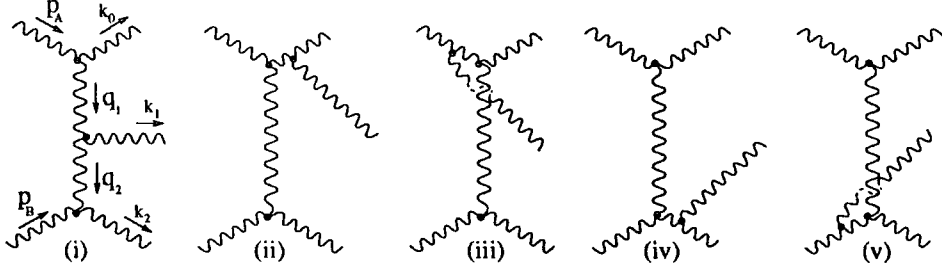
Figure 2.12: Graphs contributing to the $2 \to 3$ amplitude to $LL(s)$ accuracy in the Feynman gauge.

Firstly we deal with graph (i) of the above set. We can make the usual approximations for the upper and lower vertices, which as always are dominated by a single tensor structure, but at the central vertex we must take into account all polarisation flows. Thus we have, leaving the colour structure aside,

$$A_{(i)} \simeq \epsilon_{\mu_A}^{\lambda_A} \epsilon_{\mu_B}^{\lambda_B} \epsilon_{\mu_0}^{\lambda_0 *} \epsilon_{\mu_2}^{\lambda_2 *} \epsilon_{\mu_1}^{\lambda_1 *} \; g^3 \; g^{\mu_A \mu_0} (2p_A)^{\rho} \frac{1}{q_1^2} \Gamma^{\rho \sigma \mu_1}(q_1, -q_2, -k_1) \frac{1}{q_2^2} g^{\mu_B \mu_2}(-2p_B)^{\sigma}.$$

Then with

$$\Gamma^{\rho \eta \mu_1}(q_1, -q_2, -k_1) = (-q_1 - q_2)^{\mu_1} g^{\rho \eta} + (k_1 + q_1)^{\eta} g^{\rho \mu_1} + (q_2 - k_1)^{\rho} g^{\eta \mu_1}$$

$$\simeq (-\alpha_1 p_A + \beta_2 p_B - q_{1\perp} - q_{2\perp})^{\mu_1} g^{\rho \eta} + 2\alpha_1 p_A^{\eta} g^{\rho \mu_1} - 2\beta_2 p_B^{\rho} g^{\eta \mu_1}$$

we find that

$$A_{(i)} \simeq -2s \, (-\delta_{\lambda_A \lambda_0}) g \frac{1}{q_1^2} g \left[\alpha_1 p_A - \beta_2 p_B - (q_{1\perp} + q_{2\perp}) \right]^{\mu_1} \frac{1}{q_2^2} g(-\delta_{\lambda_B \lambda_2}) \epsilon_{\mu_1}^{\lambda_1 *}.$$

Now for the 'Bremsstrahlung' type diagram in graph (ii) of the above set. The corre-

sponding amplitude for this reads as

$$A_{(ii)} \simeq g(-\delta_{\lambda_A \lambda_0})(2p_A)^\rho \frac{g(2p_A)^{\mu_1}}{(k_0 + k_1)^2} \frac{1}{q_2^2} g(-2p_B)_\rho(-\delta_{\lambda_B \lambda_2}) \, \epsilon_{\mu_1}^{\lambda_1 *} \times \text{[Colour structure]}$$

$$= -2s \, g(-\delta_{\lambda_A \lambda_0}) \frac{1}{q_1^2} \, g\left[\frac{q_1^2}{\beta_2 s}(2p_A)\right]^{\mu_1} \frac{1}{q_2^2} \, g(-\delta_{\lambda_B \lambda_2}) \, \epsilon_{\mu_1}^{\lambda_1 *} \times \text{[Colour structure]}$$

Diagram (iii) gives exactly the same contribution apart from a minus sign and a different colour structure. By making use of our favourite colour relation (the Jacobi identity) it is clear that on summing graphs (ii) and (iii) the colour algebra gives an amplitude with the same colour structure as graph (i). Lipatov and collaborators make use of this fact to write the sum of diagrams (ii) and (iii) as an *effective* graph of type (i) with a production vertex for gluon k_1 given by [10]

$$V^{\mu_1} = \frac{q_1^2}{\beta_2 s}(2p_A)^{\mu_1}.$$

The same consideration applies to the pair of graphs (iv) and (v), which when combined give an effective graph with production vertex

$$V^{\mu_1} = \frac{q_2^2}{\alpha_1 s}(-2p_B)^{\mu_1}.$$

So, the amplitude we get from summing over all the graphs in figure 2.12 can represented in the factorised form,

$$A^{[3]}_{2\to3} = -2s \, g(-\delta_{\lambda_A \lambda_0}) \frac{1}{q_1^2} \, g\Gamma^{\mu_1}(q_1, q_2) \frac{1}{q_2^2} \, g(-\delta_{\lambda_B \lambda_2}) \epsilon_{\mu_1}^{\lambda_1 *} \tag{2.54}$$

with the colour structure corresponding to graph (i). The BFKL effective vertex Γ^{μ_1} is,

$$\Gamma^{\mu_1}(q_1, q_2) = \left(\alpha_1 + \frac{2q_1^2}{\beta_2 s}\right) p_A^{\mu_1} - \left(\beta_2 + \frac{2q_2^2}{\alpha_1 s}\right) p_B^{\mu_1} - (q_{1\perp} + q_{2\perp})^{\mu_1}, \tag{2.55}$$

$$= \left(\frac{s_{B1}}{s} + \frac{2q_1^2}{s_{A1}}\right) p_A^{\mu_1} - \left(\frac{s_{A1}}{s} + \frac{2q_2^2}{s_{B1}}\right) p_B^{\mu_1} - (q_{1\perp} + q_{2\perp})^{\mu_1}. \tag{2.56}$$

Thus we have the nice result that the full amplitude for $2 \to 3$ gluons at Born level and leading logarithmic accuracy may be represented by the single diagram in figure 2.13, with a suitably defined vertex given by (2.55).

45
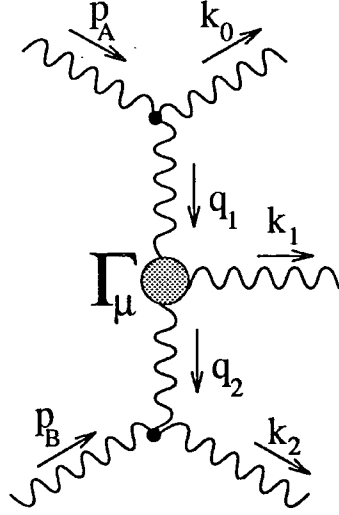
Figure 2.13: A diagrammatic representation of the BFKL form of the $gg \rightarrow ggg$ production amplitude at Born level. The colour structure for the figure is given by the usual colour rules for the respective vertices; however vertex Γ_μ is an effective vertex taking into account graphs with a different topology to the one shown.

As a check of the gauge invariance of the final amplitude, one can show that to the extent to which

$$k_1 \simeq \alpha_1 p_A + \beta_2 p_B + (q_{1\perp} - q_{2\perp})$$

then

$$k_1^\mu \Gamma_\mu(q_1, q_2) = 0$$

as required. This allows us to use the metric tensor $(-g_{\mu_i \mu_i'})$ as the spin sum for the intermediate gluon k_i when we insert the squared amplitude into the unitarity equations. For the product of two of these effective vertices we get,

$$\Gamma_i^{\mu_i}(q_i, q_{i+1})(-g_{\mu_i \mu_i'})\Gamma_i^{\mu_i'}(q_i - q, q_{i+1} - q) = 2\frac{\vec{q}_{i+1}^{\,2}(\vec{q}_i - \vec{q})^2 + \vec{q}_i^{\,2}(\vec{q}_{i+1} - \vec{q})^2}{(\vec{q}_i - \vec{q}_{i+1})^2} - 2\vec{q}^{\,2}. \quad (2.57)$$

This is independent of the α variables, so when we insert this amplitude into the phase space measure (2.52) it gives rise to a logarithmic integration over α_i.

2.5.3: 2 to (2+n) amplitudes at tree level.

The analysis of production amplitudes can be easily extended to the production of a greater number of gluons. In fact, the Born amplitude turns out to be a trivial generalisation of (2.54). This result was derived by Lipatov *et al* in such an elegant manner [11] that I feel compelled to include their analysis here. To tree level at leading logarithmic accuracy they found that the amplitude for $2 \to (2 + n)$ gluons in Multi Regge kinematics is

$$
A_{2\to 2+n} = -2s \; g(-\delta_{\lambda_A \lambda_0}) \; \frac{1}{q_1^2} \; g\Gamma^{\mu_1}(q_1, q_2) \, \epsilon_{\mu_1}^{\lambda_1 *} \; \frac{1}{q_2^2} \; g\Gamma^{\mu_2}(q_2, q_3) \, \epsilon_{\mu_2}^{\lambda_2 *} \; \frac{1}{q_3^2} \cdots
$$
$$
\times \cdots \; g\Gamma^{\mu_n}(q_n, q_{n+1}) \, \epsilon_{\mu_n}^{\lambda_n *} \; \frac{1}{q_{n+1}^2} \; g(-\delta_{\lambda_B \lambda_{n+1}}),
$$

(2.58)

with the colour structure appropriate to the following figure:
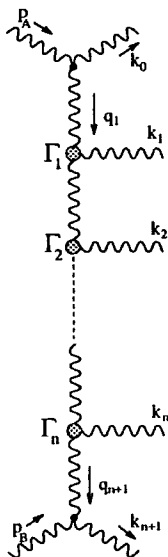
Figure 2.14: The BFKL form of the tree level production amplitude, to leading logarithmic accuracy.

It is relatively easy to show that this is correct. Let us work in the Feynman gauge and partition the Feynman graphs corresponding to the $2 \to (2 + n)$ production process into sets, which have poles in the internal momentum transfers $1/q_i^2$. That is, we define sets $\{\rho_i\}$ such that

$$
\{\rho_i\} = \left\{ \begin{array}{l} \text{The set of all leading tree level Feynman graphs for the} \\ \text{process } 2g \to (2 + n)g \text{ having a pole in } q_i^2 \end{array} \right\}.
$$

All the leading graphs have at least *one* pole in the momentum transfers; otherwise the graphs are suppressed by a power of one or more of the subenergies between emitted

partons. Thus the sets of graphs $\{\rho_i\}$ contain all information about the full amplitude to this accuracy, and the complete set of graphs which must be summed is given by

$$\{\text{Set of graphs giving the full amplitude}\} = \{\rho_1\} \cup \{\rho_2\} \cup \{\rho_3\} \cdots \cup \{\rho_{n+1}\}.$$

Consider those graphs which have a pole in q_m^2. The general form of these graphs are as displayed pictorially in figure 2.15:
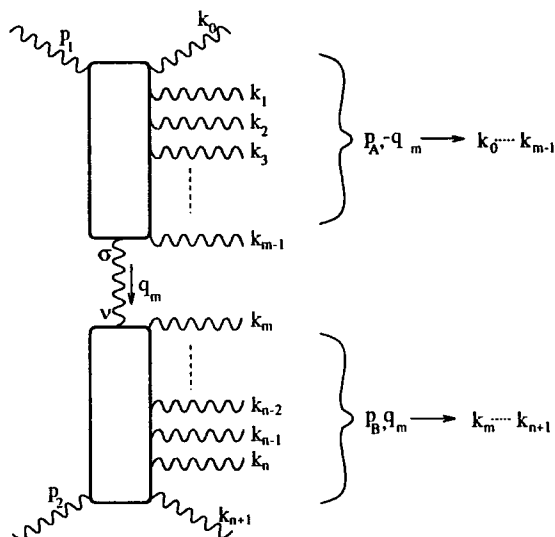
Figure 2.15: The general structure of that class of tree graphs for the amplitude $gg \rightarrow (2+n)g$ which have a pole $\sim 1/q_m^2$.

We can think of the upper blob, to which are connected gluon lines p_A, $-q_m$ and $k_0 \ldots k_{m-1}$, as being essentially the amplitude for a gluon of momentum p_A and one of momentum $-q_m \simeq \beta_m p_B$ (and polarisation also proportional to p_B) scattering to produce the m gluon system $k_0 \ldots k_{m-1}$. A similar consideration applies to the lower box, to which are connected gluons q_m, p_B and $k_m \ldots k_{n+1}$. Thus the amplitude in figure 2.15, which corresponds to the sum of amplitudes from each of the graphs in $\{\rho_m\}$, is given by

$$
\begin{aligned}
\mathcal{M}_{\{\rho_m\}} &= \mathcal{M}_\sigma(p_A, \beta_m p_B \rightarrow k_0 \ldots k_{m-1}) \cdot \frac{g^{\sigma\nu}}{q_m^2} \cdot \mathcal{M}_\nu(\alpha_m p_A, p_B \rightarrow k_m \ldots k_{n+1}) \\
&\simeq \mathcal{M}_\sigma(p_A, \beta_m p_B \rightarrow k_0 \ldots k_{m-1}) \cdot \frac{2p_B^\sigma p_A^\nu}{s q_m^2} \cdot \mathcal{M}_\nu(\alpha_m p_A, p_B \rightarrow k_m \ldots k_{n+1})
\end{aligned}
\tag{2.59}
$$

48

in which we have used the light cone decomposition of the metric tensor,

$$g^{\sigma\nu} \equiv \frac{p_A^\sigma p_B^\nu + p_B^\sigma p_A^\nu}{p_A \cdot p_B} + g_\perp^{\sigma\nu}.$$

There is now the possibility of an inductive proof of (2.58). By using the fact that those parts of the amplitude which have poles in the internal momentum transfers essentially factorise into products of smaller production amplitudes we can see that if the factorised form holds for the n values $n = 0 \ldots n_0$ then it must also hold for $n = n_0 + 1$, since it is the only form of the amplitude consistent with the requirement that the relevant pole terms coincide with (2.59). We have seen that (2.58) holds for $n = 0$ and $n = 1$; so we can prove that (2.58) holds for all integers $n = 0 \ldots \infty$.

One might worry about the gauge invariance of this argument; however the coefficients of the pole terms in $1/q_i^2$ are fixed through q_i-channel unitarity and so are necessarily gauge invariant quantities. In fact, the true method of Lipatov *et al* makes this point explicit by appealing to unitarity and dispersion relations in the momentum transfers q_i[11].

2.5.4: Loop corrections to production amplitudes.

Equation (2.58) shows that the amplitude for gluon production in multi Regge kinematics takes on a very simple form indeed, at the Born level. In fact, the simple factorised form in (2.58) is only slightly modified on accounting for loop corrections: instead of having simple gluons exchanged in the various q_i channels, the radiative corrections have the effect of transforming these gluons into *Reggeons*, as we shall now show.

We know from general considerations of analyticity of the S-matrix something about the singularity structure of production amplitudes[8]. For example, we know that in the physical region the amplitude can have multiple discontinuities only in *non-overlapping* channels. We say that two channels are overlapping if each channel has one or more momentum in common, while no channel is entirely contained within the other. Let us restrict our discussion here to the $2 \to 3$ amplitude, for which the relevant kinematics are displayed in figure 2.16 below.
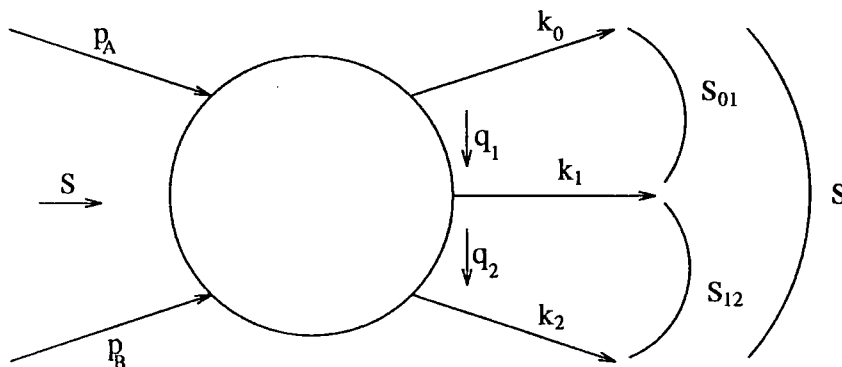
Figure 2.16: The kinematic variables for the $2 \to 3$ production process. The energies s, s_{01}, s_{12} are all greater than zero and so there may be singularities in these variables. The sets of channels $\{s_{01}, s\}$, $\{s_{12}, s\}$ are non-overlapping, whereas $\{s_{01}, s_{12}\}$ overlap and cannot have simultaneous singularities in the physical region.

The production amplitude depends upon scalar products of the various momenta,

$$A_{2 \to 3} = A_{2 \to 3}(s, s_{01}, s_{12}; q_1^2, q_2^2).$$

Our analyticity requirement precludes a simultaneous discontinuity in channels s_{01} and

50

s_{12}. The full amplitude is made up of a sum of terms having the maximal number of simultaneous discontinuities consistent with the requirement for no overlapping channels. The form of this discontinuity structure is shown diagrammatically in figure 2.17.
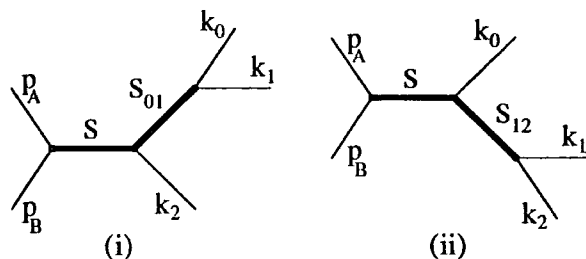
Figure 2.17: The allowable multiple discontinuities of the $2 \rightarrow 3$ production amplitude. Thick lines indicate those channels in which a discontinuity can be present.

It was shown a long time ago (see, eg. [19]) that in the region of multi Regge kinematics the following general representation of a production amplitude holds, which is analogous to the usual decomposition in (complex) angular momentum of a simple $2 \rightarrow 2$ scattering amplitude:

$$A_{2 \rightarrow 3} = \left(\frac{-1}{4i}\right)^2 \int dj_1 dj_2 \left[s^{j_1} s_{12}^{j_2-j_1} \zeta_{j_1} \zeta_{j_2 j_1} F_{12}(j_1, j_2; q_1^2, q_2^2, \eta) \right.$$
$$\left. + s^{j_2} s_{01}^{j_1-j_2} \zeta_{j_2} \zeta_{j_1 j_2} F_{01}(j_1, j_2; q_1^2, q_2^2, \eta) \right]. \tag{2.60}$$

The two terms in the representation correspond to the two sets of multiple discontinuities shown in figure 2.17 together with the crossed channels corresponding to these ($s_{ij} \rightarrow u_{ij}$ and suchlike). In the multi-Regge regime in which $u_{ij} \simeq -s_{ij}$ the effect of these crossed channels is simply to symmetrise or antisymmetrise the amplitude in $s_{ij} \rightarrow -s_{ij}$ depending on the signature associated with each ζ factor. These ζ functions are analogous to the signature factor which gives the phase to a $2 \rightarrow 2$ scattering amplitude. Explicitly, they have the form

$$\zeta_\alpha = \frac{e^{-i\pi\alpha} + \tau}{\sin \pi \alpha}, \tag{2.61}$$

$$\zeta_{\alpha_1 \alpha_2} = \frac{e^{-i\pi(\alpha_1 - \alpha_2)} + \tau_1 \tau_2}{\sin \pi(\alpha_1 - \alpha_2)}, \tag{2.62}$$

and contain all the phase structure of the amplitude: functions F_{01} and F_{12} are real analytic in their arguments. The Toller variable η is defined as

$$\eta \equiv \frac{s_{01}s_{12}}{s} \simeq \alpha_1\beta_2 s = \vec{k}^2 + m^2.$$

So far the representation has been given in its general form. For amplitudes which are dominated by the exchange of a simple Regge pole in each of the q_i-channels the functions F_{01} and F_{12} become

$$F_{01,12}(j_1, j_2; q_1^2, q_2^2, \eta) = \left(\frac{2}{\pi}\right)^2 g(q_1^2) \frac{1}{j_1 - \alpha(q_1^2)} V_{01,12}(j_1, j_2; q_1^2, q_2^2, \eta) \frac{1}{j_2 - \alpha(q_2^2)} g(q_2^2)$$

whereon we get

$$A_{2\to3} = g(q_1^2)\left[s^{\alpha_1}s_{12}^{\alpha_2-\alpha_1}\zeta_{\alpha_1}\zeta_{\alpha_2\alpha_1}V_{12} + s^{\alpha_2}s_{01}^{\alpha_1-\alpha_2}\zeta_{\alpha_2}\zeta_{\alpha_1\alpha_2}V_{01}\right]g(q_2^2),$$

or equivalently

$$A_{2\to3} = g(q_1^2)s_{01}^{\alpha_1}\left[\eta^{-\alpha_1}V_{12}\zeta_{\alpha_1}\zeta_{\alpha_2\alpha_1} + \eta^{-\alpha_2}V_{01}\zeta_{\alpha_2}\zeta_{\alpha_1\alpha_2}\right]s_{12}^{\alpha_2}g(q_2^2).$$

with $\alpha_i \equiv \alpha(q_i^2)$.

Now we can make contact with our previous result on the Reggeisation of the gluon. We found that the octet channel was dominated, to leading log accuracy, by a simple Regge pole of negative signature ($\tau = -1$) with $\alpha(q^2) = 1 + \omega(q^2)$. Now, remembering that η remains finite in the multi Regge limit ($\eta \simeq \vec{k}^2$), then to the accuracy we need we can set

$$\eta^{-\alpha} = \eta^{-(1+\omega)} \simeq \eta^{-1} + \cdots$$

and also the ζ factors simplify,

$$\zeta_\alpha = \frac{e^{-i\pi(1+\omega)} - 1}{\sin\pi(1+\omega)} \simeq \frac{2}{\pi\omega},$$

$$\zeta_{\alpha_2\alpha_1} = \frac{e^{-i\pi(\omega_2-\omega_1)} + 1}{\sin\pi(\omega_2 - \omega_1)} \simeq \frac{2}{\pi(\omega_2 - \omega_1)},$$

and so we get

$$A_{2\to3} = \frac{s_{01}s_{12}}{\eta}g(q_1^2)s_{01}^{\omega_1}\left[\frac{2}{\pi\omega_1}\frac{2}{\pi(\omega_2-\omega_1)}V_{12} - \frac{2}{\pi\omega_2}\frac{2}{\pi(\omega_2-\omega_1)}V_{01}\right]s_{12}^{\omega_2}g(q_2^2)$$

$$= \left(\frac{2}{\pi}\right)^2 sg(q_1^2)s_{01}^{\omega_1}\left(\frac{V_{01}+V_{12}}{\omega_1\omega_2}\right)s_{12}^{\omega_2}g(q_2^2).$$

By redefinitions of the various components of the amplitude this can be cast into a neat factorising form,

$$A_{2\to3} = -2s\Gamma_A(q_1)\frac{s_{01}^{\omega(q_1)}}{q_1^2}\Gamma_1(q_1,q_2)\frac{s_{12}^{\omega(q_2)}}{q_2^2}\Gamma_B(q_2) \qquad (2.63)$$

which should be compared with the Born result (2.54), from which we can pick out the various vertex factors.

By induction we can demonstrate that this factorised form of the amplitude generalises to the production of greater numbers of particles. We thus find that the amplitude for the $2g \to (2+n)g$ process in the multi Regge limit and weak coupling approximation is given by[11]

$$A_{gg\to(2+n)g} = -2s\,g(-\delta_{\lambda_A\lambda_0})\frac{s_{01}^{\omega_1}}{q_1^2}\,g\Gamma^{\mu_1}(q_1,q_2)\epsilon_{\mu_1}^{\lambda_1*}\frac{s_{12}^{\omega_2}}{q_2^2}\,g\Gamma^{\mu_2}(q_2,q_3)\epsilon_{\mu_2}^{\lambda_2*}\frac{s_{23}^{\omega_3}}{q_3^2}\cdots$$

$$\times\cdots g\Gamma^{\mu_n}(q_n,q_{n+1})\epsilon_{\mu_n}^{\lambda_n*}\frac{s_{n,n+1}^{\omega_{n+1}}}{q_{n+1}^2}g(-\delta_{\lambda_B\lambda_{n+1}}). \qquad (2.64)$$

This is a remarkably simple result, considering the complexity of the Feynman graphs which contribute to this process! Evidently there are huge cancellations occuring between the various graphs. The nature of these cancellations can be made clear by an appeal to the Ward identities, as the discussion in reference [20] shows.

The result (2.64) is displayed diagrammatically in the following figure.

53

Figure 2.18:

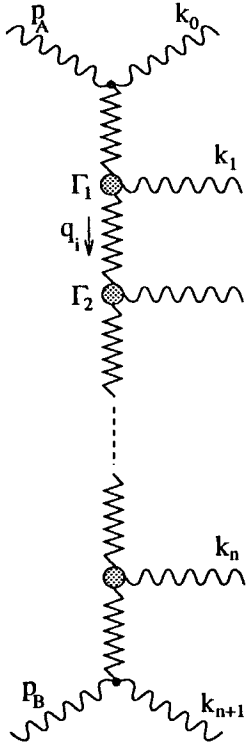The amplitude for the production process $2g \to (2+n)g$ in the multi Regge limit. The colour structure follows the usual colour rules for the diagram, vertices Γ_i are the BFKL effective vertices defined in (2.55), and the jagged lines in the q_i-channels correspond to the exchange of a *reggeised* gluon; thus exchange q_i is associated with a factor

$$\sim \frac{s_{i-1,i}^{\omega(q_i)}}{q_i^2}$$

2.5.5: BFKL equation for the scattering amplitude.

Having now found the production amplitudes to leading logarithmic accuracy, we can insert them into the unitarity equations to calculate the discontinuity of the scattering amplitude. Taking into account the form of the production amplitude given in (2.64) this can be represented diagrammatically as in figure 2.19:
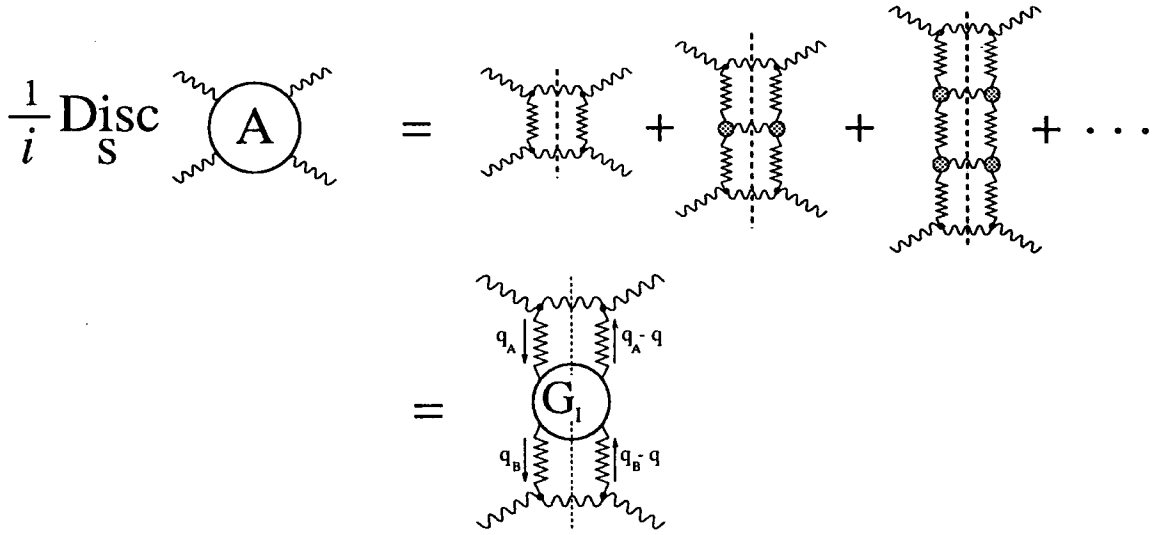
Figure 2.19: The discontinuity of the scattering amplitude written in terms of the amplitudes for the production of multiple gluons, to leading logarithmic accuracy.

This is a representation of the BFKL equation in terms of *ladder diagrams*, although it should be borne in mind that this is only an *effective representation* for the huge numbers of Feynman graphs which actually contribute to the process to leading logarithmic accuracy.

Explicitly, from (2.53) and (2.64) we find that figure 2.19 corresponds to

$$\frac{1}{i}\mathrm{Disc}_s A(s,t) = \sum_{n=0}^{\infty} 8\pi s \int \prod_{i=1}^{n} dy_i \int \prod_{j=1}^{n+1} \frac{d^2\vec{q_i}}{2(2\pi)^3}$$

$$\times g^2 \Gamma_A \Gamma_A' \frac{(s_{01}/\mu^2)^{\omega(\vec{q_1})+\omega(\vec{q_1}-\vec{q})}}{\vec{q_1}^2(\vec{q_1}-\vec{q})^2} g^2 \Gamma_1^\mu(q_1,q_2)(-g_{\mu\mu'})\Gamma_1^{\mu'}(q_1-q,q_2-q)\cdots$$

$$\times \cdots g^2 \Gamma_n^\nu(q_n,q_{n+1})(-g_{\nu\nu'})\Gamma_n^{\nu'}(q_n-q,q_{n+1}-q)\frac{(s_{n,n+1}/\mu^2)^{\omega(\vec{q}_{n+1})+\omega(\vec{q}_{n+1}-\vec{q})}}{\vec{q}_{n+1}^2(\vec{q}_{n+1}-\vec{q})^2}g^2 \Gamma_B \Gamma_B'$$

$$\times \text{ Colour structure.}$$

$$(2.65)$$

Now equation (2.65) as it stands mixes the contributions of the colour octet and singlet

channels to the full scattering amplitude. We need to seperate out the various contributions explicitly, factoring off the overall colour structure as in (2.30). This is easily done using the orthogonality of the various colour tensors and gives for the colour factors with n gluon emission

$$
\begin{aligned}
C_0^{[n]} &= \left(\frac{N_c^2}{N_c^2 - 1} \right) (N_c)^n \equiv C_0^{[0]} (\lambda_0 N_c)^n \\
C_{\bar{8}}^{[n]} &= \frac{N_c}{4} \left(\frac{N_c}{2} \right)^n \equiv C_{\bar{8}}^{[0]} (\lambda_{\bar{8}} N_c)^n
\end{aligned}
\tag{2.66}
$$

so we can associate a factor $\lambda_I N_c$ with each emitted gluon, defining $\lambda_0 = 1$ and $\lambda_{\bar{8}} = 1/2$. Let us simplify our notations for the following formal manipulations by defining

$$
\bar{\omega}_i \equiv \omega(\vec{q}_i) + \omega(\vec{q}_i - \vec{q}),
\tag{2.67}
$$

and

$$
\begin{aligned}
\mathcal{K}_I^i(\vec{q}_{i+1}, \vec{q}_i, \vec{q}) &\equiv (g^2 \lambda_I N_c) \Gamma_i^{\mu_i}(q_i, q_{i+1})(-g_{\mu_i \mu_i'}) \Gamma_i^{\mu_i'}(q_i - q, q_{i+1} - q) \\
&= (g^2 \lambda_I N_c) \left[2 \frac{\vec{q}_{i+1}^2 (\vec{q}_i - \vec{q})^2 + \vec{q}_i^2 (\vec{q}_{i+1} - \vec{q})^2}{(\vec{q}_i - \vec{q}_{i+1})^2} - 2\vec{q}^2. \right]
\end{aligned}
\tag{2.68}
$$

In terms of the rapidity variables y_i the various subenergies become

$$
\begin{aligned}
\log \left(\frac{s_{i-1,i}}{\mu^2} \right) &= \log \left(\frac{\alpha_{i-1} \beta_{i+1} s}{\mu^2} \right) \\
&\simeq y_i - y_{i-1}
\end{aligned}
\tag{2.69}
$$

So, all the factors in (2.65) which depend upon energy become simply

$$
\mu^2 e^\zeta \int_{-\frac{\zeta}{2}}^{\frac{\zeta}{2}} dy_n \int_{-\frac{\zeta}{2}}^{y_n} dy_{n-1} \cdots \int_{-\frac{\zeta}{2}}^{y_2} dy_1 \prod_{i=1}^{n+1} e^{\bar{\omega}_i(y_i - y_{i-1})}.
\tag{2.70}
$$

with $\zeta \equiv \log(s/\mu^2)$. After changing variables from the rapidities y_i to the rapidity differences $\Delta_i \equiv y_i - y_{i-1}$, this can be rewritten as

$$
\mu^2 e^\zeta \prod_{i=1}^{n+1} \int_0^\infty d\Delta_i \, e^{\bar{\omega}_i \Delta_i} . \, \delta \left(\sum_{i=1}^{n+1} \Delta_i - \zeta \right)
\tag{2.71}
$$

56

It is convenient to Mellin transform this expression, similarly to (2.48). Using

$$\frac{1}{\mu^2} \int_{\mu^2}^{\infty} \frac{ds}{s} \left(\frac{s}{\mu^2}\right)^{-j} \cdots = \frac{1}{\mu^2} \int_0^{\infty} d\zeta\, e^{-j\zeta} \cdots$$

then the Mellin transform of (2.71) can be trivially performed to give

$$\prod_{i=1}^{n+1} \frac{1}{j-1-\bar{\omega}_i} = \prod_{i=1}^{n+1} \frac{1}{j-1-\omega(\vec{q}_i)-\omega(\vec{q}_i-\vec{q})}.$$

We see that for every two-Reggeon state in the t-channel of figure 2.19 we can associate the factor

$$\frac{1}{D_i(j,\vec{q}_i,\vec{q})} = \frac{1}{j-1-\omega_i(\vec{q}_i)-\omega(\vec{q}_i-\vec{q})} \frac{1}{\vec{q}_i^{\,2}(\vec{q}_i-\vec{q})^2}.$$

This is a familiar kind of result from the Reggeon calculus ideas of the sixties and seventies[9].

So, we have that

$$\frac{1}{i}\mathrm{Disc}_s\, A_I(j,t) = \sum_{n=0}^{\infty} 8\pi\, C_I^{[0]} \int \prod_{i=1}^{n+1} \frac{d^2\vec{q}_i}{2(2\pi)^3} g^2 \Gamma_A \Gamma_A' \frac{1}{D_1} \mathcal{K}_I^1 \frac{1}{D_2} \cdots \frac{1}{D_{n+1}} g^2 \Gamma_B \Gamma_B'$$

$$= \sum_{n=0}^{\infty} 8\pi C_I^{[0]} \int \prod_{i=0}^{n+1} \frac{d^2\vec{k}_i}{2(2\pi)^3} \left[2(2\pi)^3\delta^2\left(\sum_{i=0}^{n+1}\vec{k}_i\right)\right] g^2\Gamma_A\Gamma_A' \frac{1}{D_1} \prod_{m=1}^{n} \frac{\mathcal{K}_I^m}{D_{m+1}} g^2\Gamma_B\Gamma_B'.$$

$$\tag{2.72}$$

If we rewrite this in the form shown in the second line of figure 2.19, then

$$\frac{1}{i}\mathrm{Disc}_s\, A_I(j,t) = 8\pi C_I^{[0]} \sum_{n=0}^{\infty} \int \frac{d^2\vec{q}_A}{2(2\pi)^3} \int \frac{d^2\vec{q}_B}{2(2\pi)^3} g^2\Gamma_A\Gamma_A'$$

$$\times \left\{ \int \prod_{i=1}^{n} \frac{d^2\vec{k}_i}{2(2\pi)^3} 2(2\pi)^3\delta^2\left(\sum_{i=1}^{n}\vec{k}_i - \vec{q}_A + \vec{q}_B\right) \frac{1}{D_1} \prod_{m=1}^{n} \frac{\mathcal{K}_I^m}{D_{m+1}} \right\} g^2\Gamma_B\Gamma_B' \quad \tag{2.73}$$

$$\equiv 8\pi C_I^{[0]} \int \frac{d^2\vec{q}_A}{2(2\pi)^3} \int \frac{d^2\vec{q}_B}{2(2\pi)^3} g^2\Gamma_A\Gamma_A' \, \mathcal{G}_I(\vec{q}_A,\vec{q}_B,\vec{q};j)\, g^2\Gamma_B\Gamma_B'.$$

where $\mathcal{G}_I$, which can be interpreted as essentially a two reggeon$\rightarrow$ two reggeon Green's

57

function in the old language of the Regge calculus[21], is given by

$$\mathcal{G}_I(\vec{q}_A, \vec{q}_B, \vec{q}; j) = \sum_{n=0}^{\infty} \mathcal{G}_I^{[n]}(\vec{q}_A, \vec{q}_B, \vec{q}; j) \qquad (2.74)$$

with the index n refering to the $(2 + n)$ gluons in the intermediate state in figure 2.19. Comparing (2.74) with (2.73), we get

$$\mathcal{G}_I^{[0]}(\vec{q}_A, \vec{q}_B, \vec{q}; j) = \frac{2(2\pi)^3 \delta^2(\vec{q}_A - \vec{q}_B)}{j - 1 - \bar{\omega}_A} \frac{1}{\vec{q}_A^{\,2}(\vec{q}_A - \vec{q})^2}, \qquad (2.75)$$

and for the higher $\mathcal{G}_I^{[n]}$

$$\begin{aligned}
\mathcal{G}_I^{[n]} &= \int \prod_{i=1}^{n} \frac{d^2\vec{k}_i}{2(2\pi)^3} \, 2(2\pi)^3 \delta^2 \left(\sum_{i=1}^{n} \vec{k}_i - \vec{q}_A + \vec{q}_B \right) \frac{1}{D_1} \prod_{m=1}^{n} \frac{\mathcal{K}_I^m}{D_{m+1}} \\
&= \int \frac{d^2\vec{q}_n}{2(2\pi)^3} \frac{\mathcal{K}_I^n(\vec{q}_B, \vec{q}_n, \vec{q})}{D_B} \left[\int \prod_{i=2}^{n-1} \frac{d^2\vec{q}_i}{2(2\pi)^3} \frac{1}{D_1} \prod_{m=1}^{n-1} \frac{\mathcal{K}_I^m}{D_{m+1}} \right].
\end{aligned} \qquad (2.76)$$

Equation (2.76) shows that the higher $\mathcal{G}_I^{[n]}$ satisfy a recursion relation, due to the ladder structure of figure 2.19. In fact equation (2.76) reads as

$$\begin{aligned}
\mathcal{G}_I^{[n]}(\vec{q}_A, \vec{q}_B, \vec{q}; j) &= \frac{1}{D_B} \int \frac{d^2\vec{q}'}{2(2\pi)^3} \mathcal{K}_I(\vec{q}_B, \vec{q}', \vec{q}) \mathcal{G}_I^{[n-1]}(\vec{q}_A, \vec{q}', \vec{q}; j) \\
&\equiv \frac{1}{D_B} \mathcal{K}_I \odot \mathcal{G}_I^{[n-1]}
\end{aligned} \qquad (2.77)$$

for $n = 1 \ldots \infty$, with $\odot$ standing symbolically for the convolution in transverse momentum q'. Equation (2.77) means that the full $\mathcal{G}_I$ must satisfy an integral equation, in the form of a Bethe-Salpeter equation for the two-Reggeon $\rightarrow$ two-Reggeon Green's function, which is given by

$$\mathcal{G}_I = \mathcal{G}_I^{[0]} + \frac{1}{D_B} \mathcal{K}_I \odot \mathcal{G}_I. \qquad (2.78)$$

This equation is portrayed in figure 2.20, and is the BFKL equation for the scattering amplitude which embodies all leading logarithmic corrections[11, 12, 18, 20].
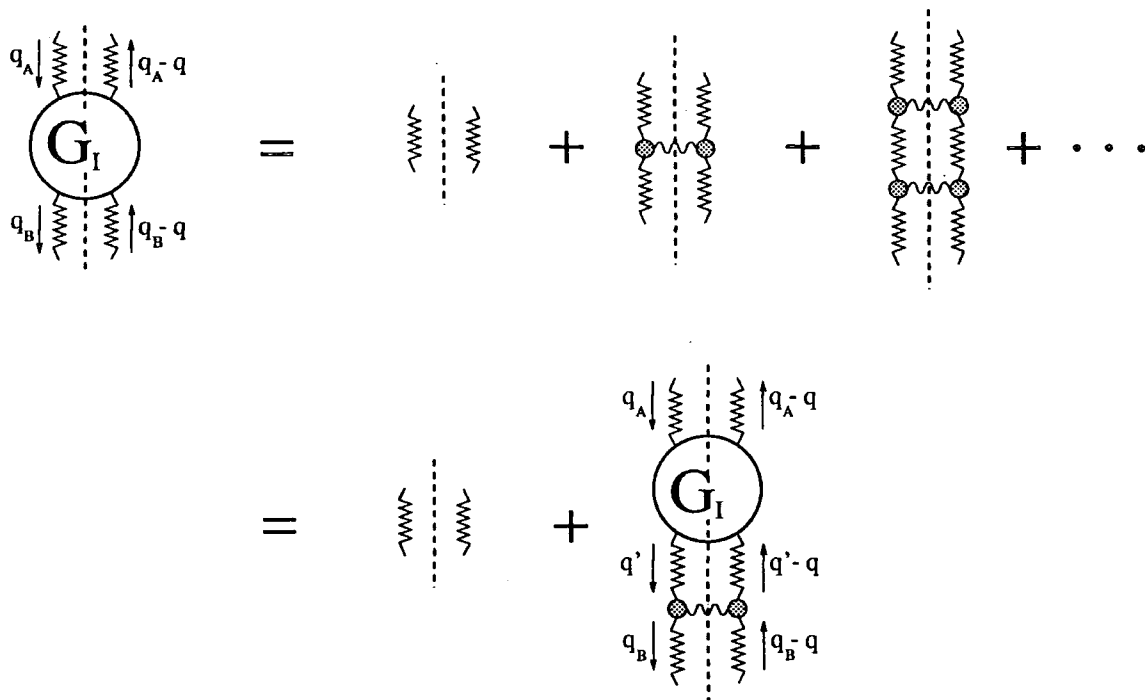
Figure 2.20: Diagrammatic representation of equations (2.74) and (2.78) for the two reggeon→ two reggeon Green's function $\mathcal{G}_I$.

As equation (2.78) stands, it is not clear that the infrared divergences corresponding to real and virtual emission cancel out. This does however happen for the vacuum channel, as we can show by rewriting this equation in a slightly different form. We start by reshuffling terms to give

$$\mathcal{G}_I(\vec{q}_A, \vec{q}_B, \vec{q}; j) = \mathcal{G}_I^{[0]}(\vec{q}_A, \vec{q}_B, \vec{q}; j) \left(\frac{j - 1 - \bar{\omega}_B}{j - 1} \right)$$
$$+ \frac{1}{2(2\pi)^3 (j - 1)} \int d^{2+\epsilon} \vec{q}\,' \frac{\mathcal{K}_I(\vec{q}_B, \vec{q}\,', q)}{\vec{q}_B^2 (\vec{q}_B - \vec{q}\,')^2} \mathcal{G}_I(\vec{q}_A, \vec{q}\,', \vec{q}; j) + \frac{\bar{\omega}_B}{j - 1} \mathcal{G}_I(\vec{q}_A, \vec{q}_B, \vec{q}; j). \tag{2.79}$$

Now, we have that

$$\omega(\vec{q}) = -\frac{g^2 N_c \, \vec{q}^{\,2}}{2(2\pi)^3} \int \frac{d^{2+\epsilon} \vec{q}\,'}{\vec{q}\,'^2 (\vec{q}\,' - \vec{q}\,)^2}$$
$$= -\frac{g^2 N_c \, \vec{q}^{\,2}}{2(2\pi)^3} \int \frac{d^{2+\epsilon} \vec{q}\,'}{\vec{q}\,'^{\,2} + (\vec{q} - \vec{q}\,')^2} \left\{ \frac{1}{\vec{q}\,'^{\,2}} + \frac{1}{(\vec{q} - \vec{q}\,')^2} \right\}$$
$$= -2 \frac{g^2 N_c \, \vec{q}^{\,2}}{2(2\pi)^3} \int \frac{d^{2+\epsilon} \vec{q}\,'}{\vec{q}\,'^{\,2} + (\vec{q} - \vec{q}\,')^2} \frac{1}{(\vec{q} - \vec{q}\,')^2} \tag{2.80}$$

59

so our equation can be rewritten as[11]

$$
\mathcal{G}_I(\vec{q}_A, \vec{q}_B, \vec{q}; j) = \frac{2(2\pi)^3 \delta^2(\vec{q}_A - \vec{q}_B)}{j-1} \frac{1}{\vec{q}_B^2(\vec{q}_B - \vec{q})^2}
$$

$$
+ \frac{N_c g^2}{2(2\pi)^3(j-1)} \int d^{2+\epsilon} \vec{q}' \left\{ 2\lambda_I \left(\frac{\vec{q}_B^2(\vec{q}' - \vec{q})^2 + \vec{q}'^2(\vec{q}_B - \vec{q})^2}{(\vec{q}_B - \vec{q}')^2} - \vec{q}^2 \right) \frac{\mathcal{G}_I(\vec{q}_A, \vec{q}', \vec{q}; j)}{\vec{q}_B^2(\vec{q}_B - \vec{q})^2} \right.
$$

$$
- 2 \left(\frac{\vec{q}_B^2}{\vec{q}'^2 + (\vec{q}_B - \vec{q}')^2} \frac{1}{(\vec{q}_B - \vec{q}')^2} \right) \mathcal{G}_I(\vec{q}_A, \vec{q}_B, \vec{q}; j)
$$

$$
\left. - 2 \left(\frac{(\vec{q}_B - \vec{q})^2}{\vec{q}'^2 + (\vec{q}_B - \vec{q} - \vec{q}')^2} \frac{1}{(\vec{q}_B - \vec{q} - \vec{q}')^2} \right) \mathcal{G}_I(\vec{q}_A, \vec{q}_B, \vec{q}; j) \right\},
$$

and finally

$$
\mathcal{G}_I(\vec{q}_A, \vec{q}_B, \vec{q}; j) = \frac{2(2\pi)^3 \delta^2(\vec{q}_A - \vec{q}_B)}{j-1} \frac{1}{\vec{q}_B^2(\vec{q}_B - \vec{q})^2}
$$

$$
+ \frac{N_c g^2}{2(2\pi)^3(j-1)} \int d^{2+\epsilon} \vec{q}' \left\{ 2\lambda_I \left(\frac{\vec{q}_B^2(\vec{q}' - \vec{q})^2 + \vec{q}'^2(\vec{q}_B - \vec{q})^2}{(\vec{q}_B - \vec{q}')^2} - \vec{q}^2 \right) \frac{\mathcal{G}_I(\vec{q}_A, \vec{q}', \vec{q}; j)}{\vec{q}_B^2(\vec{q}_B - \vec{q})^2} \right.
$$

$$
- 2 \left(\frac{\vec{q}_B^2}{\vec{q}'^2 + (\vec{q}_B - \vec{q}')^2} \frac{1}{(\vec{q}_B - \vec{q}')^2} \right) \mathcal{G}_I(\vec{q}_A, \vec{q}_B, \vec{q}; j)
$$

$$
\left. - 2 \left(\frac{(\vec{q}_B - \vec{q})^2}{(\vec{q}' - \vec{q})^2 + (\vec{q}_B - \vec{q}')^2} \frac{1}{(\vec{q}_B - \vec{q}')^2} \right) \mathcal{G}_I(\vec{q}_A, \vec{q}_B, \vec{q}; j) \right\}.
$$

(2.81)

For the colour singlet channel, for which $\lambda_0 = 1$, any potential divergence as $\vec{q}' \to \vec{q}_B$ now explicitly cancels out between the real and virtual emission terms, so we can now safely take the limit $\epsilon \to 0^+$. For the colour octet channel, for which $\lambda_{\bar{8}} = \frac{1}{2}$, we must find that equation (2.79) reproduces our original result that the gluon lies on a Regge trajectory, in order for the whole analysis to be consistent. If we introduce the function g such that

$$
g(\vec{q}', \vec{q}; j) = \vec{q}'^2(\vec{q}' - \vec{q})^2 \times \int \frac{d^{2+\epsilon} \vec{q}_A}{2(2\pi)^3} \mathcal{G}_I(\vec{q}_A, \vec{q}', \vec{q}; j)
$$

then equation (2.79) becomes

$$
g(\vec{q}_B, \vec{q}; j) = \left(\frac{1}{j-1} \right)
$$

$$
+ \frac{N_c g^2}{j-1} \int \frac{d^{2+\epsilon} \vec{q}'}{2(2\pi)^3} \left[\frac{\vec{q}_B^2}{\vec{q}'^2(\vec{q}_B - \vec{q}')^2} + \frac{(\vec{q}_B - \vec{q})^2}{(\vec{q}' - \vec{q})^2(\vec{q}_B - \vec{q}')^2} - \frac{q^2}{\vec{q}'^2(\vec{q}' - \vec{q})^2} \right] g(\vec{q}', \vec{q}; j)
$$

$$
- \frac{N_c g^2}{j-1} \int \frac{d^{2+\epsilon} \vec{q}'}{2(2\pi)^3} \left[\frac{\vec{q}_B^2}{\vec{q}'^2(\vec{q}_B - \vec{q}')^2} + \frac{(\vec{q}_B - \vec{q})^2}{\vec{q}'^2(\vec{q}_B - \vec{q} - \vec{q}')^2} \right] g(\vec{q}_B, \vec{q}; j)
$$

which has a solution $g(\vec{q}_B, \vec{q}; j) = g(\vec{q}; j)$ independent of $\vec{q}_B$, and given by

$$g(\vec{q}; j) = \frac{1}{j - 1 - \omega(\vec{q})}$$

with $\omega(\vec{q})$ defined exactly as before. This is a highly nontrivial check of the gluon's Reggeisation and demonstrates the self consistency of the formalism[11, 15].

2.6: The model for small-x processes.

2.6.1: Scattering of bound states.

The analysis of the previous sections was devoted to the scattering of the fundamental particles of QCD — quarks and gluons — whereas in reality we deal with initial and final states which are colourless composites of these basic constituents. We shall need further phenomenological assumptions in order to apply the results of the previous sections to these processes.

As always in perturbative QCD, our starting point will be to allow ourselves (the luxury of) a Fock state decomposition of the incoming hadrons into the fundamental fields. Such a decomposition would be valid for the scattering of stable, heavy quark bound states — so called "Onium" states — with mass $M^2 \gg \Lambda^2$ [2]. The characteristic length scale associated with these bound states is much smaller than that associated with lighter states like the proton, $R \sim 1/M \ll R_p$, and hence these states essentially decouple from gluons of small transverse momenta $\vec{k}^2 \sim \Lambda^2$. (In physical terms, such gluons can only resolve the net colour charge of the whole Onium state — that is, zero). Another process would be the scattering of some high energy photon coupling through a very heavy, stable quark-antiquark pair[13]. This is an even cleaner situation since the $Q\bar{Q}$ wavefunction can here be calculated through the pointlike coupling of the photon to the $Q\bar{Q}$ pair.

We shall outline the treatment of $\gamma\gamma$ scattering here since it is of direct relevance to the deep inelastic scattering process. As in section 2.5 we determine the total cross section for $\sigma_{TOT}(\gamma\gamma \to X)$ mediated by heavy quarks by summing over the production amplitudes,

$$\sigma_{TOT}(\gamma\gamma \to X) = \sum_n |A^{[LL]}(\gamma\gamma \to Q\bar{Q} + ng + Q'\bar{Q}')|^2.$$

The crucial observation is that to leading logarithmic accuracy a reggeon couples to only *one* of the partons in the photon [13] (cf. the coulomb gauge analysis in which gluon reggeisation was explicitly due to vertex corrections only). This allows us to apply the BFKL formalism to these processes with only a very minor modification: the full amplitude for n gluon production simply factorises into a product of independent pieces

$$A^{[LL]}(\gamma\gamma \to Q\bar{Q} + ng + Q'\bar{Q}') = \sum_{i=Q,\bar{Q}} \sum_{j=Q',\bar{Q}'} \Psi_i \Psi_j \, A_{ij}^{[LL]}(ij \to ij + ng)$$

with Ψ_i, Ψ_j being the amplitudes to find parton i,j inside the two photons, and $A_{ij}^{[LL]}$ being the fundamental production amplitude calculated in section 2.5. This equation is depicted in the following diagram.
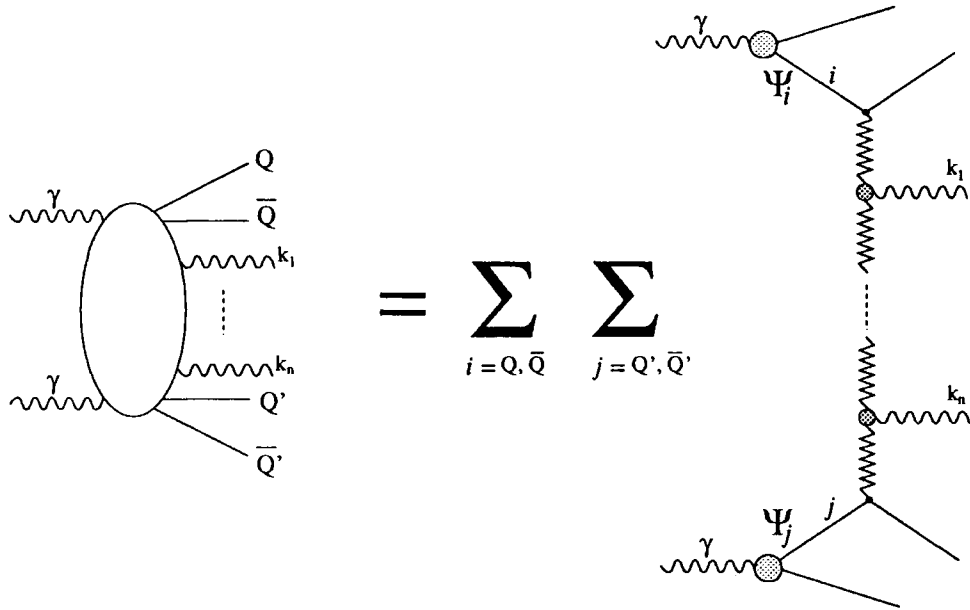
Figure 2.21: Factorisation of the $\gamma\gamma \to Q\bar{Q} + ng + Q'\bar{Q}'$ amplitude to leading logarithmic accuracy.

On squaring this amplitude and summing over the number of produced gluons we find that we can write the following expression for the Mellin transformed discontinuity,

similarly to (2.73),

$$\frac{1}{i}\text{Disc}_s A(\gamma\gamma \to \gamma\gamma) = 8\pi C_0^{[0]} \int \frac{d^2\vec{q}_A}{2(2\pi)^3} \int \frac{d^2\vec{q}_B}{2(2\pi)^3} \Gamma_A(\vec{q}_A,\vec{q};j)\,\mathcal{G}_0(\vec{q}_A,\vec{q}_B,\vec{q};j)\,\Gamma_B(\vec{q}_B,\vec{q};j) \tag{2.82}$$

where the 'impact factors' Γ_A (Γ_B) will now depend on $\vec{q},j$ and $\vec{q}_A$ ($\vec{q}_B$) due to the fact that the incoming photons are not seen as pointlike in QCD.
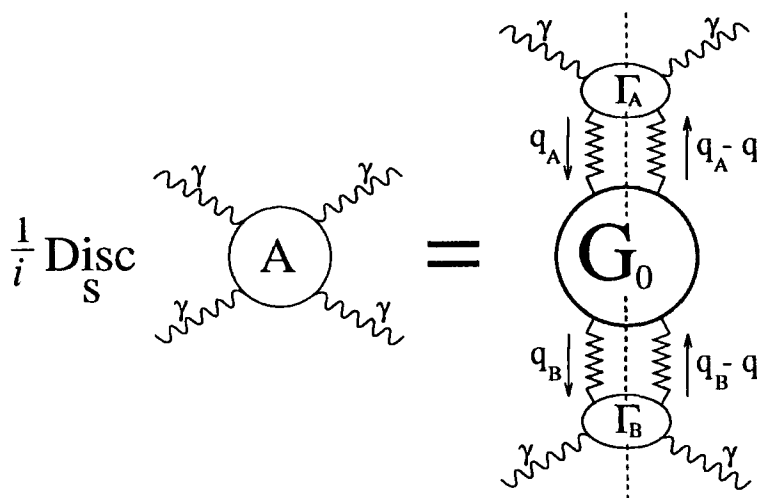
Figure 2.22: Equation (2.82) for the discontinuity of the $\gamma\gamma$ scattering amplitude to leading logarithmic accuracy.

2.6.2: Application to Deep Inelastic scattering.

We assume that the factorisation in (2.82) can be applied to the situation in which one of the photons is replaced by a proton, in which case we get information on the small-x limit of deep inelastic scattering. Inverting (2.82) through to x space we get

$$F_{T,L}(x,Q^2) \sim 8\pi C_0^{[0]} \int_x^1 \frac{dx'}{x'} \int \frac{d^2\vec{k}}{2(2\pi)^3} \int_{x'}^1 \frac{dx_0}{x_0} \int \frac{d^2\vec{k}_0}{2(2\pi)^3}$$

$$\times F_{T,L}^{[0]}(x/x',\vec{k},Q^2)\,\mathcal{G}_0(\vec{k},\vec{k}_0,\vec{q}=0;x'/x_0)\,\mathcal{F}_p(x_0,\vec{k}_0) \tag{2.83}$$

with $\mathcal{F}_p$ and $F_{T,L}^{[0]}$ being the impact factors corresponding to the proton and photon respectively. We note that the transverse momentum integrations run over all areas of phase space, including the area of very small transverse momenta. There are no infrared divergences associated with these integrals though; although $\mathcal{G}_0$ is singular as $\vec{k}_0 \to 0$ ($\vec{k} \to 0$) these singularities are compensated by corresponding zeroes in $\mathcal{F}_p$ and $F_{T,L}$, corresponding to the fact that the proton and photon are globally colourless[13, 15].

There may be no infrared divergence in (2.83), but we see that there will be a contribution to the structure functions from the region of small virtualities where we have no faith in the validity of perturbative QCD. The function $\mathcal{F}_p(x_0, k_0^2)$ corresponds to some 'non-perturbative' input distribution of gluons before perturbative leading logarithmic corrections have been accounted for. We might expect it therefore to have a large component in the infrared region $\vec{k}_0^2 \sim \Lambda^2$. Indeed, in the phenomenology which follows we shall see that the infrared uncertainties associated with (2.83) can be very significant.

Usually equation (2.83) is rewritten in terms of a new function f, defined up to numerical factors by

$$f(x, \vec{k}) \sim \vec{k}^4 \int_x^1 \frac{dx_0}{x_0} \int \frac{d^2 k_0}{2(2\pi)^3} \, \mathcal{G}_0(\vec{k}, \vec{k}_0, \vec{q} = 0; x/x_0) \, \mathcal{F}_p(x_0, \vec{k}_0). \tag{2.84}$$

In terms of this function f the factorisation formula takes the form [22]

$$F_{T,L}(x, Q^2) = \int_x^1 \frac{dx'}{x'} \int \frac{d^2 \vec{k}}{\pi \vec{k}^4} \, F_{T,L}^{[0]}(x/x', \vec{k}, Q^2) \, f(x', \vec{k}), \tag{2.85}$$

with the unintegrated gluon distribution $f(x, \vec{k})$ satisfying the BFKL equation at zero momentum transfer; which, from equation (2.81), is given by

$$f(x, \vec{k}) = f_0(x, \vec{k}) + \frac{N_c \alpha_s}{\pi^2} \int_x^1 \frac{dx'}{x'} \int_0^\infty \frac{d^2 \vec{k}'}{(\vec{k} - \vec{k}')^2} \left(f(x', \vec{k}') \frac{\vec{k}^2}{\vec{k}'^2} - f(x', \vec{k}) \frac{\vec{k}^2}{\vec{k}'^2 + (\vec{k} - \vec{k}')^2)} \right).$$
$$\tag{2.86}$$

2.6.3: Unitarisation corrections : the GLR equation.

The leading logarithmic approximation of the previous section leads to a very steep behaviour of $f(x, \vec{k})$, and hence also $F_2(x, Q^2)$, of the form[12]

$$f(x, \vec{k}) \sim \frac{x^{-\lambda}}{\sqrt{\log(1/x)}}. \tag{2.87}$$

This is in contradiction with the Froissart bound on total cross sections, which means that cross sections cannot grow more rapidly than

$$\sigma_{TOT} \sim \log^2 s$$

in the limit $s \to \infty$. Of course, strictly speaking our leading logarithmic analysis has assumed that $g^2 \log s \sim 1$, and in naively taking the limit $s \to \infty$ with g^2 fixed we violate this requirement.

One simple model to tame the power law growth in (2.87) is set out in [20]. The motivation of the model again seems to lie with Regge calculus ideas. We note that there is no reason in principle why a reggeon cannot be exchanged twice in the same amplitude — indeed, unitarity requires such contributions to exist. So, for example, we must allow for multiple exchange of the BFKL ladders if we are to satisfy unitarity. These multiple exchanges of Reggeons can be accounted for through the Regge calculus, in which the input reggeons and their interactions are derived from QCD by explicit calculations.

The authors of [20] treated the BFKL pomeron of the previous sections as the fundamental, 'input' Reggeon of the theory — by analogy with the ideas in subsection 2.2.2 — and proceeded to compute the triple pomeron coupling. However, we have seen that the 'pomeron' in QCD is not a fundamental object; and in consequence it is not a moving Regge pole but rather corresponds to a fixed cut in the angular momentum plane. Futhermore, it is *super*critical in the sense that the tip of this singularity lies to the right of unity. The theoretical basis of the GLR equation is therefore open to doubt, and in recent papers it has been shown that the approximation of treating the BFKL pomeron as an entity in itself with no Reggeon substructure does overlook some contributions which are of the same order, formally [23]. It may however be a good first approximation to the unitarity corrections.

To derive the GLR equation we consider the deep inelastic scattering process in the limit $Q^2 \to \infty, W^2/Q^2 \to \infty$; a doubly logarithmic limit. The first observation we can make is the dominance of the triple pomeron coupling arising as a consequence of the idea of *enhancement* [24, 20]. This idea first arose in connection with models of the old 'soft' pomeron as a critical Regge pole with trajectory $\alpha(\vec{q}) \simeq 1 - \alpha'\vec{q}^2$. We note that the crucial region of importance in these models is the region $j \sim 1$, where the branch points due to many-pomeron exchange coalesce. Consider the relative contributions of the diagrams in figure 2.23.

(a)   (b)
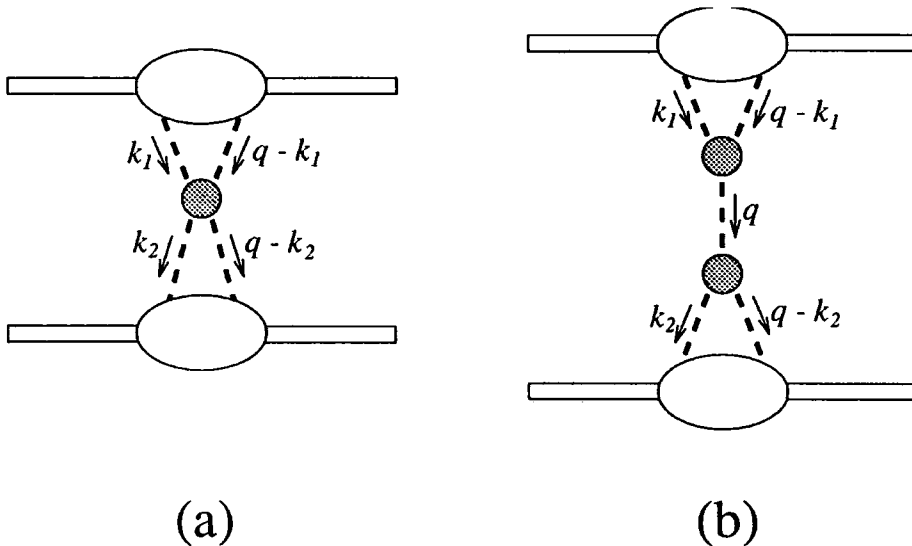
Figure 2.23: Graphs in pomeron field theory, involving

(a) A fundamental four-pomeron vertex,

(b) Three-pomeron vertices.

The contribution from figure 2.23(a) is given by

$$
\int d^2\vec{k}_1 \int d^2\vec{k}_2 N_2(\vec{k}_1, \vec{q}) \frac{1}{j - 1 + \alpha'\vec{k}_1^2 + \alpha'(\vec{k}_1 - \vec{q})^2}
$$
$$
\times \; \gamma_{\mathrm{PP}}^{\mathrm{PP}}(\vec{k}_1, \vec{k}_2, \vec{q}) \frac{1}{j - 1 + \alpha'\vec{k}_2^2 + \alpha'(\vec{k}_2 - \vec{q})^2} N_2(\vec{k}_2, \vec{q})
\tag{2.88}
$$

In the region $j \to 1$, the pomeron propagators give large factors $\sim 1/(j-1)$. This being the case, we can see why the three-pomeron coupling should have a special status as we show on the next diagram 2.23(b). This gives rise to a contribution to the scattering amplitude

of

$$\int d^2 \vec{k}_1 \int d^2 \vec{k}_2 N_2(\vec{k}_1, \vec{q}) \frac{1}{j - 1 + \alpha' \vec{k}_1^2 + \alpha'(\vec{k}_1 - \vec{q})^2} \gamma_{\mathbf{P}}^{\mathbf{PP}}(\vec{k}_1, \vec{q})$$

$$\times \frac{1}{j - 1 + \alpha' \vec{q}^2} \gamma_{\mathbf{PP}}^{\mathbf{P}}(\vec{k}_2, \vec{q}) \frac{1}{j - 1 + \alpha' \vec{k}_2^2 + \alpha'(\vec{k}_2 - \vec{q})^2} N_2(\vec{k}_2, \vec{q})$$

(2.89)

which contains an extra pomeron propagator compared to (2.88), and so is enhanced provided that the three pomeron coupling is not anomalously small.

In fact, in the asymmetric limit we are taking, in which $Q^2 \to \infty$, we can simplify the situation further by realising that a single orientation of the three pomeron vertex dominates in this limit, namely $\gamma_{\mathbf{PP}}^{\mathbf{P}} \gg \gamma_{\mathbf{P}}^{\mathbf{PP}}$. Thus if we write the general expansion of the cross section in terms of pomeron Green's functions

$$\sigma(s) \sim \sum_{n,m=1}^{\infty} N_m(\vec{k}_1 \cdots \vec{k}_m, \vec{q} = 0) \mathcal{G}_n^m(\vec{k}_1 \cdots \vec{k}_m; \vec{l}_1 \cdots \vec{l}_n; \vec{q} = 0) N_n(\vec{l}_1 \cdots \vec{l}_n; \vec{q} = 0) \quad (2.90)$$

we can truncate to just those contributions with a single pomeron coupling to the photon,

$$\sigma(s) \sim \sum_{n=1}^{\infty} N_1(\vec{k}; \vec{q} = 0) \mathcal{G}_n^1(\vec{k}; \vec{l}_1 \cdots \vec{l}_n; \vec{q} = 0) N_n(\vec{l}_1 \cdots \vec{l}_n; \vec{q} = 0) \quad (2.91)$$

where the Green's function $\mathcal{G}_n^1$ is constructed through a sequence of elementary $1 \to 2$ bare pomeron branchings with vertex factor $\gamma_{\mathbf{PP}}^{\mathbf{P}}$. These are the so-called *fan diagrams* of [20].
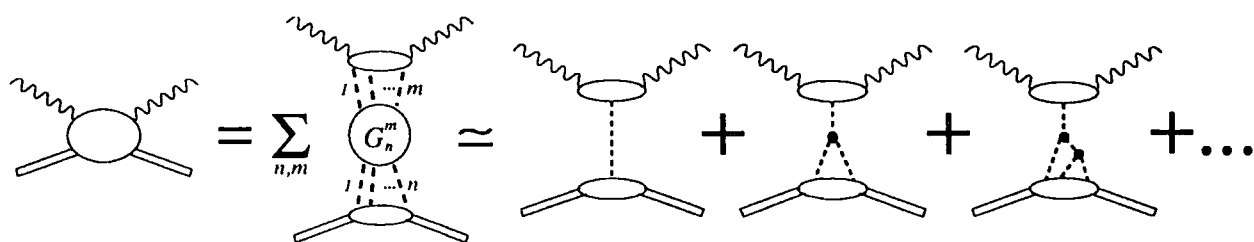
Figure 2.24: The representation of the scattering amplitude in terms of pomeron Green's functions in Reggeon Field Theory. The GLR equation sums the *fan diagrams* constructed purely from the triple-pomeron vertex $\gamma_{\mathbf{PP}}^{\mathbf{P}}$, as shown.

We can rewrite the summation in (2.91) as shown in diagram 2.25.
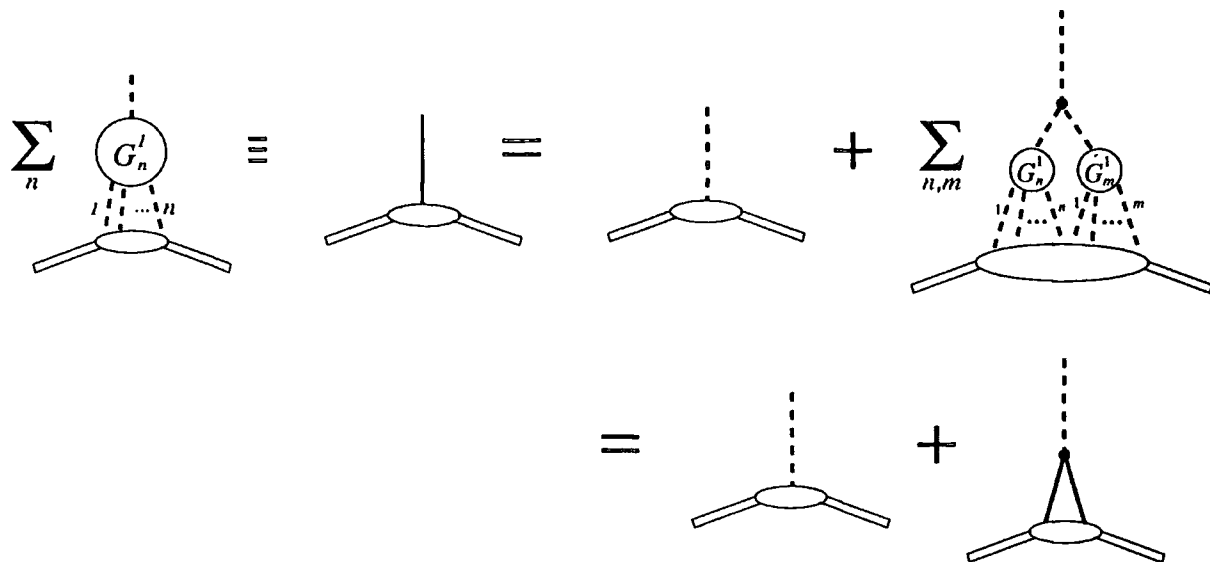
Figure 2.25: The equation for the 'full pomeron'. Broken lines denote the 'bare' pomeron propagator; Full lines denote the 'full' pomeron, defined as shown.

The equation summing these diagrams, along with the BFKL resummation, is given by [20, 25, 26]

$$
f(x, \vec{k}) = f_0(x, \vec{k}) + \frac{N_c \alpha_s}{\pi^2} \int_x^1 \frac{dx'}{x'} \int_0^\infty \frac{d^2 \vec{k}'}{(\vec{k} - \vec{k}')^2} \left(f(x', \vec{k}') \frac{\vec{k}^2}{\vec{k}'^2} - f(x', \vec{k}) \frac{\vec{k}^2}{\vec{k}'^2 + (\vec{k} - \vec{k}')^2)} \right)
$$
$$
- \frac{4\pi^3}{N_c^2 - 1} \left(\frac{\alpha_s N_c}{\pi} \right)^2 \frac{1}{k^2} \int_x^1 \frac{dx'}{x'} x'^2 G^{(2)}(x', \vec{k}^2)
$$

(2.92)

where the two-gluon distribution $G^{(2)}$ is given for a nucleon target by

$$
G^{(2)}(x', \vec{k}^2) \simeq \frac{1}{\frac{4}{3}\pi R^3} \frac{3R}{2} \left[g(x', \vec{k}^2) \right]^2 = \frac{9}{8\pi R^2} \left[g(x', \vec{k}^2) \right]^2,
$$

(2.93)

with, to doubly logarithmic accuracy,

$$
xg(x, Q^2) \simeq \int^{Q^2} \frac{d\vec{k}^2}{\vec{k}^2} f(x, \vec{k}).
$$

(2.94)

The parameter R in (2.93) is the effective transverse radius within which the gluons are distributed in the nucleon. If they are distributed homogeneously across the whole

of the proton, we should have $R \simeq 5$ GeV^{-1}; however there are arguments [27] that the gluons may be concentrated in a smaller region than this, in which case the effective value of R can be smaller, $R \sim 2$ GeV^{-1}.

If we take equation (2.92) at face value, we find that the nonlinear term will tame the power-law growth as $x \to 0$; in fact, ultimately the equation predicts that the unintegrated gluon density will *saturate*, reaching a limiting value independent of x, that is

$$f(x, \vec{k}^2)\Big|_{x \to 0} \to f_{sat}(\vec{k}^2) \sim \frac{\vec{k}^2 R^2}{\alpha_s} \qquad (2.95)$$

However, in reality further corrections beyond (2.92) will have to be considered long before we reach this limiting region.

References.

[1] S. Catani et al, Nucl. Phys. **B361**, 645 (1991)

[2] A.H. Mueller, Nucl. Phys. **B415**, 373 (1994)

[3] G. Marchesini, Univeristy of Milano preprint IFUM 486-FT, November 1994

[4] P.D.B. Collins, *Introduction to Regge theory and high energy scattering*, Cambridge University Press, 1977

[5] R.J. Eden, P.V. Landshoff, D.I. Olive and J.C. Polkinghorne, *The analytic S-matrix*, Cambridge University Press, 1966

[6] A.D. Martin and T.D. Spearman, *Elementary Particle Theory*, North-Holland publishing, 1970

[7] P.V. Landshoff, Proc. XXVII Rencontre de Moriond (Editions Frontieres, 1992, ed. J. Tran Thanh Van); A. Donnachie and P.V. Landshoff, Phys. Lett. **B236** (1992) 227; Z. Phys. **C61**, 139 (1994)

[8] A.R. White, Int. J. Mod. Phys. **A6**, 1859 (1991); Int. J. Mod. Phys. **A8**, 4755 (1993)

[9] *Regge Theory of low-p_t Hadronic Interactions*, edited by L. Caneschi, North-Holland 1989

[10] L.N. Lipatov, Sov. J. Nucl. Phys. **23**, 338 (1976)

[11] E.A. Kuraev, L.N. Lipatov and V.S. Fadin, Sov. Phys. JETP **44**, 443 (1976)

[12] E.A. Kuraev, L.N. Lipatov and V.S. Fadin, Sov. Phys. JETP **45**, 199 (1977)

[13] Ya. Ya. Balitskii and L.N. Lipatov, Sov. J. Nucl. Phys. **28**, 822 (1978)

[14] T. Muta, *Foundations of Quantum Chromodynamics*, World Scientific, 1987

[15] J. Bartels, Nucl. Phys. **B151**, 293 (1979); Nucl. Phys. **B175**, 365 (1980)

[16] H. Cheng and C.Y. Lo, Phys. Rev. **D15**, 2959 (1977)

[17] A.L. Mason, Nucl. Phys. **B117**, 493 (1976); Nucl. Phys. **B120**, 275 (1977)

[18] T. Jaroszewicz, Acta Physica Polonica **B11**, 965 (1980)

[19] J. Bartels, Phys. Rev. **D11**, 2977 (1975) and **D11**, 2989 (1975)

[20] L.V. Gribov, E.M. Levin and M.G. Ryskin, Phys. Rep. **100**, 1 (1983)

[21] J.B. Bronzan and R.L. Sugar, Phys. Rev. **D17**, 585 (1978)

[22] S. Catani, M. Ciafaloni and F. Hautmann, Phys. Lett. **B242**, 91 (1990); Nucl. Phys. **B366**, 135 (1991); S. Catani, M. Ciafaloni and F. Hautmann, Proc. of the Workshop "Physics at HERA", DESY, Hamburg, Germany, October 1992, eds. W. Buchmüller and G. Ingelman, Vol. 2 (1992) p690

[23] J. Bartels and M. Wüsthoff, Z. Phys. **C66**, 157 (1995); J. Bartels, Phys. Lett. **B298**, 204 (1993)

[24] V.N. Gribov, Sov. Phys. JETP **26**, 414 (1968)

[25] A.H. Mueller and J. Qiu, Nucl. Phys. **B268**, 427 (1986)

[26] E.M. Levin, *Orsay lectures on low-x deep inelastic scattering*, LPTHE preprint 91/02 (1991)

[27] V.M. Braun *et al*, Phys. Lett. **B302**, 291 (1993)

3

Implications of the BFKL formalism for structure functions.

3.1: Introduction

With the advent of the DESY electron-proton collider HERA, attention has been focussed upon the behaviour of the structure functions $F_i(x, Q^2)$ for deep inelastic scattering in the small-x region, typically $x \sim 10^{-3}$ and $Q^2 \sim 10$ GeV^2. This is a region hitherto unexplored by experiment in which novel effects may be expected to occur. Perturbative QCD predicts, via a leading $\log(1/x)$ summation of multiple soft gluon emissions, that the structure functions will have a singular $x^{-\lambda}$ behaviour at small x, with λ possibly as large as 0.5. The summation is carried out by the BFKL equation [1-10] and the resulting behaviour is therefore said to arise from the BFKL (or bare QCD) pomeron, which has intercept $\alpha_P = 1 + \lambda$ considerably above unity. Ultimately, with decreasing x, the singular behaviour must be suppressed by shadowing corrections and eventually by non-perturbative effects.

Prior to the results from HERA, with experiment not having imparted its guidance, the behaviour as $x \to 0$ had been the subject of much speculation. Parton distributions had to be extrapolated towards small x in various ways depending on the prevailing theoretical prejudice. Figure 3.1 gives some indication of the wide range of behaviour which had to be considered in sets of parton distributions available before HERA came on line [11]. In line with Regge phenomenology of total hadronic cross sections, the D_0 set of partons showed a fairly 'flat' behaviour, $F_2(x, Q_0^2) \sim x^{-0.08}$ for Q_0^2 of a few GeV^2. By contrast the D_- set of partons displayed the very steep behaviour $F_2(x, Q_0^2) \sim x^{-0.5}$ motivated by the BFKL formalism. Both sets of partons D_-, D_0 described the whole range of existing precise deep

inelastic data equally well.
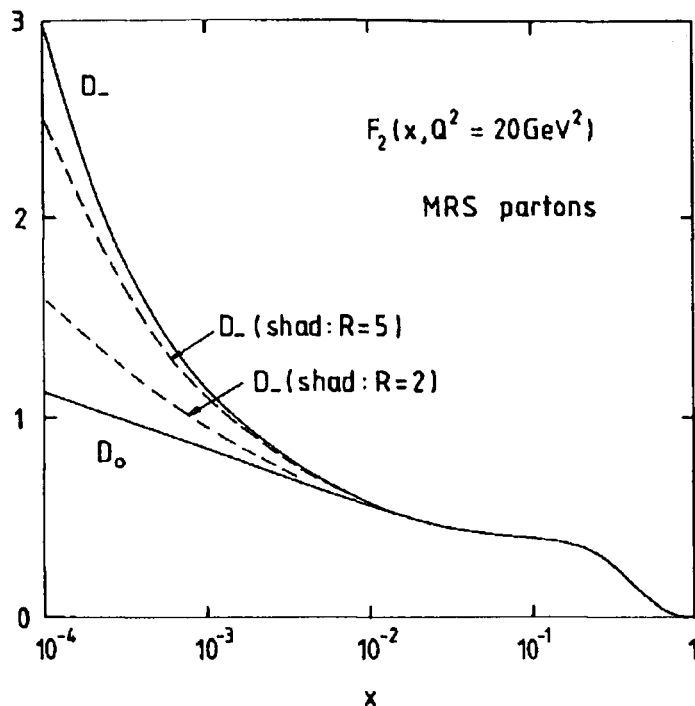
Figure 3.1: Extrapolations of F_2 at $Q^2 = 20$ GeV^2 to small x based on MRS partons [11]. Sets D_- and D_0 have xg, xq_{sea} "starting" distributions (that is at $Q_0^2 = 4$ GeV^2) which behave respectively as $x^{-\frac{1}{2}}$ and x^0 at small x. The dashed curves show the effect of conventional parton shadowing with $R = 5$ GeV^{-1} together with the more extreme "hot spot" shadowing with $R = 2$ GeV^{-1}.

The dashed curves in figure 3.1, obtained from steep parton distributions which contain shadowing corrections, show that the screening effects were expected to be small in this x region if the gluons are distributed evenly across the proton. We emphasize that the small x predictions shown in figure 3.1 are simply extrapolations of parametric forms determined from data which, apart from one or two measurements, populate the $x \gtrsim 0.05$ region. A missing ingredient is any constraint on the size of the BFKL component. The gluon distribution has not been required to satisfy the BFKL equation at small x; simply a leading $x^{-\frac{1}{2}}$ behaviour has been imposed on the "starting" distribution at some $Q^2 = Q_0^2$, and also on the sea quark distributions which are themselves driven by the gluon. We should add, though, that it was subsequently shown that the form of the gluon was quite compatible with that obtained by numerical solution of the BFKL equation [12].

Here we present more quantitative predictions of the behaviour of $F_2(x, Q^2)$, and the longitudinal structure function $F_L(x, Q^2)$, as $x \to 0$. In the previous chapter we outlined a theoretical framework to analyse this limit. We found that the leading logarithmic contribution can be represented in the form of effective ladder diagrams, with the virtual radiative corrections leading to gluon Reggeisation [1- 6] (or equivalently to the introduction of a non-Sudakov form factor [7- 9]). These ladder diagrams are a universal feature of all small-x processes driven by the gluon. For instance they occur in the perturbative QCD description of the structure functions F_2 and F_L, heavy quark-pair and J/ψ production, prompt photon production, deep inelastic diffraction and deep inelastic events containing an identified forward jet. As a result of this BFKL resummation, the gluon distribution develops a sharp $x^{-\lambda}$ growth as x decreases, with $\lambda \sim 0.5$. This singular behaviour of the gluon should manifest itself in all the processes listed above since they incorporate the universal gluon ladder. In particular, since the density of gluons increases rapidly with decreasing x the sea quark distributions are increasingly driven by the gluon distribution, via $g \to q\bar{q}$. This component may be calculated in perturbative QCD. The relevant diagram is shown in figure 3.2.
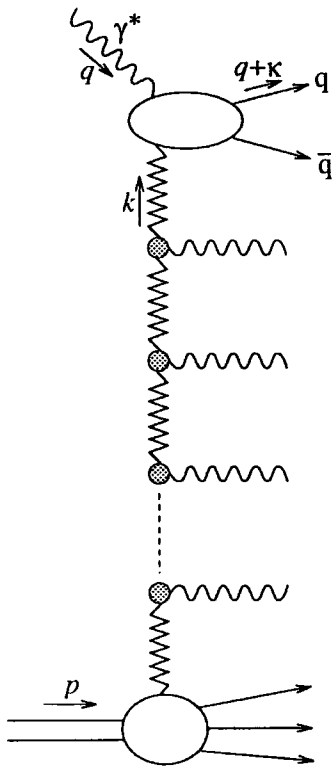
Figure 3.2:

Diagrammatic representation of a gluon "ladder" contribution to the deep-inelastic structure functions of the proton. q, κ, k and p denote the particle 4-momenta.

This contribution to the (transverse and longitudinal) deep inelastic structure functions

73

may therefore be written in the factorizable form [13,14]

$$F_{T,L}(x,Q^2) \;=\; \int_x^1 \frac{dz}{z} \int \frac{d\vec{k}^2}{\vec{k}^4} f\left(x/z, \vec{k}^2\right) F_{T,L}^{(0)}(z, \vec{k}^2, Q^2) \qquad (3.1)$$

see figure 3.3, where x/z is the longitudinal momentum fraction carried by the gluon which dissociates into the $q\bar{q}$ pair. The function $F^{(0)}$ denotes the quark box (and crossed box) approximation to the photon-gluon subprocess shown in the upper part of figure 3.3. In other words $F^{(0)}$, or rather to be dimensionally correct $F^{(0)}/\vec{k}^2$, may be regarded as the structure function of a gluon of approximate virtuality $\vec{k}^2$. The gluon density function f in (3.1) denotes the sum of the 'ladder diagrams' shown symbolically in the lower part of figure 3.3.
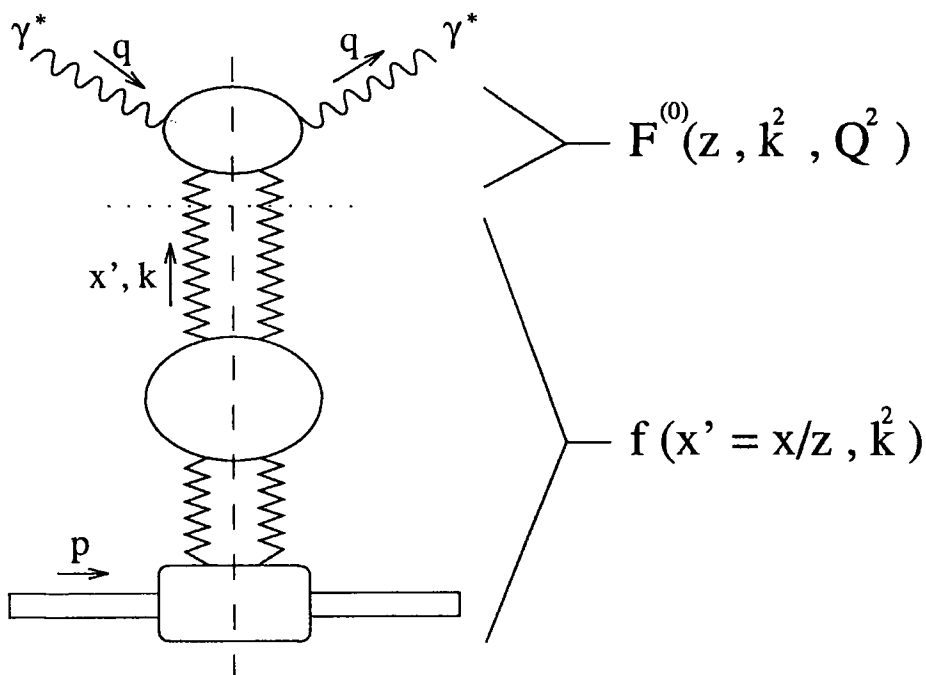
Figure 3.3: Diagrammatic representation of the factorization formula of eq. (3.1).

In the leading $\log(1/x)$ approximation, f is given as the solution of the BFKL equation; for this reason it is the "unintegrated" gluon density

$$f(x, \vec{k}^2) \;\simeq\; \left.\frac{\partial(xg(x, Q^2))}{\partial \ell n Q^2}\right|_{Q^2 = \vec{k}^2 \gg \Lambda^2}. \qquad (3.2)$$

The function $g(x, Q^2)$, which enters (3.2), is the traditional gluon distribution whose Q^2 evolution is controlled by the Altarelli-Parisi equations and whose form is determined by the parton analyses of the deep-inelastic structure function data. It is therefore instructive to see how the general factorizable form (3.1) reduces to the Altarelli-Parisi evolution of $q\bar{q}$ radiation from a gluon. In the Altarelli-Parisi treatment in the leading log Q^2 approximation the integrations over the transverse momenta are dominated by the contributions from the strongly ordered configuration $\vec{k}^2 \ll \vec{\kappa}^2 \ll Q^2$, where the momenta k, κ and q are shown on figure 3.2 and where $Q^2 \equiv -q^2$. In this limit there is no contribution to F_L and so we need only consider $F_2(x, Q^2)$. If we keep only the strongly-ordered contribution and we recall that z is the momentum fraction of the gluon carried by the quark (or antiquark) which is struck by the photon, then $F^{(0)}$ of (3.1) is given by

$$F_2^{(0)}(z, \vec{k}^2, Q^2)/\vec{k}^2 \;=\; \int_{k^2}^{Q^2} \frac{d\vec{\kappa}^2}{\vec{\kappa}^2} 2 \sum_q e_q^2 \frac{\alpha_s(\vec{\kappa}^2)}{2\pi} z P_{qg}(z) \qquad (3.3)$$

where P_{qg} is the Altarelli-Parisi splitting function. Thus (3.1) becomes

$$F_2(x, Q^2) \;=\; \int_x^1 dz \int^{Q^2} \frac{d\vec{\kappa}^2}{\vec{\kappa}^2} \int^{\vec{\kappa}^2} \frac{d\vec{k}^2}{\vec{k}^2} f\left(\frac{x}{z}, \vec{k}^2\right) 2 \sum_q e_q^2 \frac{\alpha_s(\vec{\kappa}^2)}{2\pi} P_{qg}(z) \qquad (3.4)$$

and hence, using (3.2), we have

$$\frac{\partial F_2}{\partial \ell n Q^2} \;=\; 2 \sum_q x e_q^2 \frac{\alpha_s(Q^2)}{2\pi} \int_x^1 \frac{dz}{z} P_{qg}(z) g\left(\frac{x}{z}, Q^2\right), \qquad (3.5)$$

that is the conventional Altarelli-Parisi evolution of F_2 driven by $g \to q\bar{q}$.

There are at least two reasons why the leading log Q^2 evolution, (3.5), is inadequate in the small x region. The first is due to the BFKL effects and the second arises from shadowing. We discuss these effects in turn. A crucial observation is that it is the dominance of the region of strong ordering of the transverse momenta which leads to the nested logarithmic integrations of (3.4). However at small x where the leading $\log(1/x)$ terms dominate it is important to retain the full Q^2 dependence and not just the leading log Q^2 terms. This is accomplished by the BFKL equation for the unintegrated distribution f which sums the ladder diagrams over the full phase space of the transverse momenta and not simply the strongly ordered part. In the case of fixed α_s the BFKL equation may be approximately solved analytically. The leading small x behaviour is found to be

$$f(x, \vec{k}^2) \;\; \propto \;\; (\vec{k}^2)^{\frac{1}{2}} \frac{x^{-\lambda}}{\sqrt{\ell n(1/x)}} \left[1 + O\left(\frac{1}{\ell n(1/x)}\right) \right] \tag{3.6}$$

where

$$\lambda \;\; = \;\; \frac{3\alpha_s}{\pi} 4\ell n 2. \tag{3.7}$$

We note, in particular, the factor $(\vec{k}^2)^{\frac{1}{2}}$ which may be traced to the anomalous dimension having magnitude $\frac{1}{2}$ [1-10]. Due to this factor the region of strongly ordered transverse momenta is no longer dominant. The integrals are no longer of logarithmic $d\vec{k}^2/\vec{k}^2$ form and we must use the exact $\vec{k}^2$ dependence of $F^{(0)}$ as well as integrating over the full region of phase space of the transverse momenta. This has been found to have profound effects on the predictions for heavy quark photo- and electro-production [13]. (The cross sections can increase by a factor of 3 when the effects of shifted anomalous dimension are included.)

As x decreases, the singular $x^{-\lambda}$ behaviour of f will eventually be tamed by shadowing effects. These stop f growing with decreasing x and lead to an x independent saturation limit which grows linearly with $\vec{k}^2$ [6], that is

$$f_{sat}(x, \vec{k}^2) \;\; \sim \;\; R^2 \vec{k}^2 \tag{3.8}$$

where the radius R specifies the (transverse) region in which the gluons are concentrated

within the proton. As before, the $\vec{k}^2$ behaviour requires that we must integrate over the full domain of the transverse momenta.

The above two formulae, (3.6) and (3.8), overestimate their respective effects. The numerical solution of the BFKL equation shows, particularly when the effects of the running of α_s are included, that the approximate analytic form (3.6) considerably overestimates the actual solution [15]. Secondly, the numerical solution of the BFKL equation with the non-linear shadowing contribution included shows that the saturation limit (3.8) is approached rather slowly and that it is irrelevant for the $x \gtrsim 10^{-4}$ region which will be probed at HERA [12]. In particular we are able to obtain more definitive estimates of the size of the shadowing corrections than hitherto.

It is illuminating to consider the full content of the factorization formula (3.1) for $F_{T,L}(x, Q^2)$. The formula, with the exact functions $F_{T,L}^{(0)}$ arising from the quark box and crossed box diagrams, does not describe just photon-gluon interactions in which the exchanged quark and gluon are constituents of the proton. For sufficiently small Q^2, the formula also describes the situation in which the exchanged quark is better regarded as a constituent of the photon; that is when the quark lies in the photon (rather than the proton) hemisphere and when $\vec{k}^2 \gg \vec{\kappa}^2 \gtrsim Q^2$, where the momenta are defined in figure 3.2. These kinematic conditions could also apply to the gluon and then figure 3.2 would describe a semi-hard interaction between this gluon constituent of the photon and a gluon constituent of the proton (the next gluon down the chain with $\vec{k}'^2 \gg \vec{k}^2 \gtrsim Q^2$). Since we shall integrate over the full momentum phase space of the outgoing particles in figure 3.2 all these contributions are automatically included. Formula (3.1) does not, however, include the vector-meson-dominance component of the photon.

The primary purpose of this chapter is to use (3.1) to estimate the deep-inelastic structure functions F_2 and F_L at small x using the exact solution f of the BFKL equation (with and without the shadowing term) and using the exact forms of the photon-gluon couplings, $F_{T,L}^{(0)}$. In this way we are able to make predictions for the contribution to F_2 and F_L in the small x region arising from the leading $\log(1/x)$ gluon summation, which in turn drives the sea quark contributions via $g \to q\bar{q}$. At this point however we should note that the transverse integrals in (3.1) and the BFKL equation itself extend down into the region of small transverse momenta, $\vec{k}^2 < 1, 2 \text{ GeV}^2$, where we would have doubts about

the reliability of perturbative QCD. As a first approximation, we will impose a cut-off on the transverse momenta of the emitted gluons along the ladder, requiring $\vec{k}^2 > k_0^2$ in order to stay within the perturbative region. On top of this perturbative contribution to the structure functions we will have to add a contribution from the region of small virtualities which we have ignored. We estimate this remaining ("background") contribution to F_2 using phenomenologically known structure functions (and parton distributions) at larger x. The background contributions to F_2 and F_L turn out to be approximately independent of x in the small x region, and to be small for F_L. The resulting predictions, however, are subject to several ambiguities: the choice of the infra-red cut-off, the size of the shadowing radius parameter R, etc. We quantify these uncertainties in the numerical sections 3.4 and 3.5.

It is worth mentioning that there are dynamical calculations of parton distributions [16] in which the sea quark and gluon distributions at large scales are obtained by evolving with Altarelli-Parisi equations from "valence" quark (and "valence" gluon) distributions at some (very) low Q^2 scale. A similar attempt to calculate the gluon and sea quark distributions entirely within perturbative QCD is presented in ref. [17]. These calculations are ambitious and speculative in that they stretch the application of pertubative QCD to very low scales, but since they do not take into account the BFKL leading $\log(1/x)$ terms implied by perturbative QCD they do not generate the complete small x behaviour of F_2 and F_L. The validity of using perturbative QCD to dynamically generate parton distributions from valence-like input at low Q^2 has recently been questioned [18]; see also the discussion in subsection 1.2.2.

3.2: The photon-gluon impact factor.

We consider the process $\gamma^* g \to g q \bar{q}$, from which the impact factor $F^{(0)}(z, \vec{k}^2, Q^2)$ can be extracted. The relevant diagrams are shown the following figure.
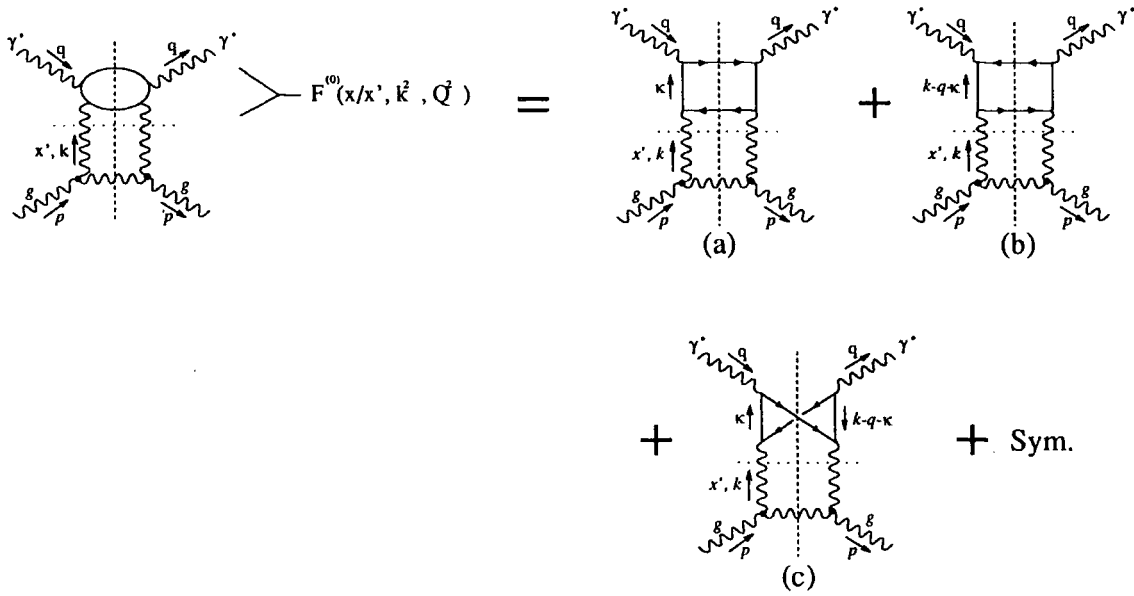
Figure 3.4: The diagrams contributing to the process $\gamma^* g \to g q \bar{q}$ in the high energy region $s \to \infty$.

The $\gamma^* g$ centre of mass energy for this process is given by $s = (p + q)^2 \simeq Q^2/x$ for small x. Let us note in passing, that in the limit $s \to \infty$ these diagrams actually dominate over the Born diagrams by a *power of energy*. This is due to the fact that these diagrams have spin-1 gluons in the t-channel, rather than the spin-$\frac{1}{2}$ fermions of the lowest order graphs, and is an indication of the problems that one is faced with in the high energy (small-x) region.

The contribution from diagram (a) to the inelastic scattering tensor $W_{\mu\nu}$ is given by the normal Feynman rules supplemented by the conventional factor of $1/2\pi$ in the definition of $W_{\mu\nu}$, see (1.3) and the figure following it. So diagram (a) yields

$$W_{\mu\nu}^{(a)} = \frac{1}{2\pi} \sum_q e_q^2 (g^2 T_F)(g^2 C_A)$$

$$\times \int \frac{d^4\kappa}{(2\pi)^4} \int \frac{d^4k}{(2\pi)^4} \frac{N_{\mu\nu}}{k^4\kappa^4} 2\pi\delta((p-k)^2) \, 2\pi\delta((\kappa-k)^2 - m^2) \, 2\pi\delta((\kappa+q)^2 - m^2)$$

(3.9)

with the numerator factor

$$N_{\mu\nu} \simeq 4Tr\left[\gamma_\mu(\not{k}+\not{q}+m)\gamma_\nu(\not{k}+m)\not{p}(\not{k}-\not{\kappa}-m)\not{p}(\not{\kappa}+m)\right].$$

(3.10)

Let us introduce the lightlike vector q', where

$$q_\mu = q'_\mu - xp_\mu$$

and decompose four vectors κ, k into the usual Sudakov parameters,

$$\kappa^\mu = \alpha p^\mu - \beta q'^\mu + \kappa_\perp^\mu$$
$$k^\mu = a p^\mu - b q'^\mu + k_\perp^\mu$$

(3.11)

in terms of which the mass shell conditions become

$$(p-k)^2 = (1-a)bs - \vec{k}^2 = 0,$$

(3.12)

$$(k-\kappa)^2 - m^2 = (a-\alpha)(\beta-b)s - (\vec{\kappa}-\vec{k})^2 - m^2 = 0,$$

(3.13)

$$(\kappa+q)^2 = (\alpha-x)(1-\beta)s - \vec{\kappa}^2 - m^2 = 0.$$

(3.14)

We use these relations to fix b, a and α respectively. Having done this, we get

$$W_{\mu\nu} \simeq \sum_q e_q^2 \frac{\alpha_s T_F}{4s} \int \frac{d\beta}{\beta(1-\beta)} \int \frac{d^2\vec{\kappa}}{(2\pi)^2} \int \frac{d^2\vec{k}}{\pi\vec{k}^4} \left[\frac{N_{\mu\nu}}{\kappa^4}\right] \left(\frac{\alpha_s C_A}{\pi}\right).$$

(3.15)

The term $\frac{\alpha_s C_A}{\pi}$ corresponds to the term $f(x/z, \vec{k}^2)$ in the factorisation formula (3.1). The integration over z is here implicitly included in the integral over β and κ. The propagator

k^2 is well approximated by $(-\vec{k}^2)$ for small-x, while a little algebra shows that the $\kappa^2 - m^2$ propagator can be rewritten as

$$\kappa^2 - m^2 = -\alpha\beta s - \vec{\kappa}^2 - m^2 = -\left[\frac{\beta(1-\beta)Q^2 + \vec{\kappa}^2 + m^2}{(1-\beta)}\right] \equiv -\frac{D_1}{(1-\beta)}.$$

To evaluate $N_{\mu\nu}$ we make use of the master formulae,

$$Tr\left[\gamma^{\mu_1}\gamma^{\mu_2}\cdots\gamma^{\mu_n}\right] = g^{\mu_1\mu_2}Tr\left[\gamma^{\mu_3}\gamma^{\mu_4}\cdots\gamma^{\mu_n}\right] - g^{\mu_1\mu_3}Tr\left[\gamma^{\mu_2}\gamma^{\mu_4}\cdots\gamma^{\mu_n}\right] + \cdots$$
$$\cdots + (-1)^n g^{\mu_1\mu_n}Tr\left[\gamma^{\mu_2}\gamma^{\mu_3}\cdots\gamma^{\mu_{n-1}}\right]$$

for n even and

$$Tr\left[\gamma^{\mu_1}\gamma^{\mu_2}\cdots\gamma^{\mu_n}\right] = 0$$

for n odd. We can decompose $W_{\mu\nu}$ in terms of the functions F_T, F_L defined as in (1.4) by noting that

$$F_L(x, Q^2) = p^\mu p^\nu W_{\mu\nu} \times \frac{xQ^2}{(p.q)^2},$$
$$F_T(x, Q^2) = -\frac{x}{2}\, g_\perp^{\mu\nu}\, W_{\mu\nu}. \tag{3.16}$$

This observation simplifies the calculation of the trace factor since it shows that we do not need to know the terms in $N_{\mu\nu}$ which are proportional to p_μ and p_ν in order to be able to extract F_T and F_L. If we look at the tensor structures which can appear in (3.10), we see that the only ones which give a nonzero result under the projections in (3.16) are

$$N_{\mu\nu} = C_1\, g_{\mu\nu} + C_2\left[(\kappa + q)_\mu \kappa_\nu + \kappa_\mu(\kappa + q)_\nu\right] + C_3\, \kappa_\mu \kappa_\nu + (p_\mu \text{ and } p_\nu \text{ terms}).$$

Explicit calculation gives for each of these pieces

$$C_1 = -2s^2\frac{\beta}{(1-\beta)}\vec{\kappa}^2 + [m^2 \text{ terms}]$$

$$C_2 = -4\beta^2 s^2,$$

and C_3 turns out to be zero. On projecting out the transverse and longitudinal components from (3.16) this leaves

$$N_T = 8Q^2 s\frac{\beta}{1-\beta}\, \vec{\kappa}^2\left[\beta^2 + (1-\beta)^2\right] + [m^2 \text{ terms}], \tag{3.17}$$

81

3: Implications of the BFKL formalism for structure functions.

$$N_L = 32Q^4 s \frac{\beta}{1-\beta} \left[\beta^2(1-\beta)^2 \right] \tag{3.18}$$

which we can put into (3.15) to give

$$F_T^{(a)} = 2\sum_q e_q^2 T_F \frac{Q^2}{4\pi^2} \int \frac{d^2\vec{k}}{\pi\vec{k}^4} \int_0^1 d\beta \int d^2\vec{\kappa} \ \alpha_s \left[\beta^2 + (1-\beta)^2 \right] \frac{\vec{\kappa}^2}{D_1^2} f(a,\vec{k}),$$

$$F_L^{(a)} = 2\sum_q e_q^2 T_F \frac{Q^4}{\pi^2} \int \frac{d^2\vec{k}}{\pi\vec{k}^4} \int_0^1 d\beta \int d^2\vec{\kappa} \ \alpha_s \left[\beta^2(1-\beta)^2 \right] \frac{1}{D_1^2} f(a,\vec{k}). \tag{3.19}$$

As mentioned above we have identified the factor $\frac{\alpha_s C_A}{\pi}$ in (3.9) as the gluon distribution $f(a,\vec{k})$.

Proceeding similarly we find that the total contribution from all the graphs in figure 3.4 can be written in the form, [13,19,20]

$$F_T(x,Q^2) = 2\sum_q e_q^2 T_F \frac{Q^2}{4\pi^2} \int \frac{d^2\vec{k}}{\pi\vec{k}^4} \int_0^1 d\beta \int d^2\vec{\kappa} \ \alpha_s$$

$$\times \left\{ m^2 \left(\frac{1}{D_1^2} + \frac{1}{D_2^2} - \frac{2}{D_1 D_2} \right) + \left[\beta^2 + (1-\beta)^2 \right] \left[\frac{\vec{\kappa}^2}{D_1^2} + \frac{(\vec{\kappa}-\vec{k})^2}{D_2^2} - 2\frac{\vec{\kappa}.(\vec{\kappa}-\vec{k})}{D_1 D_2} \right] \right\} f(a,\vec{k}),$$

$$F_L(x,Q^2) = 2\sum_q e_q^2 T_F \frac{Q^4}{\pi^2} \int \frac{d^2\vec{k}}{\pi\vec{k}^4} \int_0^1 d\beta \int d^2\vec{\kappa} \ \alpha_s \left[\beta^2(1-\beta)^2 \right]$$

$$\times \left[\frac{1}{D_1^2} + \frac{1}{D_2^2} - \frac{2}{D_1 D_2} \right] f(a,\vec{k}), \tag{3.20}$$

where

$$D_1 = \vec{\kappa}^2 + \beta(1-\beta)Q^2 + m^2,$$
$$D_2 = (\vec{\kappa}-\vec{k})^2 + \beta(1-\beta)Q^2 + m^2. \tag{3.21}$$

For the charm quark we take $m = m_c \simeq 1.7\text{GeV}^2$, while the light u,d,s quarks we take to be massless. It turns out to be possible to perform the azimuthal integration in (3.20) analytically, on changing variables to [13,13]

$$\vec{\kappa}' = \vec{\kappa} - (1-\beta)\vec{k}.$$

The resulting formulae are however quite lengthy, and we do not reproduce them here.

3: Implications of the BFKL formalism for structure functions.

The z integration of (3.1) is implicit in the $d^2\vec{\kappa}$ and $d\beta$ integrations. Indeed z is fixed in terms of $\vec{\kappa}$ and β through the relations in (3.13), (3.14). If we note that $a = x/z$ then these equations give

$$
\begin{aligned}
z &= \left[1 + \frac{\vec{\kappa}^2 + m^2}{(1-\beta)Q^2} + \frac{(\vec{\kappa} - \vec{k})^2 + m^2}{\beta Q^2} \right]^{-1} \\
&= \left[1 + \frac{\vec{\kappa}'^2 + m^2}{\beta(1-\beta)Q^2} + \frac{\vec{k}^2}{Q^2} \right]^{-1}.
\end{aligned}
\tag{3.22}
$$

The requirement that $0 < z < 1$ is clearly satisfied. Of course the integration regions in (3.20) must be additionally constrained by the condition

$$
z(\beta, \vec{\kappa}^2, \vec{k}^2, Q^2) > x
\tag{3.23}
$$

so that the argument $x' = x/z$ of f satisfies the requirement $x' < 1$. The argument of α_s has been taken to be $\vec{\kappa}'^2 + m_0^2$ in the equations in (3.20), which allows integration over the entire region of $\vec{\kappa}'$, since for small $\vec{\kappa}'^2$ the "mass" m_0 serves as a regulator by "freezing" the coupling to $\alpha_s(m_0^2)$. For light quarks we take $m_0^2 = 1\,\text{GeV}^2$; the results are not very sensitive to variations of m_0 around this value. For the charm quark contribution we set $m_0^2 = m_c^2$.

The expressions in (3.20) for the deep-inelastic structure functions are the explicit realisation of the factorization formula (3.1). Therefore, provided the gluon distribution $f(z, k^2)$ is known, we can calculate F_T and F_L. For small z the function $f(z, k^2)$ is calculated in the leading $\log(1/z)$ approximation from the BFKL equation, which may be written in the integro-differential form

$$
\frac{\partial f(z, k^2)}{\partial \log(1/z)} = \frac{3\alpha_s(k^2)}{\pi} k^2 \int_{k_0^2}^{\infty} \frac{dk'^2}{k'^2} \left\{ \frac{f(z, k'^2) - f(z, k^2)}{|k'^2 - k^2|} + \frac{f(z, k^2)}{(4k'^4 + k^4)^{\frac{1}{2}}} \right\}
\tag{3.24}
$$

$$
\equiv K \otimes f.
$$

If we incorporate the effects of parton shadowing the equation becomes [6,12]

$$\frac{\partial f(z,k^2)}{\partial \log(1/z)} = K \otimes f - \frac{81}{16k^2R^2}\alpha_s^2(k^2)[zg(z,k^2)]^2 \qquad (3.25)$$

where

$$zg(z,k^2) = \int_{\tilde{k}_0^2}^{k^2} \frac{dk'^2}{k'^2}f(z,k'^2) \qquad (3.26)$$

with $\tilde{k}_0^2 = 1$ GeV^2 [12]. Eq. (3.26) is the inverse (3.2). The additional term, quadratic in g, in (3.25) is the leading order shadowing contribution; the negative sign leading to a suppression in the growth of the gluon density with decreasing z, which arises from the recombination of gluons. It is the iteration of (3.25) that generates the "fan" diagrams in which the lines correspond to the BFKL ladders [6]. For investigations of shadowing, the crucial parameter is R, which specifies the size of the region in which the gluons are concentrated within the proton.

Finally we mention a possible simplifying assumption that could be considered for the factorization formula (3.1). To leading $\log(1/x)$ accuracy we may ignore the z dependence of $f(x/z,k^2)$ in (3.1). This is justified since

$$\left(\log\frac{x}{z}\right)^n = (\log x)^n[1 + O(1/\log x)].$$

The technical advantage of using this approximation is that the constraint (3.23), which requires $x/z < 1$, does not have to be imposed on the region of integration. For example in a recent calculation by Levin and Ryskin [21], which motivated the present study, the saturation limit (3.8) was used for f (at least for low Q^2). In such a case f would be independent of x and the simplifying approximation is reasonable. In general the simplifying approximation, $f(x/z,k^2) \to f(x,k^2)$ is expected to overestimate the magnitude, but to lead to a satisfactory prediction for the shape, of the small x behaviour of F_T and F_L. For instance if $f(x',k^2) \sim x'^{-\lambda}$ then the approximation would amount to the omission of a factor z^λ in the implicit z integration.

84

3.3: Analytic properties of the BFKL formalism.

A central problem in small x physics is the stability of the solutions of the BFKL or Lipatov equation [1-10] to contributions from the infrared and ultraviolet regions of the transverse momenta of the emitted gluons. This is reflected in the dependence of the solutions to the choice of the transverse momentum cut-offs. Several general properties of the solutions of the BFKL equation are known, which are scattered widely in the literature [2, 3, 6, 10, 22, 23]. In this section we draw these together and attempt to present a reasonably self-contained and coherent discussion.

3.3.1: Analytic solution of the BFKL equation.

The BFKL equation reads as:

$$f(x, \vec{k}) = f_0(x, \vec{k}) + \frac{N_c \alpha_s}{\pi^2} \int_x^1 \frac{dx'}{x'} \int_0^\infty \frac{d^2 \vec{k}'}{(\vec{k} - \vec{k}')^2} \left(f(x', \vec{k}') \frac{\vec{k}^2}{\vec{k}'^2} - f(x', \vec{k}) \frac{\vec{k}^2}{\vec{k}'^2 + (\vec{k} - \vec{k}')^2} \right)$$
$$(3.27)$$

For axially symmetric solutions, $f(x, \vec{k}) = f(x, \vec{k}^2)$, the integration over azimuthal angle can be performed analytically, leaving an integral equation in just the two variables x and $\vec{k}^2$:

$$f(x, k^2) = f_0(x, k^2) + \bar{\alpha}_s \int_x^1 \frac{dx'}{x'} \int_0^\infty \frac{dk'^2}{k'^2} k^2 \left(\frac{f(x', k'^2) - f(x', k^2)}{|k'^2 - k^2|} + \frac{f(x', k^2)}{(4k'^4 + k^4)^{\frac{1}{2}}} \right),$$
$$(3.28)$$

where we have introduced $\bar{\alpha}_s \equiv \frac{N_c \alpha_s}{\pi}$ and dropped the vector notation from $\vec{k}^2$. The function $f(x, k^2)$, the unintegrated gluon distribution, gives the probability to find a gluon in the parent hadron with longitudinal momentum fraction x and transverse momentum k^2. To be precise, f is related to the more familiar integrated gluon distribution, $g(x, Q^2)$, by

$$\int_0^{Q^2} \frac{dk^2}{k^2} f(x, k^2) \simeq x g(x, Q^2).$$

Although the integration over the transverse momentum in (3.28) does not contain any cutoff parameters, it should be emphasized that it is free from both infrared and ultraviolet divergences. However the solution contains infrared and ultraviolet singularities, which will

85

manifest themselves as non-trivial anomalous dimension(s); we amplify this comment in the discussion below (3.54).

Equation (3.28) takes the general form,

$$f(x, k^2) = f_0(x, k^2) + \bar{\alpha}_s \int_x^1 \frac{dx'}{x'} \int_0^\infty \frac{dk'^2}{k'^2} \mathcal{K}(k^2/k'^2) \times f(x', k'^2) \qquad (3.29)$$

in which the scale-invariant kernel $\mathcal{K}(k^2/k'^2)$ is

$$\mathcal{K}(k^2/k'^2) = \frac{1}{|k'^2/k^2 - 1|} + C\delta(k'^2/k^2 - 1) \quad \text{where} \qquad (3.30a)$$

$$C = \int_0^\infty \frac{d\hat{k}^2}{\hat{k}^2} \left(\frac{1}{(1 + 4\hat{k}^4/k^4)^{\frac{1}{2}}} - \frac{1}{|\hat{k}^2/k^2 - 1|} \right). \qquad (3.30b)$$

We have implicitly assumed some regularisation of the infrared divergences; these divergencies cancel out in the final integral equation anyway.

Inspecting the form of equation (3.29) it is clear on dimensional grounds that a function $\phi \sim (k^2)^\omega$ is an eigenfunction of the kernel $\mathcal{K}$, that is,

$$\int_0^\infty \frac{dk'^2}{k'^2} \mathcal{K}(k^2/k'^2) \times (k'^2)^\omega = \tilde{\mathcal{K}}(\omega)(k^2)^\omega \qquad (3.31)$$

provided that the integral converges. Noting that, for fixed k^2, $\mathcal{K}(k^2/k'^2) \sim k^2/k'^2$ for $k'^2 \to \infty$, and $\mathcal{K}(k^2/k'^2) \sim$ constant for $k'^2 \to 0$, then the integral will converge over the region $0 < \mathcal{R}e\ \omega < 1$.

Transforming to the basis of eigenfunctions of operator $\mathcal{K}$, as usual, simplifies the solution of the equation enormously. Denoting the integral transform (actually a Mellin transform) of an arbitrary function $\phi(t)$ as

$$\mathcal{M}_{t \to \omega}[\phi(t)] = \int_0^\infty \frac{dt}{t}(t)^{-\omega}\phi(t) \equiv \tilde{\phi}(\omega) \qquad (3.32)$$

and applying this to equation (3.30a) one gets (using the change of variables $k^2/k'^2 \to u$),

$$\tilde{f}(x, \omega) = \tilde{f}_0(x, \omega) + \bar{\alpha}_s \int_x^1 \frac{dx'}{x'} \int_0^\infty \frac{dk^2}{k^2} \int_0^\infty \frac{dk'^2}{k'^2} \mathcal{K}(k^2/k'^2)(k^2)^{-\omega} f(x', k'^2) \quad (3.33a)$$

$$= \tilde{f}_0(x,\omega) + \bar{\alpha}_s \int_x^1 \frac{dx'}{x'} \int_0^\infty \frac{du}{u} \int_0^\infty \frac{dk'^2}{k'^2} \mathcal{K}(u)(uk'^2)^{-\omega} f(x',k'^2) \qquad (3.33b)$$

$$\equiv \tilde{f}_0(x,\omega) + \bar{\alpha}_s \int_x^1 \frac{dx'}{x'} \widetilde{\mathcal{K}}(\omega) \times \tilde{f}(x',\omega) \qquad (3.33c)$$

It turns out (and the calculation is carried out explicitly in Appendix A) that the integration for $\widetilde{\mathcal{K}}(\omega)$ can be performed analytically, and the result given in a compact form,

$$\widetilde{\mathcal{K}}(\omega) = \int_0^\infty \frac{du}{u} u^{-\omega} \widetilde{\mathcal{K}}(u) \qquad (3.34a)$$

$$= 2\psi(1) - \psi(\omega) - \psi(1-\omega) \qquad (3.34b)$$

with the ψ-function defined in terms of Euler's Γ-function as $\psi(x) = \frac{d}{dx}\log\Gamma(x)$. We saw that (3.34a) was defined only for $0 < \mathcal{R}e\ \omega < 1$; however we can take (3.34b) as defining $\widetilde{\mathcal{K}}(\omega)$ over the full ω plane, by analytic continuation. The essential features of this function as ω varies along the real axis are shown in figure 3.5.
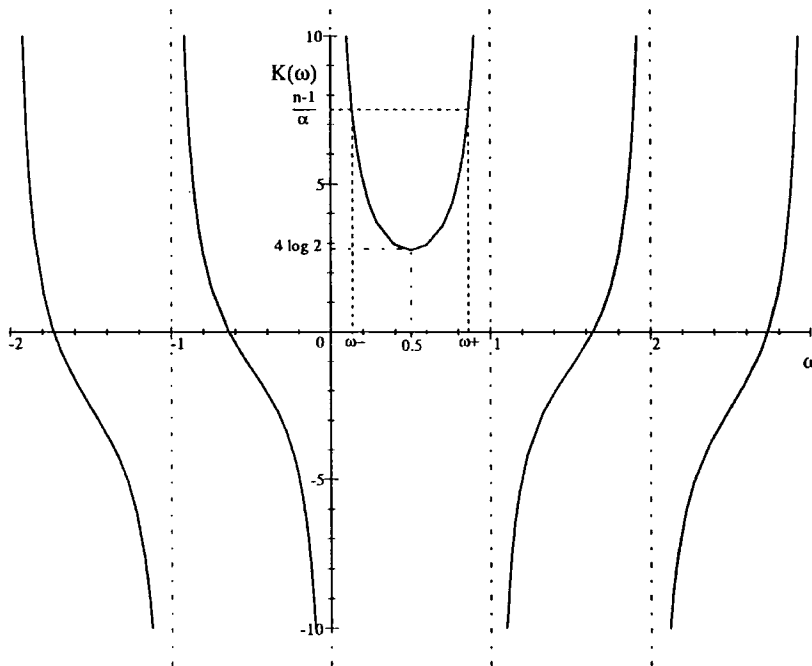
Figure 3.5: A plot of the eigenvalue $\widetilde{\mathcal{K}}(\omega)$ against ω, for ω on the real axis. The points $\omega_\pm(n)$ are some of the singularities in the ω-plane (corresponding to the anomalous dimension of the gluon field) generated by the BFKL equation when $n > 1 + \lambda$ and is real. The position of these singularities are those values of ω for which $n - 1 - \bar{\alpha}_s\widetilde{\mathcal{K}}(\omega) = 0$. For $\frac{n-1}{\bar{\alpha}_s}$ large, $\omega_- \to \frac{\bar{\alpha}_s}{(n-1)}$, thus reproducing the leading order DGLAP result for the anomalous dimension at small n.

87

Our original function $f(x, k^2)$ can be reconstructed from $\tilde{f}(x, \omega)$ through the standard inversion of the Mellin transform,

$$f(x, k^2) = \int_{\sigma - i\infty}^{\sigma + i\infty} \frac{d\omega}{2\pi i} (k^2)^\omega \tilde{f}(x, \omega), \qquad (3.35)$$

where the integral is taken along a line parallel to the imaginary axis in the complex ω-plane. The placing of this line such that the integral converges appropriately: in the present case, we have the restriction $0 < \sigma < 1$ due to the poles in $\tilde{\mathcal{K}}(\omega)$ for $\omega \to 0$ and $\omega \to 1$. It is convenient to choose $\sigma = \frac{1}{2}$ since $\tilde{\mathcal{K}}$ is real along this line and has a saddle point at $\omega = \frac{1}{2}$.

Thus, the Mellin transform in k^2 has resulted in the following equation for $\tilde{f}(x, \omega)$:

$$\tilde{f}(x, \omega) = \tilde{f}_0(x, \omega) + \bar{\alpha}_s \int_x^1 \frac{dx'}{x'} \tilde{\mathcal{K}}(\omega) \tilde{f}(x', \omega). \qquad (3.36)$$

It is useful to perform the analogous transform also in the x-variable,

$$\widetilde{\mathcal{F}}(n, \omega) = \int_0^1 \frac{dx}{x} x^{n-1} \tilde{f}(x, \omega) \qquad (3.37)$$

since after applying this transform to (3.36) the equation reduces to the trivial algebraic form

$$\widetilde{\mathcal{F}}(n, \omega) = \widetilde{\mathcal{F}}_0(n, \omega) + \frac{\bar{\alpha}_s}{(n-1)} \tilde{\mathcal{K}}(\omega) \widetilde{\mathcal{F}}(n, \omega) \qquad (3.38)$$

with solution

$$\widetilde{\mathcal{F}}(n, \omega) = \frac{(n-1)\widetilde{\mathcal{F}}_0(n, \omega)}{\left(n - 1 - \bar{\alpha}_s \tilde{\mathcal{K}}(\omega)\right)}. \qquad (3.39)$$

This represents the general solution of the equation (3.28) in the $\omega - n$ representation. We can now invert the integral transforms and study the properties of the solution in $x - k^2$ space. The inversion formula for $n \to x$ is exactly analogous to (3.35),

$$f(x) = \int_{\sigma - i\infty}^{\sigma + i\infty} \frac{dn}{2\pi i} x^{-n+1} \mathcal{F}(n). \qquad (3.40)$$

The line of integration here is to the right of all singularities of $\mathcal{F}(n)$ in the complex n plane to ensure that $f(x)$ vanishes for $x > 1$. Noting that the factor x^{-n+1} goes to zero very rapidly for $\mathcal{R}e\, n \to -\infty$ we can deform the contour of integration to encircle each singularity in the left hand plane as shown in figure 3.6.
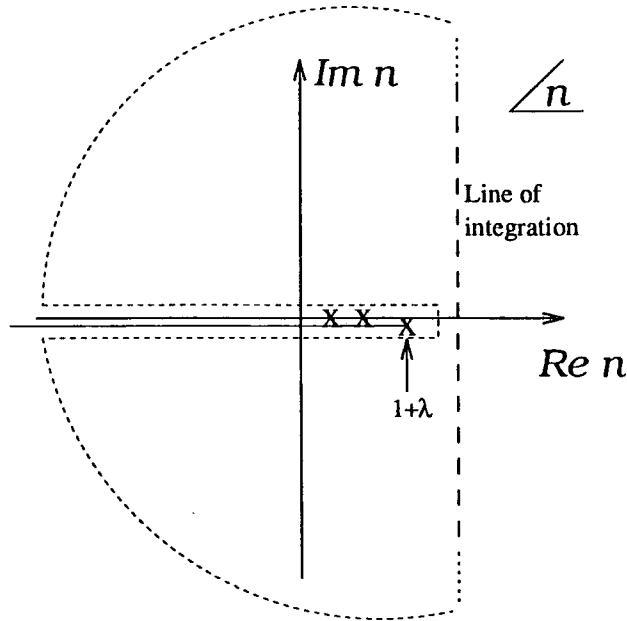
Figure 3.6: The contour of integration in the inversion of the Mellin transform by equation (3.40). Crosses denote pole singularities in the n-plane, and the endpoint of a cut singularity on the real axis at $n = 1 + \lambda$, the singularity generated by the BFKL equation.

This contour integral will pick up contributions from the singularities of $\mathcal{F}(n)$, shown as crosses in figure 3.6. The dominant contribution for $x \to 0$ will come from the rightmost singularity of $\mathcal{F}(n)$. Hence it is of interest to understand the singularity structure generated by the BFKL equation. From (3.39) we can see that the singularities of $\mathcal{F}(n, \omega)$ are those of the driving term, $\mathcal{F}_0(n, \omega)$, plus additional singularities from the zeroes of the denominator, at

$$n = 1 + \bar{\alpha}_s \, \widetilde{\mathcal{K}}(\omega). \tag{3.41}$$

As ω varies along the line of integration $\omega = \frac{1}{2} - i\infty \to \frac{1}{2} + i\infty$ then $\widetilde{\mathcal{K}}(\omega)$ increases from $-\infty$ through to a maximum of $4 \log 2$ at $\omega = \frac{1}{2}$ and back through to $-\infty$. Thus the n-plane singularity associated with (3.41) moves from $-\infty \to 1 + \bar{\alpha}_s 4 \log 2 \to -\infty$. We therefore notice that the BFKL equation gives rise to a *cut* singularity in the n-plane starting at $n = 1 + \bar{\alpha}_s 4 \log 2 \equiv 1 + \lambda$ and extending back to $n \to -\infty$. This cut singularity is displayed on figure 3.6 slightly detached from the real axis, for clarity. In the following section we will explicitly invert the two Mellin transforms to get an approximate solution

for the asymptotic behaviour of $f(x, k^2)$.

3.3.2: Asymptotic form of the solution.

We have arrived at the following solution to the BFKL equation in $n - \omega$ space:

$$\widetilde{\mathcal{F}}(n, \omega) = \frac{(n-1)\widetilde{\mathcal{F}}_0(n, \omega)}{\left(n - 1 - \bar{\alpha}_s \widetilde{\mathcal{K}}(\omega)\right)}.$$

Take the case for which $f_0(x, k^2) = f_0(k^2)$, arising from the two-gluon exchange driving term. This gives rise to a double Mellin transform of the type

$$\widetilde{\mathcal{F}}_0(n, \omega) = \frac{\tilde{\rho}(\omega)}{(n-1)} \tag{3.42}$$

where the singularity at $n = 1$ corresponds to the x^0 behaviour of f_0. We noted previously that the BFKL equation gives rise to a singularity at $n = 1 + \lambda > 1$ so asymptotically the BFKL resummation will dominate the driving term. The first inverse Mellin transform $n \to x$ is now very simple,

$$\tilde{f}(x, \beta) = \int_{\sigma - i\infty}^{\sigma + i\infty} \frac{dn}{2\pi i} x^{-n+1} \frac{\tilde{\rho}(\omega)}{\left(n - 1 - \bar{\alpha}_s \widetilde{\mathcal{K}}(\omega)\right)} = \tilde{\rho}(\omega) x^{-\bar{\alpha}_s \widetilde{\mathcal{K}}(\omega)}. \tag{3.43}$$

The second Mellin transform can not in general be performed analytically, since it depends on the nature of $\tilde{\rho}(\omega)$. However, an approximate solution can be obtained by noting that the $x^{-\bar{\alpha}_s \widetilde{\mathcal{K}}(\omega)}$ factor in $\tilde{f}$ means that the transform integral for $\omega \to k^2$ is strongly dominated by the region around $\omega = \frac{1}{2}$ where $\widetilde{\mathcal{K}}$ takes on its maximum value along the contour. This allows for a saddle point approximation of the integral, expanding $x^{-\bar{\alpha}_s \widetilde{\mathcal{K}}(\omega)}$ as a Gaussian around $\omega = \frac{1}{2}$. Let us define $\omega = 1/2 + i\nu$ and

$$\tilde{\rho}(1/2 + i\nu) = \exp\left(\log\left(\tilde{\rho}(1/2 + i\nu)\right)\right) = \exp(A - Bi\nu - \frac{C}{2}\nu^2 + \cdots), \tag{3.44}$$

$$\widetilde{\mathcal{K}}(1/2 + i\nu) \simeq \widetilde{\mathcal{K}}_0 - \frac{\widetilde{\mathcal{K}}_0''}{2}\nu^2 + \cdots, \tag{3.45}$$

where $\widetilde{\mathcal{K}}_0 = 4\log 2$, and $\widetilde{\mathcal{K}}_0'' = 28\zeta(3)$ (the Riemann zeta function $\zeta(3) \simeq 1.202$). The

inverse Mellin transform then gives us

$$
f(x, k^2) = \int_{\frac{1}{2}-i\infty}^{\frac{1}{2}+i\infty} \frac{d\omega}{2\pi i} (k^2)^\omega \tilde{\rho}(\omega) x^{-\bar{\alpha}_s \widetilde{\mathcal{K}}(\omega)}
$$

$$
\simeq \tilde{\rho}(1/2) \frac{(k^2)^{\frac{1}{2}}}{2\pi} x^{-\bar{\alpha}_s \widetilde{\mathcal{K}}_0} \int_{-\infty}^{\infty} d\nu \, \exp\left[-\frac{1}{2}(C + \widetilde{\mathcal{K}}_0'' \log(1/x))\nu^2 + (\log k^2 - B)i\nu \right]
$$

$$
= \tilde{\rho}(1/2)(k^2)^{\frac{1}{2}} \frac{x^{-\lambda}}{\sqrt{2\pi(\widetilde{\mathcal{K}}_0'' \log(1/x) + C)}} \exp\left[\frac{-\log^2(k^2/\bar{k}^2)}{2(\widetilde{\mathcal{K}}_0'' \log(1/x) + C)} \right].
$$

$$
(3.46)
$$

(Here we have defined $\log \bar{k}^2 \equiv B$, by analogy with the case where the driving term is a gluon of definite transverse momentum $k^2 = \bar{k}^2$, i.e. $\rho(k^2) = \delta(k^2 - \bar{k}^2)$, for which the parameter B as defined in (3.44) is exactly $\log \bar{k}^2$)

We have reproduced the solution of the gluon distribution originally obtained by Lipatov *et al.* with its characteristic $x^{-\lambda}$ behaviour, with $\lambda = \bar{\alpha}_s 4 \log 2$, modulated by a $(\log(1/x))^{-\frac{1}{2}}$ factor.

Formula (3.46) also displays explicitly the diffusion pattern of the solution of the BFKL equation, that is a Gaussian distribution in $\log(k^2)$ with a width which grows as $(\log(1/x))^{\frac{1}{2}}$ as x decreases. The position of the maximum of the Gaussian distribution (given by $\log(\bar{k}^2)$ of (3.46)), as well as the normalisation of the solution, is controlled by the boundary conditions, that is by $f(x_0, k^2)$. The rate of diffusion, however, is independent of the boundary conditions.

The approximate analytic solution (3.46) only applies for $x \ll x_0$, x_0 being the starting point of our evolution (which was simply set to one above). We assume, simply for the purposes of illustration, that this form applies for all $x \leq x_0$. Fig. 3.7 shows the width of the Gaussian $\log k^2$ distribution of $f(x, k^2)/(k^2)^{\frac{1}{2}}$ as x decreases from x_0. At x_0 the "width" is given by the boundary conditions $f(x_0, k^2)/(k^2)^{\frac{1}{2}}$, though in practice this input distribution will not have a perfect Gaussian form in $\log k^2$. In Fig. 3.7 we use dashed curves to emphasize the approximate nature of the treatment for $x \sim x_0$. It should be noted also that in a realistic treatment we find that the gluon distribution $f(x, k^2)$ samples k^2 uncomfortably close to the infrared (non-perturbative) region.
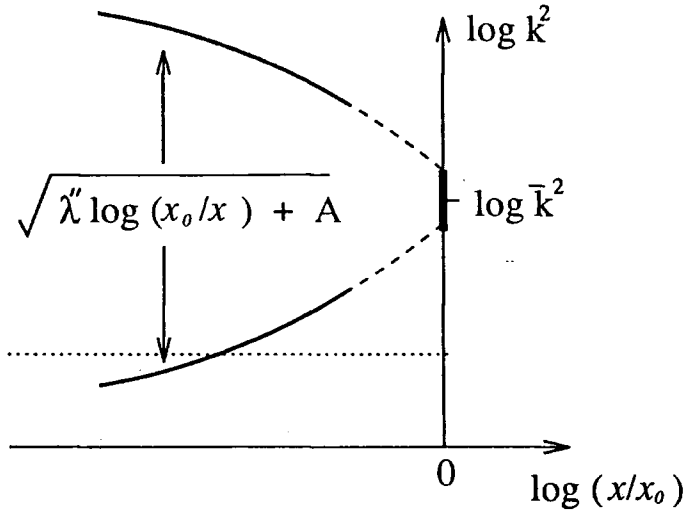
Figure 3.7: The variation in the width of the Gaussian $\log k^2$ distribution of $f(x, k^2)/(k^2)^{\frac{1}{2}}$ as we evolve down in x below the starting value x_0.

3.3.3: Examples of diffusion in transverse momentum.

The diffusion in $\log k^2$ with decreasing x is a major problem in the applicability of the BFKL equation since it can lead to an increasingly large contribution from the infrared and ultraviolet regions of k^2 where the equation is not expected to be valid. We may illustrate diffusion using two physical examples from deep-inelastic electron-proton scattering.

Given the unintegrated gluon distribution $f(x, k^2)$ we can, in principle, calculate the behaviour of the deep-inelastic structure functions $F_{2,L}(x, Q^2)$ at small x through the so-called k_T factorization theorem [13, 14]. Then

$$F_i(x, Q^2) \;=\; \int \frac{dk'^2}{k'^4} \int_x^1 \frac{dx'}{x'} f\left(\frac{x}{x'}, k'^2\right) F_i^{(0)}(x', k'^2, Q^2) \tag{3.47}$$

with $i = 2, L$. Symbolically we may write $F = f \otimes F^{(0)}$, see Fig. 3.8a, where f describes the gluon ladder and $F^{(0)}$ the quark-box amplitude for gluon-virtual photon fusion. It should be noted that the integration over k'^2 extends down to $k'^2 = 0$ and so knowledge of $f(x/x', k'^2)$ in this region is, in principle, necessary for getting absolute predictions for $F_{2,L}(x, Q^2)$.

3: Implications of the BFKL formalism for structure functions.

To illustrate the effect of diffusion in k^2 we use the $LL(1/x)$ approximation to simplify (3.47) to

$$F_i(x, Q^2) = \int \frac{dk^2}{k^4} f(x, k^2) B_i(k^2, Q^2) \qquad (3.48)$$

where the "impact factors" B_i are

$$B_i(k^2, Q^2) = \int_0^1 \frac{dx'}{x'} F_i^{(0)}(x', k^2, Q^2). \qquad (3.49)$$

Now we may equally well rewrite the convolution (3.48) by factorizing at an intermediate link x_1 along the gluon chain in Fig. 3.8a,

$$F_i(x, Q^2) = \int \frac{dk^2}{k^4} f(x_1, k^2) f_u\left(\frac{x}{x_1}, k^2\right) \qquad (3.50)$$

where f_u is a solution of the BFKL equation but with the boundary condition fixed at the "upper" end of the chain by the quark-box impact factor $B_i(k^2, Q^2)$. The diffusion pattern is now determined by boundary conditions at both ends of the gluon ladder [22]. To be specific, it is given by

$$\frac{f(x_1, k^2) f_u\left(\frac{x}{x_1}, k^2\right)}{k^2} \sim \frac{x^{-\lambda}}{\sqrt{\log(x_0/x_1)\log(x_1/x)}} \exp\left(-\frac{\log^2(k^2/\bar{k}^2)}{2\lambda''\log(x_0/x_1)} - \frac{\log^2(k^2/\bar{k}_u^2)}{2\lambda''\log(x_1/x)}\right) \qquad (3.51)$$

where $\bar{k}_u^2$ is determined by $B_i(k^2, Q^2)$ and so $\bar{k}_u^2 \sim Q^2$. The variation of the width of the diffusion pattern, as x_1 varies between x and x_0, is sketched in Fig. 3.8a. Even for large Q^2, the boundary conditions at x_0 mean that the infrared region is penetrated leading to uncertainty in the predictions for $F_i(x, Q^2)$.

This problem is overcome for deep-inelastic (x, Q^2) events containing an energetic measured jet (x_j, k_j^2), see Fig. 3.8b,[24 - 26, 15]. We then have a $\delta(k^2 - k_j^2)$ distribution at the "bottom" of the gluon ladder and k_j^2 can be chosen sufficiently large such that $f(x, k^2)$ does not diffuse appreciably into the infrared region for physically accessible values of x/x_j, see Fig. 3.8b.
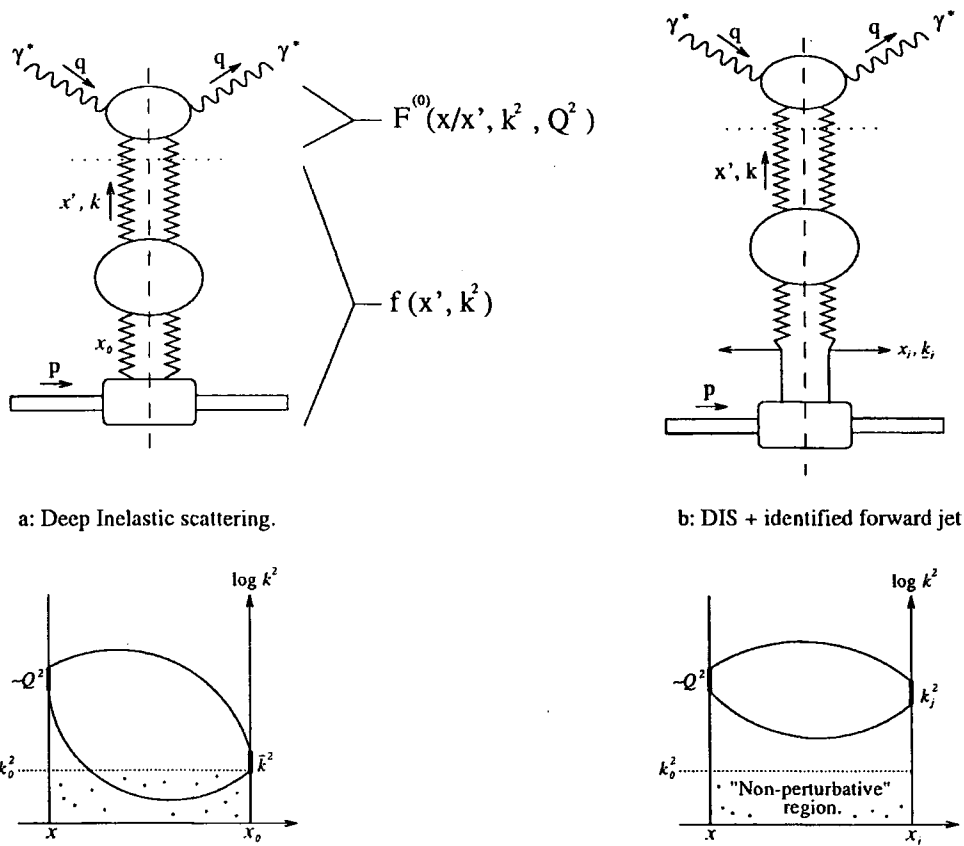
Figure 3.8: The upper diagrams show a gluon "ladder" contribution to small x processes,

(a) for deep-inelastic scattering and

(b) for deep-inelastic scattering together with an energetic jet.

The quark box factor $F^{(0)}$ implicitly includes the contribution of the crossed box. The lower sketches show the variation of the width of the $\log k^2$ distributions of (3.51) as a function of x_1.

3.3.4: Sensitivity to the infra red region.

The convolution in transverse momentum which appears in the BFKL equation extends down into the region of small virtualities, for which we have no faith in the validity of perturbative QCD. In the present section we therefore analyse the extent to which this infra-red region affects the predictions of the BFKL equation. In order to gain some analytic insight into the problem we will here make the simplest change to the BFKL equation possible, and just introduce some cutoff in the convolution integral, disregarding the infra-red region completely. (An alternative approach would be to introduce some form of "non-perturbative" gluon propagator and couplings and study the dependence on the exact form of these functions for small k^2.) We shall find that, in the case of fixed coupling, the position of the leading singularity in the ω-plane is unaffected by the imposition of any infrared cutoff, which means that the $x^{-\lambda}$ behaviour remains essentially unchanged.

Firstly, let us just demonstrate in more detail the nature of the singularity generated by the basic BFKL equation. We found earlier the solution in $n - \omega$ space given by

$$\widetilde{\mathcal{F}}(n,\omega) = \frac{(n-1)\widetilde{\mathcal{F}}_0(n,\omega)}{(n-1) - \bar{\alpha}_s \widetilde{\mathcal{K}}(\omega)} \qquad (3.52)$$

Let us now transform $\omega \to k^2$,

$$\mathcal{F}(n,k^2) = \int_{\frac{1}{2}-i\infty}^{\frac{1}{2}+i\infty} \frac{d\omega}{2\pi i}(k^2)^\omega \widetilde{\mathcal{F}}(n,\omega). \qquad (3.53)$$

It follows from the form of this inversion integral that the leading behaviour of $\mathcal{F}(n,k^2)$ as $k^2 \to 0$ ($k^2 \to \infty$) is controlled by the nearest singularity $\omega_+(n)$ ($\omega_-(n)$) which lies to the right (left) of the contour of integration in the ω plane, that is

$$\mathcal{F}(n,k^2) \sim (k^2)^{\omega_+} \text{ for } k^2 \to 0 \qquad (3.54)$$

(and similarly as $(k^2)^{\omega_-}$ as $k^2 \to \infty$). These $\omega_\pm$ singularities come from the zeroes of the denominator in (3.52), and the value ω_- is equal, by definition, to the anomalous dimension of the twist-2 gluonic operator analytically continued to small nonintegral values of n. As

we shall see later, gauge invariance requires the driving term in the BFKL equation to behave as

$$f_0(x, k^2) \sim k^2 \text{ as } k^2 \to 0$$

which corresponds to a pole at $\omega = 1$ for $\tilde{f}_0(x, \omega)$. Thus the presence of the anomalous dimension ω_+ changes the small k^2 behaviour of $\mathcal{F}(n, k^2)$ from $\sim k^2$ to $\sim (k^2)^{\omega_+}$ with $\omega_+(n) < 1$. It is in this way that the infrared singularities of the BFKL equation manifest themselves.

To determine the values of $\omega_\pm(n)$ we can recall that the neighbourhood of $\omega \sim 1/2$ is the critical region, and by expanding

$$\bar{\alpha}_s \widetilde{\mathcal{K}}(\omega) \simeq \lambda + \frac{1}{2}\lambda''(\omega - \frac{1}{2})^2$$

we see from (3.52) that $\widetilde{\mathcal{F}}(n, \omega)$ has two nearby poles at

$$\omega = \frac{1}{2} \pm \sqrt{2(n - 1 - \bar{\alpha}_s\lambda)/\lambda''} \equiv \omega_\pm(n). \tag{3.55}$$

(See figure 3.5). These poles move together and pinch the contour in (3.53) when $n = 1 + \lambda$ and so generate a singularity in $\mathcal{F}(n, k^2)$ at this point. By completing the contour in (3.53) in the left- or right-hand ω-plane, according to whether k^2 is large or small, we get

$$\mathcal{F}(n, k^2) = \frac{(k^2)^{\omega_\pm}\widetilde{\mathcal{F}}_0(n, \omega_\pm)}{\omega_+ - \omega_-} = \frac{\sqrt{\frac{1}{2}\lambda''}\,(k^2)^{\omega_\pm}\,\widetilde{\mathcal{F}}_0(n, \omega_\pm)}{2\sqrt{n - 1 - \lambda}} \tag{3.56}$$

which explicitly exhibits the $1/\sqrt{n - 1 - \lambda}$ branch cut singularity. If we insert this result into (3.40), fold back the contour in the n-plane to circle the branch cut, and perform the n-integration we get the asymptotic behaviour given in (3.46), namely

$$f(x, k^2) \sim x^{-\lambda}[\log(1/x)]^{-\frac{1}{2}} \tag{3.57}$$

for small x.

Now let us see how we can analyse the BFKL equation when we apply a cutoff to the transverse momentum integrations. The equation to be solved is of the form,

$$f(x, k^2) = f_0(x, k^2) + \bar{\alpha}_s \int_x^1 \frac{dx'}{x'} \int_0^\infty \frac{dk'^2}{k'^2} \mathcal{K}(k^2/k'^2) \Theta(k'^2 - k_0^2) f(x', k'^2), \qquad (3.58)$$

for which a solution can be found through Wiener-Hopf methods. We split $f(x, k^2)$ up into two functions,

$$f(x, k^2) = f^+(x, k^2) + f^-(x, k^2)$$

where $f^+(x, k^2)$ and $f^-(x, k^2)$ are zero for $k^2 > k_0^2$ and $k^2 < k_0^2$ respectively. By performing a Mellin transform in both x, k^2 space we get

$$\widetilde{\mathcal{F}}^+(n, \omega) + \widetilde{\mathcal{F}}^-(n, \omega) = \widetilde{\mathcal{F}}_0(n, \omega) + \frac{\bar{\alpha}_s}{(n-1)} \widetilde{\mathcal{K}}(\omega) \widetilde{\mathcal{F}}^-(n, \omega), \qquad (3.59)$$

with $0 < \mathcal{R}e\ \omega < 1$ for the inversion integral. The function $\widetilde{\mathcal{F}}^-$ (resp. $\widetilde{\mathcal{F}}^+$) has no singularities to the right (resp. left) of the contour of integration in the inverse Mellin transform, so that it vanishes in the appropriate region of k^2. If we initially take n large and positive, then each function in the above equation will have no poles or zeroes within some strip in the ω plane given by $\frac{1}{2} - \delta < \mathcal{R}e\ \omega < \frac{1}{2} + \delta$, say. This allows us to decompose $1 - \frac{\bar{\alpha}_s}{(n-1)} \widetilde{\mathcal{K}}(\omega)$ as

$$A(n, \omega) \equiv 1 - \frac{\bar{\alpha}_s}{(n-1)} \widetilde{\mathcal{K}}(\omega) = \frac{A^-(n, \omega)}{A^+(n, \omega)}$$

where A^- (resp. A^+) has no poles or zeroes for $\mathcal{R}e\ \omega > \frac{1}{2} - \delta$ (resp. $\mathcal{R}e\ \omega < \frac{1}{2} + \delta$). The equation then becomes

$$\widetilde{\mathcal{F}}^-(n, \omega) A^-(n, \omega) + \widetilde{\mathcal{F}}^+(n, \omega) A^+(\omega) = A^+(n, \omega) \widetilde{\mathcal{F}}_0(n, \omega)$$

Again, we can decompose $A^+ \times \widetilde{\mathcal{F}}_0$ into two functions $B^- + B^+$, with each B being analytic in the appropriate region. Then, we have

$$\widetilde{\mathcal{F}}^-(n, \omega) A^-(n, \omega) - B^-(n, \omega) = -\widetilde{\mathcal{F}}^+(n, \omega) A^+(\omega) + B^+(n, \omega). \qquad (3.60)$$

By construction, the left hand side is analytic for $\mathcal{R}e\ \omega > \frac{1}{2} - \delta$ while the right hand side is analytic for $\mathcal{R}e\ \omega < \frac{1}{2} + \delta$. Each side must therefore be analytic in the entire finite

97

complex ω plane, ie. be equal to some entire function $E(n,\omega)$. So, finally,

$$\widetilde{\mathcal{F}}^-(n,\omega) = \frac{[E(n,\omega) + B^-(n,\omega)]}{A^-(n,\omega)}. \qquad (3.61)$$

It can be seen that the poles of $\widetilde{\mathcal{F}}^-$ arise from zeroes of $A^-(n,\omega)$ and correspond to those singularities of the original equation (with *no* cutoff) which lie to the left of $\omega = \frac{1}{2}$. The leading singularity for large k^2 is the rightmost of these, at $\omega = \omega_-(n)$. Thus on inverting the transform $\omega \to k^2$ we have $f^-(n,k^2) \sim (k^2)^{\omega_-(n)} \sim 1 + \log k^2 \omega_-(n) + \cdots$. Since $\omega_-(n) \simeq 1/2 - \sqrt{2(n-1-\lambda)/\lambda''}$ this expression has a square root branch cut, $\widetilde{\mathcal{F}}(n,k^2) \sim \sqrt{n-1-\lambda}$, rather than the $1/\sqrt{n-1-\lambda}$ singularity of the equation with no cutoff. However the tip of each branch cut lies at the same point, so the leading power growth remains the same. In fact, on performing the transform $n \to x$ we find that the leading behaviour becomes

$$f(x,k^2) \sim x^{-\lambda}[\log(1/x)]^{-\frac{3}{2}}. \qquad (3.62)$$

(Clearly, we find the same behaviour if we have an ultraviolet, and no infrared, cutoff - the roles of $\widetilde{\mathcal{F}}^-$ and $\widetilde{\mathcal{F}}^+$ are simply interchanged.) Finally, we note that the infrared cutoff eliminates infrared singularities and so $\mathcal{F}(n,k^2) \sim k^2$ as $k^2 \to 0$ rather than the anomalous behaviour shown in (3.54).

So far, the leading small-x behaviour, $x^{-\lambda}$, has remained intact under mutilations of the integration region in k'^2. However, if we introduce both an infrared and ultraviolet cutoff then the exponent λ becomes cutoff dependent [23].

3.3.5: Fixed and running coupling.

We have seen that the exponent λ controlling the small x behaviour, $x^{-\lambda}$, of the gluon is given by the maximal eigenvalue of the BFKL kernel. If we use a fixed value of α_s in the BFKL equation, (3.28), then the eigenvalue spectrum is continuous, and remains so in the presence of either an infrared or ultraviolet cut-off. Moreover the maximum eigenvalue (the branch point of the cut) does not change.

The situation is different if we introduce both an infrared cut-off k_0^2 and an ultraviolet cut off k_{max}^2 [23]. Then the eigenvalue spectrum becomes discrete. The maximum eigenvalue, λ_{max}, and the separation between the eigenvalues can be shown to depend on the quantity $t = k_{max}^2/k_0^2$. For large $\log t$ the distance between the eigenvalues becomes proportional to $1/\log t$ and

$$\lambda_{max} = \lambda_{max}(t = \infty) + O(1/\log t), \qquad (3.63)$$

so in the limit $t \to \infty$ we do indeed recover the continuous spectrum.

So far we have considered a fixed value of the coupling, α_s, in the BFKL equation, (3.28). So, strictly speaking, the exponent λ in the $x^{-\lambda}$ behaviour we have found is defined only up to an arbitrary factor α_s. Clearly, in order to extract any phenomenology from the BFKL equation it is necessary somehow to constrain this parameter, which will require further phenomenological assumptions. Rather than choose the coupling arbitrarily, it seems more satisfactory to introduce a running coupling into the BFKL equation, $\alpha_s \to \alpha_s(k^2)$, and allow the *dynamics* to choose the effective value of α_s. By expanding

$$\alpha_s(k^2) = \alpha_s(\bar{k}^2) \left[1 + \sum_{n=1}^{\infty} \left(\frac{\beta_0}{4\pi} \alpha_s(\bar{k}^2) \log(\bar{k}^2/k^2) \right)^n \right]$$

we see that this approximation contains the genuine leading log results with fixed $\alpha_s = \alpha_s(\bar{k}^2)$ ($\bar{k}^2$ arbitrary) plus a further selection of terms which actually go infinitely far down in non-leading logarithms.

For phenomenological work then, we make this physically reasonable replacement of fixed with running coupling, although there is no rigorous proof that this is correct. Indeed the author doubts that there can be any such proof in a formal sense: inasmuch as it genuinely does go down infinitely far in nonleading logarithms, it does not seem clear what the approximation means, formally. At present the main justification for a running coupling is that in the strongly ordered k^2 limit the BFKL equation will produce the Altarelli-Parisi equation in the double leading logarithm approximation if we take $\alpha_s = \alpha_s(k^2)$. However, strictly speaking this consideration can only determine the argument of α_s up to a finite factor, since for example $\alpha_s(3k^2) \sim \alpha_s(k^2)$ in the limit for which the DLLA result would apply. While irrelevant asymptotically, such a factor could be important in

99

the non-asymptotic scales probed by experiment. Considerations like these make it clear that much work still needs to be done in understanding the formal basis of the BFKL formalism, and its relationship to the standard analysis of deep inelastic scattering. There have been recent developments in this regard, notably [27] (see also [28]).

The introduction of running α_s has the effect of suppressing the importance of the ultraviolet cut-off and enhancing the dependence on the infrared behaviour. Moreover in this case, even with no ultraviolet cut-off, the eigenvalue spectrum of $\tilde{K}(\omega)$ is discrete, with $\lambda_{\max}$ sensitive to the choice of the infrared cut-off k_0^2. In the following two sections we quantify this effect and apply the modified (running coupling) form of the BFKL equation to structure functions.

3.4: Numerical predictions (I).

We calculate the leading $\log(1/x)$ contributions to $F_2 = F_T + F_L$ and F_L using eqs. (3.20) . We first solve the integro-differential BFKL equation (3.25) for $f(z, k^2)$ by evolving down in z from boundary conditions at $z = z_0 = 10^{-2}$ specified in terms of the known gluon distribution $g(z_0, Q^2)$. The procedure is described in detail in ref. [12]. Above z_0, where the BFKL effect is expected to be negligible we simply use the known gluon distribution to calculate $f(z, k^2)$ via (3.2). The "known" parton distributions that we use for $z \geq z_0$ are those of set D_0 of ref. [11]; to be precise we use D_0-type distributions which have been obtained by a global leading order fit [29] to the deep inelastic data, rather than those obtained in the next-to-leading order analysis of ref. [11].

In summary the gluon distribution $f(x, k^2)$, or $g(x, Q^2)$, is determined from the BFKL equation for $x < x_0$, and from deep inelastic data via the Altarelli-Parisi evolution equations for $x \geq x_0$. Though the continuity of g at $x = x_0$ is assured, there can be a mismatch of the derivatives on account of the different rates of Q^2 evolution in the two regions, see ref. [12]. We take up the discussion of this point in section 3.4.1. However it turns out, fortuitously, that the smoothest matching across the $x = x_0$ boundary occurs for $Q^2 \simeq 10-20$ GeV^2 [12]; the Q^2 region most pertinent to investigate the small x behaviour at HERA.

We show results for the structure functions $F_{2,L}$ at $Q^2 = 10$ and 20 GeV^2 corresponding to two choices ($k_0^2 = 1$ and 2 GeV^2) of the lower cut-off of the integration over the transverse momentum k of the gluon in the BFKL equation, (3.24), and in the convolution formulae of (3.20). Also we present results with the shadowing term (quadratic in g) omitted from (3.25), and with it included for two different choices of R, where πR^2 is the transverse area within which the gluons are concentrated in the proton. We chose either $R = 5$ GeV^{-1} (corresponding to gluons uniformly spread across the proton) or $R = 2$ GeV^{-1} (gluons concentrated in "hot-spots" within the proton). We then calculated F_2 and F_L from (3.20) using the different solutions that we obtained for $f(z, k^2)$.

Before we present the above QCD predictions for F_2 and F_L we must note that they are not the only contributions to the structure functions. They simply represent the leading $\log(1/x)$ gluon contributions, which we denote $F_2^{[LL]}$ and $F_L^{[LL]}$. These contributions are indeed expected to dominate at small x, but they decrease rapidly with increasing x. The remaining contributions to the structure functions (which we denote F_2^{rem} and F_L^{rem}) are

calculated from the Altarelli-Parisi equations with the $1/z$ term omitted from the splitting function $P_{gg}(z)$. Again we use the "D_0" set of parton distributions [11,29].
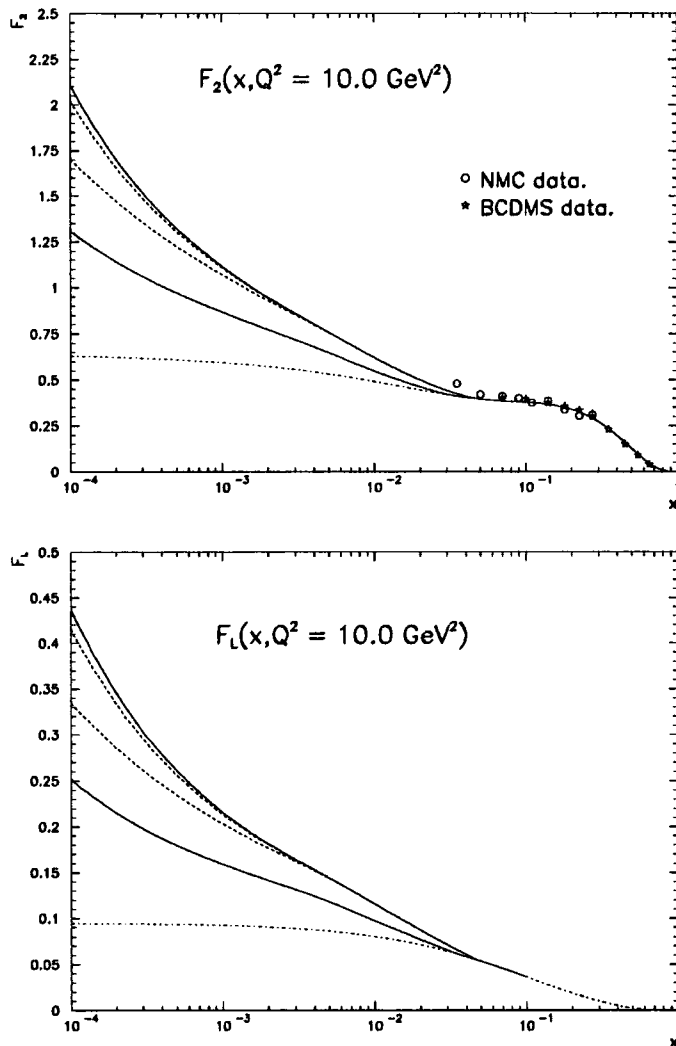
Figure 3.9: Perturbative QCD predictions of the behaviour of the structure functions $F_2(x, Q^2)$ and $F_L(x, Q^2)$ at $Q^2 = 10$ GeV^2 and small x. The continuous curves are with shadowing neglected, while the upper (lower) dashed curves have shadowing effects included with $R = 5$ GeV^{-1} ($R = 2$ GeV^{-1}). For the upper three curves the infrared cut-off in (3.24) is chosen to be $k_0^2 = 1$ GeV^2, while the lower of the two continous curves give the unshadowed result for $k_0^2 = 2$ GeV^2. The dash-dotted curves are the background (non-BFKL) contributions. The data are from the NMC [30] and the BCDMS collaboration [31] (and are for $Q^2 = 15$ GeV^2, to be exact).

102
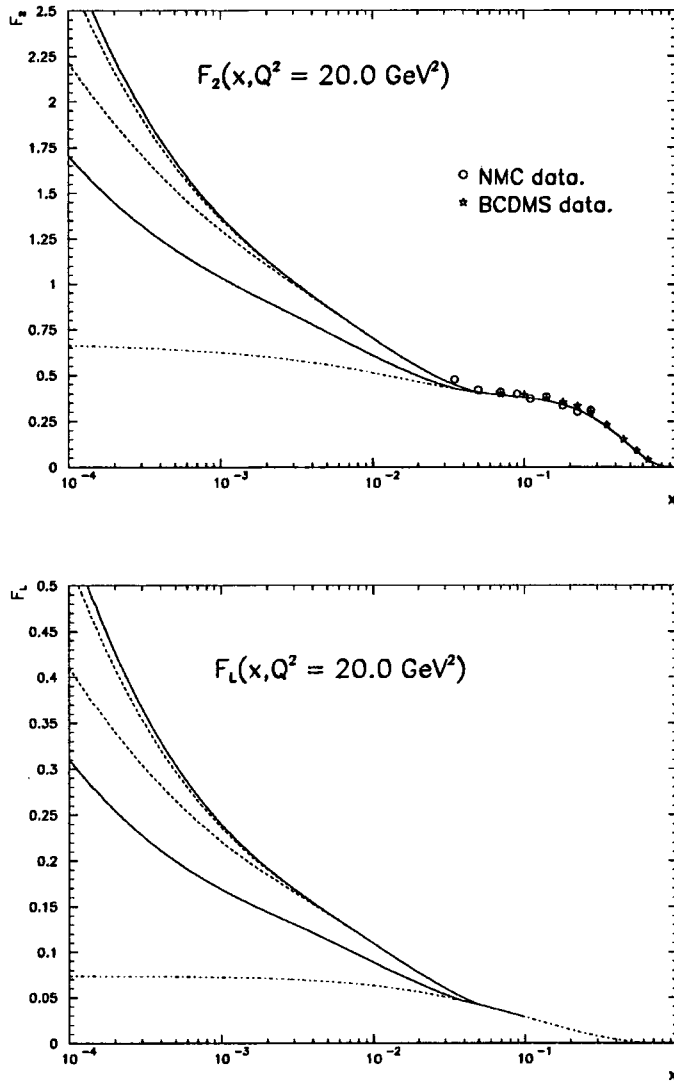
Figure 3.10: As for figure 3.5 but for $Q^2 = 20$ GeV^2.

The results at $Q^2 = 10$ and 20 GeV^2 are shown in figures 3.9 and 3.10 respectively. The background contributions F_2^{rem} and F_L^{rem} are shown by the dash-dotted curves. The agreement between the curves and the available data for F_2 shows that our input distributions for $x > x_0 = 0.01$ are satisfactory. The main purpose of this work is to use this "experimental" input to make theoretical extrapolations of $F_2(x, Q^2)$ and $F_L(x, Q^2)$ into the small x region based on perturbative QCD. The results are shown by the continuous curves in figures 3.9 and 3.10 if shadowing is neglected, and by dashed curves if shadowing effects are included. Two examples of shadowing are shown: conventional shadowing cor-

103

responding to gluons uniformly distributed through the entire proton ($R = 5$ GeV^{-1}) and a more extreme scenario in which they are concentrated in "hot spots" ($R = 2$ GeV^{-1}) within the proton. Recall that the shadowing term in (3.25) is proportional to $1/R^2$.

We may compare the results of figures 3.9 and 3.10 with extrapolations based on sets of partons obtained from global analyses of deep inelastic data, see for example MRS [11]. We see that the unshadowed predictions are similar to the parametric extrapolation based on the D$_-$ set of partons [11], see figure 3.1. Recall that for the D$_-$ set a $x^{-\frac{1}{2}}$ factor was specially incorporated into the gluon and sea quark "starting" distributions ($xg(x, Q_0^2)$ and $x\bar{q}(x, Q_0^2)$)) to mock up the shape due to the BFKL effect. The magnitude of the BFKL effect in F_2 obtained from the D$_-$ set is simply the result of extrapolation of a phenomenologically-determined parametric form to small x; in contrast in this work we solve the BFKL equation in the small x region with phenomenologically-determined boundary conditions at $x = x_0$. From figures 3.9 and 3.10 we see that our predictions of the shadowing corrections are significantly smaller than those obtained in MRS [11] (or KMRS [32]). The present calculation has the advantage that it does not depend on assumed input parametric forms at $Q^2 = Q_0^2$ in the small x region. Rather our extrapolation is based on the known phenomenological behaviour for $x > x_0$ and follows directly from solving the BFKL equation with shadowing terms incorporated. In this sense it may be regarded as an "absolute" prediction.

The origin of the larger shadowing corrections found in the MRS [11] (and KMRS [32]) structure function analyses can be traced to the assumption that the sea quark "starting" distributions in the region $x < x_0$ are taken to have shadowing corrections proportional to those of the gluon, that is

$$\bar{q}_{\text{shad}}(x, Q_0^2) = \bar{q}_{\text{unshad}}(x, Q_0^2) \frac{g_{\text{shad}}(x, Q_0^2)}{g_{\text{unshad}}(x, Q_0^2)},$$

see eq. (35) of ref. [32]. It could be argued that a more reliable estimate would have been to take the argument of x in the gluon to be significantly greater than that of the sea quark to allow for the effects of the $g \rightarrow q\bar{q}$ convolution. In contrast, in the present calculation the effects of the $g \rightarrow q\bar{q}$ convolution are automatically included, by construction, and so the shadowing predictions should be more reliable than previous estimates. Actually

even the shadowing of the gluon distribution calculated dynamically turns out [12] to be smaller than that found in the parametrization adopted by KMRS [32] and MRS [11]. This explains the weaker shadowing corrections in the longitudinal structure function than that found in refs. [32, 11].
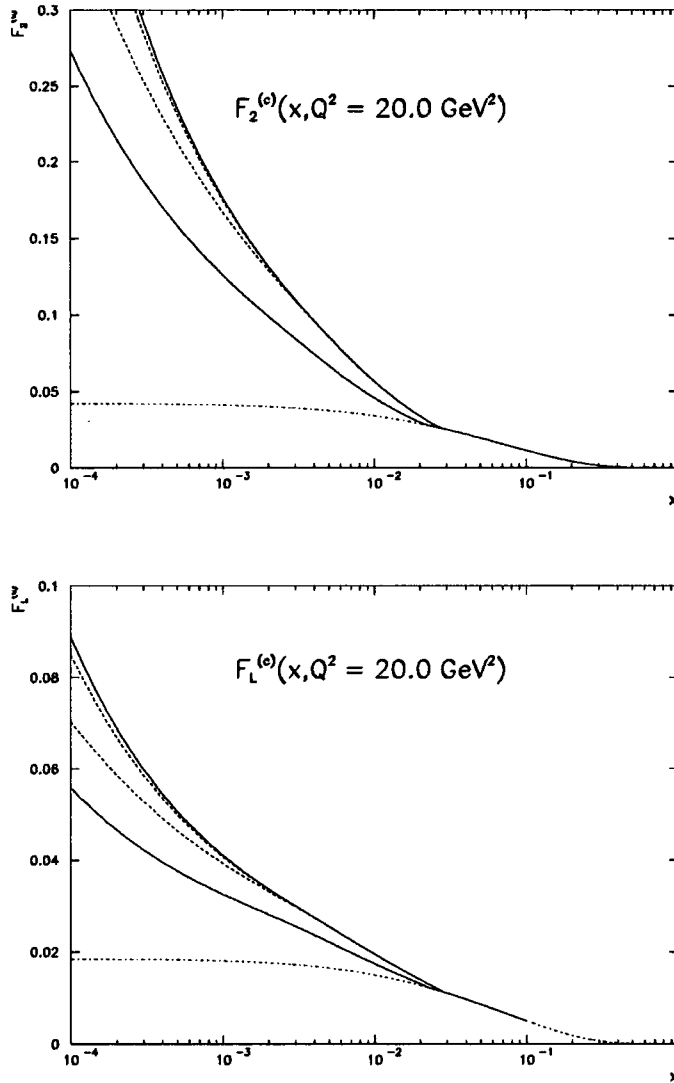
Figure 3.11: As for figure 3.10, but showing only the $c\bar{c}$ contribution to $F_2(x, Q^2)$ at $Q^2 = 20 \text{ GeV}^2$.

Our perturbative QCD estimates may appear to be parameter free and to give, in principle, "absolute" extrapolations of F_2 and F_L into the small x region. In practice there are significant ambiguities associated with the infrared (or non-perturbative) region. There is a dependence on the choice of cut-off k_0^2 in (3.24) used to calculate $f(x', k^2)$ and

105

in the convolution formulae of (3.20). For example the lower continuous curves in figures 3.9 and 3.10 show the reduction in the estimates of F_2 and F_L arising from increasing k_0^2 from 1 to 2 GeV^2. The reduction can be traced equally to (i) the change of effective slope and magnitude of the solution $f(z, k^2)$ of the BFKL equation, and (ii) infrared effects in the convolution integrals in (3.20).

Moreover our estimates depend on contributions from low values of κ' in (3.20). To quantify this dependence we introduce a non-zero mass m_q for the light quarks. For example if we were to change m_q from 0 to 1 GeV^2 our predictions for F_2 at $x \sim 10^{-3}$ would decrease by about 20%. This latter uncertainty is absent in the $c\bar{c}$ contribution, which we show separately in figure 3.11. Further discussion of heavy quark production, which incorporates the small x BFKL effects can be found in refs. [13,14,33] (see also [34]).

3.4.1: Discussion

We have applied the factorization formula (3.1) to give an estimate of the deep-inelastic structure functions F_i at small x, using the phenomenologically determined parton distributions at larger x, that is in the region $x > 0.01$ or so. The procedure we followed is to first solve the BFKL equation to determine the (unintegrated) gluon distribution f in the small x region and then to convolute the result with exact gluon-virtual photon couplings $F_i^{(0)}$ as determined by the quark box diagrams. Symbolically formula (3.1) may thus be written in the form

$$F_i \;=\; f \otimes F_i^{(0)}, \tag{3.64}$$

with $i = 2$ or L.

The above determination of the structure functions F_i at small x should be compared with the extrapolations based on the Altarelli-Parisi equations alone. The Altarelli-Parisi equations give the log Q^2 evolution of parton densities in terms of a set of "starting" distributions at some scale $Q_0^2 \gg \Lambda_{QCD}^2$, chosen sufficiently high for perturbative QCD to be applicable. In this way the x, Q^2 behaviour of parton densities are given in terms of parametric forms at $Q^2 = Q_0^2$ with the parameters determined by fitting to the deep inelastic structure function data. At present, however, the data do not extend into the small

x region (for $Q^2 \gg \Lambda_{QCD}^2$), and the expectations for the structure functions at small x are therefore entirely dependent on the particular parametric forms that are assumed for the $x \to 0$ behaviour of the gluon and sea quark distributions. The parametric forms, although theoretically motivated, are to a large extent arbitrary. Consequently extrapolations into the small x domain from the region of the available data can, at best, just indicate general trends.

In contrast, the small x behaviour of the structure functions obtained via the factorization formula (3.64) results directly from QCD dynamics, at least in principle. Here the (unintegrated) gluon distribution, f, is calculated at small x by evolving the BFKL equation in $\log(1/x)$ from boundary conditions at $x = x_0 = 0.01$ which are specified by parton distributions determined from data at $x > x_0$. We therefore have, via (3.64), a theoretical prediction of the small x behaviour of the structure functions $F_{2,L}(x, Q^2)$ with the normalisation determined by the data at larger x. In particular we are able to make, for the first time, a quantitative prediction of the size of the shadowing corrections to F_2 and F_L. These corrections are found to be smaller than previous estimates and are almost certainly undetectable from structure function measurements at $x \sim 10^{-3}$.

Although the procedure to calculate F_2 and F_L is well-defined, in practice there are ambiguities (which, however, should not alter the conclusion concerning the relative size of the shadowing corrections). First we have the dependence on the lower cut-off k_0^2 required for the integration over the transverse momentum in the BFKL equation, (3.24), for $f(x, k^2)$. The exchanged gluons along the ladder are required to have transverse momenta of magnitude greater than k_0. The value of λ in the effective $x^{-\lambda}$ behaviour which emerges for f at small x is sensitive to the choice of k_0^2. For instance if k_0^2 is chosen to be 0.5, 1 or 2 GeV^2 we find, after numerically solving the BFKL equation, that $\lambda = 0.54, 0.46$ or 0.41 respectively. Moreover the same cut-off is necessary in the k_T convolution integrals in (3.20). The k_0^2-dependent ambiguity is displayed in figures 3.9 and 3.10. The uncertainty is a reflection of uncalculable non-perturbative QCD effects.

A second ambiguity has its origin in the different Q^2 dependences which occur in the small and larger x regions. It is well-known [12] that the Q^2 dependence of the gluon distribution which emerges from the BFKL equation is more rapid than that which results from the Altarelli-Parisi equation. However we have required the solution of the BFKL equation to satisfy boundary conditions at $x = x_0 = 0.01$ which are obtained from the

107

Altarelli-Parisi equation. Although the continuity of $f(x, Q^2)$ is ensured at $x = x_0$, the differing Q^2 dependences lead to artificial structure in the x dependence just below the boundary, $x = x_0$. Only for a small region of Q^2 will smoothness across the boundary be obtained [12]. Fortunately the region is $Q^2 = 10\text{-}20$ GeV^2, the region most pertinent to experiments at HERA. Since $F_2^{[LL]}$ is a relatively small contribution at $x = 0.01$ the artificial structure would be barely noticeable in $F_2(x, Q^2)$ at the other values of Q^2. The main reason to draw attention to the deficiency is that it points to other contributions which could be important. The source of the problem is that the BFKL equation is based on the leading $\log(1/x)$ approximation, while to obtain a reliable Q^2 dependence it is necessary to include non-leading $\log(1/x)$ contributions. Eventually it should be possible to overcome this problem by solving a more general evolution equation [9] for the gluon distribution which embodies both BFKL effects and the complete Altarelli-Parisi equation.

In summary we have formulated a procedure, based on perturbative QCD, which makes predictions of the structure functions $F_{2,L}(x, Q^2)$ for deep-inelastic electron-proton scattering in the small x regime. In principle, the procedure overcomes the considerable uncertainties associated with the conventional parametric extrapolations to small x. In practice, we have seen it has its own ambiguities. The predicted values of the structure functions at $Q^2 = 10$ and 20 GeV^2, including the effects of shadowing and displaying the theoretical uncertainties, are shown in figures 3.9 - 3.11.

3.5: Numerical predictions (II).

3.5.1: Treatment of the infrared region.

We shall use a running coupling $\alpha_s(k^2)$ in the BFKL equation and so we will need to focus attention on how to deal with the infrared region. The simplest procedure [35] is to introduce a cut-off k_0^2 (as in section 3.4) so the BFKL equation becomes

$$-x\frac{\partial f}{\partial x} = \frac{3\alpha_s(k^2)}{\pi}k^2 \int_{k_0^2}^{\infty} \frac{dk'^2}{k'^2}\left[\frac{f(x,k'^2)-f(x,k^2)}{|k'^2-k^2|} + \frac{f(x,k^2)}{(4k'^4+k^4)^{\frac{1}{2}}}\right] \quad (3.65)$$

where (for simplicity) the same cut-off is used in the real emission term and in the virtual corrections. To calculate F_2 we would impose the same cut-off on the convolution integral (3.47) which occurs in the k_T-factorization theorem.

The above cut-off which completely eliminates the infrared region $k^2 < k_0^2$ is rather drastic. Clearly a better procedure which incorporates this region, at least in an approximate way, is desirable. The problem is that the BFKL equation is not expected to be valid when the gluon momenta enter the non-perturbative region of small k^2. One way to overcome the problem is to introduce 'non-perturbative' (albeit phenomenological) gluon propagators which are finite at $k^2 = 0$ [36, 37] and hence to eliminate the potential infrared singularities of the solution. The most systematic procedure however is to somehow factor out the nonperturbative region in a similar manner as happens in the DGLAP equations. Some progress along these lines has been made in [14, 27].

During the Durham workshop "HERA - the new frontier for QCD" our discussions (in particular with Jochen Bartels, Jeff Forshaw and Genya Levin) focussed on the problems with the BFKL equation due to the region of small transverse momenta. The notion was put forward that accounting for the constraint that the solution of the BFKL equation (and the driving term) vanish as $k^2 \to 0$ ought to suppress the importance of this region [38]. This requirement that

$$f(x, k^2) \sim k^2 \qquad \text{as } k^2 \to 0 \quad (3.66)$$

is a consequence of gauge invariance or to be precise of the colour neutrality of the probed proton [6, 10]. In the present section then, we attempt to go beyond the simple k^2 cutoff

109

approximation and to model the low k^2 region in a more systematic fashion. We assume that the small-k^2 behaviour of the gluon distribution is driven by a form factor $G(k^2)$ such that

$$f(x, k^2) \sim \text{Const.} \ [1 - G(k^2)] \tag{3.67}$$

for $k^2 \to 0$. We take

$$1 - G(k^2) = 1 - \frac{k_a^2}{k^2 + k_a^2} = \frac{k^2}{k^2 + k_a^2}, \tag{3.68}$$

where the parameter k_a^2 is related to the radius of the gluonic form factor of the proton. If this is taken to be of the same magnitude as the radius characterising the hadronic electromagnetic form factor then we would have $k_a^2 \simeq 0.5$ GeV^2; however estimates based on the QCD sum rules prefer a larger value, $k_a^2 \simeq 1 - 2$ GeV^2.

We then proceed by splitting the integration region for real gluon emission (the term involving $f(x, k'^2)$) in (3.65) up into two parts, namely

Region(A) : 0 to k_0^2

Region (B) : k_0^2 to ∞.

In region (B) the BFKL equation as it stands is taken to hold. In region (A) we assume that k_0^2 is sufficiently small that the behaviour given in (3.67) is a good approximation. If we parametrise $f(x, k'^2 < k_0^2)$ in this form, then the integral (A) can be calculated analytically, and in this way we have a physically motivated approximation for the infrared contribution to the BFKL equation (3.65). As a further modification to the low-k^2 region we 'freeze' the argument of α_s by using $\alpha_s(k^2 + a^2)$, with $a^2 = 1$ GeV^2, in both the evolution equation and in the factorisation formula (3.47) used to calculate F_2 and F_L.

The modified BFKL equation can then be used to evolve the gluon distribution down in x starting from a suitable input distribution $f(x_0, k^2)$. This boundary condition must be consistent with Altarelli-Parisi evolution for large k^2, that is

$$f^{\text{AP}}(x_0, k^2) = \left. \frac{\partial(x_0 g(x_0, Q^2))}{\partial \log Q^2} \right|_{Q^2 = k^2 \gg \Lambda^2} \tag{3.69}$$

where we take $g(x_0, Q^2)$ from the Altarelli-Parisi evolution of MRS partons [29]. The

boundary condition must also have a small k^2 behaviour consistent with our approximations, so we take

$$f(x_0, k^2) = (1 - G(k^2))f^{\mathrm{AP}}(x_0, k^2 + a^2) \qquad (3.70)$$

for $k^2 > k_0^2$, whereas for $k^2 < k_0^2$ we "freeze" the evolution of f^{AP} at $k_0^2 + a^2$. The parameter $a^2 = 1$ GeV^2 just softens the low-k^2 behaviour of f^{AP} which tends to be unreliable. The important fact is that the input distributions approach $f^{\mathrm{AP}}(x_0, k^2)$ for large k^2, as they must, and also embody a suitable behaviour for smaller k^2.

In preparation to see the diffusion in k^2 develop as we proceed to small x, we plot the boundary conditions in the form $f(x_0, k^2)/(k^2)^{\frac{1}{2}}$ as suggested by (3.46). Sample distributions are shown in Fig. 3.12 for different choices of k_a^2 and k_0^2.
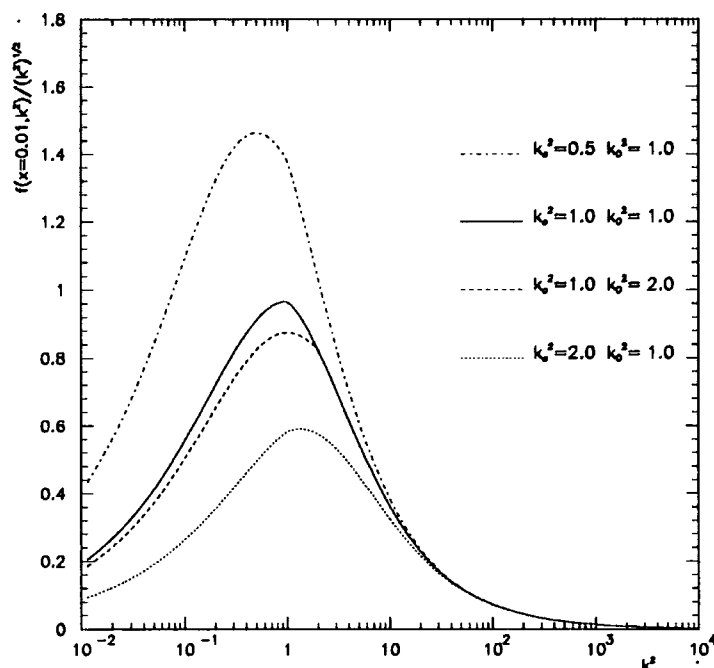

Figure 3.12: The boundary conditions for $f/(k^2)^{\frac{1}{2}}$ at $x = 0.01$ used to solve the modified BFKL equation, for various choices of k_a^2 and k_0^2. ($k_0^2 = 1$ GeV^2 where it is not specified).

We see the input distributions have an approximate Gaussian form in $\log k^2$. Fig. 3.13 shows the evolution of the distribution, for the choice $k_a^2 = k_0^2 = 1$ GeV^2, as we proceed to smaller x using (3.65) and (3.67). We see both the diffusion to large k^2 and the $x^{-\lambda}$ type growth. There is no diffusion into the infrared region since we impose the phenomenological form

(3.67). The diffusion to large k^2 is more apparent in Fig. 3.14 which shows the distributions of Fig. 3.13 normalised to a common value. Even in the limit of very small x, the rate of this diffusion will differ from that given by the analytic form (3.46), since here we are using a running coupling α_s.
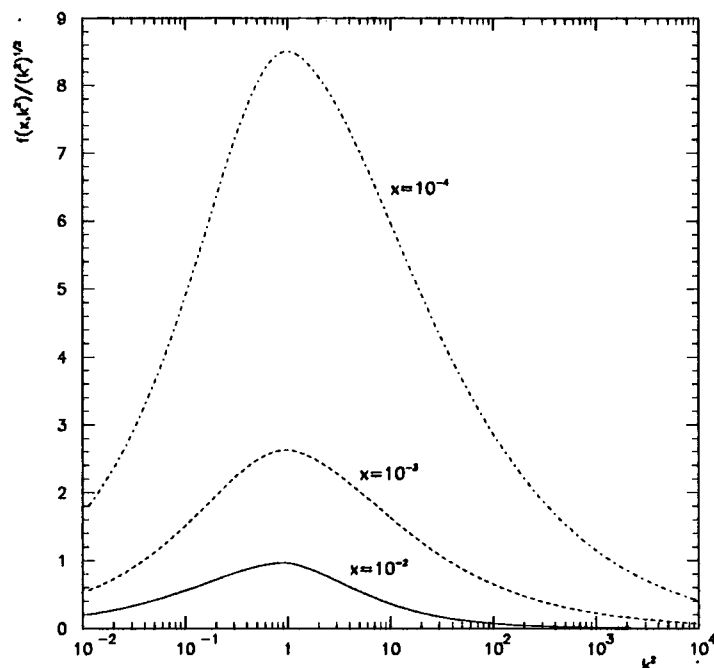
Figure 3.13: The evolution of $f/(k^2)^{\frac{1}{2}}$ as we step down in x using the modified BFKL equation with $k_a^2 = k_0^2 = 1 \ \mathrm{GeV}^2$.
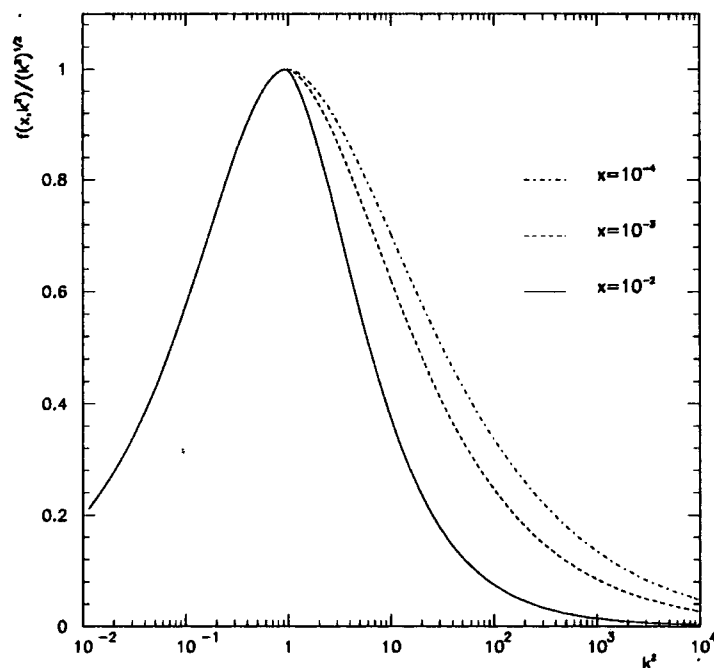
Figure 3.14: As for Fig. 3.13 but with the distributions normalised to a common value at $k^2 = 1$ GeV^2.

112

# 3.5.2: Consistency constraint on the infrared region.

The numerical solution $f(x, k^2)$ of the BFKL equation, modified as above, is found to be much more sensitive to the choice of k_a^2 than to k_0^2, see ref. [39]. Therefore here we choose $k_0^2 = 1$ GeV^2, and we concentrate on investigating the sensitivity of the results to variations of k_a^2. However as may be anticipated from the discussion in section 3.3 it is the magnitude of f, and not the shape, which is particularly sensitive to k_a^2. That is, with decreasing x, an $x^{-\lambda}$ behaviour sets in with a numerical value of λ only weakly dependent on k_a^2 [39].

There is a consistency requirement between the "input" and "output gluon" which, in principle, can be used to estimate the value of k_a^2. The constraint is that the gluon distribution calculated from

$$xg(x, Q^2) \simeq \int_0^{Q^2} \frac{dk^2}{k^2} f(x, k^2), \tag{3.71}$$

the inverse relation to (3.69), should match the phenomenological input gluon distribution. The comparison is shown in Fig. 3.15 for different choices of k_a^2. Here we use as input at $x_0 = 0.01$ a gluon [29] satisfying the leading order Altarelli-Parisi equations (the dotted curve), but based on the D$_0$ type parametrizations of ref. [11]. Fig. 3.15 shows that there is good agreement between the "input" and "output" gluons for $k_a^2 \approx 1$ GeV^2. (In Fig3.15 we also compare our input gluon with the gluons of the D$_0'$ and D$_-'$ next-to-leading order analyses of ref. [40]). In practice, it would be misleading to impose this constraint too rigorously. The input gluon is not well known at $x_0 = 0.01$, particularly at the low values of Q^2 which are necessary for this comparison. Nevertheless it is encouraging that the estimate of k_a^2 appears reasonable, and suggests that we should consider QCD predictions with k_a^2 chosen in a range of about 0.5 to 2 GeV^2.
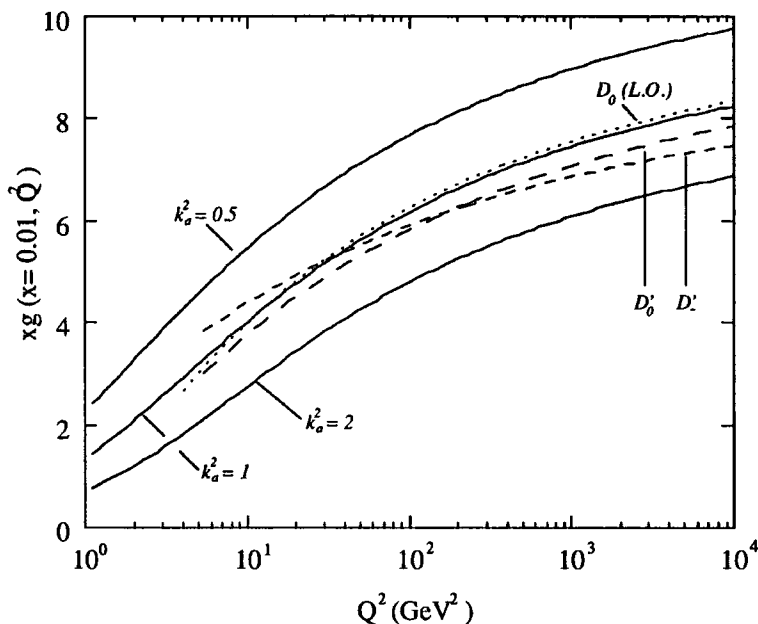
Figure 3.15: The self consistency of the gluon at $x = 0.01$. The dotted curve is the input gluon [29] and the continuous curves show the output gluon obtained from $f(x, k^2)$ via (3.71), where f itself is determined from the input gluon with different choices of k_a^2 (but with $k_0^2 = 1$ GeV^2). The dashed curves, which correspond to the D$_0'$ and D$_-'$ gluons of ref. [40], are to illustrate the ambiguity in the input gluon.

3.5.3: Numerical predictions for structure functions.

We may use the solution $f(x, k^2)$ of the modified BFKL equation to predict the structure functions $F_i(x, Q^2)$ at small x via the factorization theorem (3.47). The factorization formula has the symbolic form

$$F_i^{[LL]} = f \otimes F_i^{(0)} \tag{3.72}$$

and gives the contribution to F_i arising from the BFKL resummation of soft gluons. Recall that $F_i^{(0)}$ describes the quark box (and "crossed" box) photon-gluon fusion process shown in the upper part of Fig. 3.10a. The gluon is off-mass-shell with virtuality approximately equal to k'^2. The explicit formula for $F_i^{(0)}(x', k'^2, Q^2)$ can be found in refs. [13, 35] and section 3.2.

114

Before we can obtain a realistic estimate for the structure functions F_i we must include the background non-BFKL contributions F_i^{Bg}. A reasonable choice at small x is to assume that F_i^{Bg} gradually increases like $x^{-0.08}$ with decreasing x (as might be expected from a "soft" pomeron with intercept $\alpha_P(0) = 1.08$ [41]). To be precise we take

$$F_i^{\mathrm{Bg}}(x, Q^2) \;=\; F_i^{\mathrm{Bg}}(x_0, Q^2)(x/x_0)^{-0.08} \tag{3.73}$$

with $x_0 = 0.1$. The values we use for $F_i^{\mathrm{Bg}}(x_0, Q^2)$ are listed in the figure captions. The resulting predictions for the small x behaviour of $F_i = F_i^{[LL]} + F_i^{\mathrm{Bg}}$ with $i = 2, L$ are shown in Figs. 3.16 - 3.19 for various values of Q^2. In each figure the continuous curves show the predictions for two choices of the infrared parameter k_a^2, namely $k_a^2 = 1$ and 2 GeV^2.
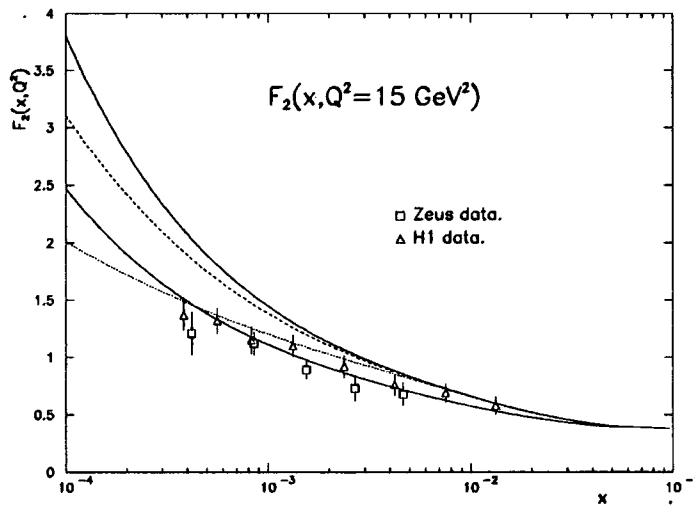
Figure 3.16: The perturbative QCD predictions for $F_2(x, Q^2)$ at $Q^2 = 15$ GeV^2 obtained from the k_T factorisation formula, (3.47). The continuous curves correspond to the infrared parameter $k_a^2 = 1$ and 2 GeV^2 respectively, with shadowing neglected. The dashed curves show the suppression caused by conventional ($R = 5$ GeV^{-1}) and "hot-spot" ($R = 2$ GeV^{-1}) shadowing for the choice $k_a^2 = 1$ GeV^2. The data are from the H1[42] and ZEUS [43] collaborations. The background contribution is given by (3.73) with $F_2^{\mathrm{Bg}}(x_0) = 0.384$.

115
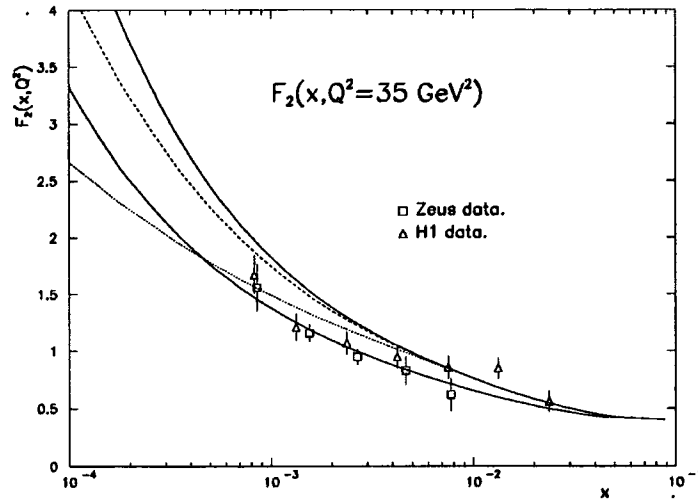
Figure 3.17: As for Fig. 3.16 but for $Q^2 = 35$ GeV^2 with $F_2^{Bg}(x_0 = 0.1) = 0.391$.

The recent HERA measurements of F_2 are shown on Figs. 3.16 and 3.17. There is general agreement between QCD and the data. In particular they both show a dramatic increase with decreasing x, and lie well above a straightforward extrapolation of the fixed target measurements that exist for $x > 10^{-2}$ [30, 31]. Certainly the data indicate support for the $x^{-\lambda}$ type behaviour arising from the BFKL leading $\log(1/x)$ resummation. But before we draw conclusions we must consider the effects of shadowing corrections.
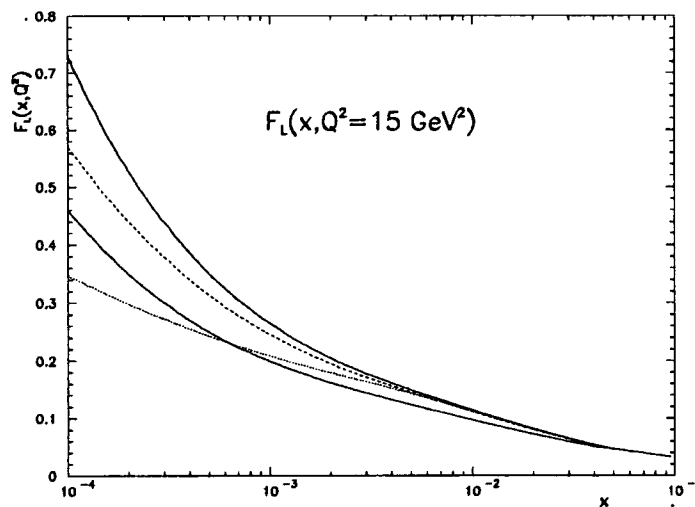
Figure 3.18: The curves are as for Fig. 3.16 but for the longitudinal structure function $F_L(x, Q^2 = 15\text{GeV}^2)$. The background contribution is given by (3.73) with $F_L^{Bg} = 0.04$ at $x_0 = 0.1$ and $Q^2 = 15$ GeV^2. **116**
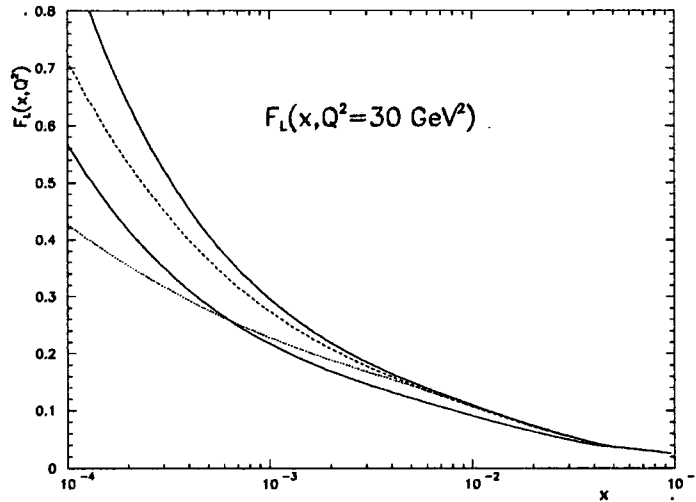
Figure 3.19: As for Fig. 3.18 but at $Q^2 = 30$ GeV^2.

3.5.4: Inclusion of shadowing.

The growth of the gluon density with decreasing x means that there is an increased probability that the gluons will interact and recombine. To allow for the effects of this recombination or parton shadowing we incorporate an additional term in (3.65)

$$-x\frac{\partial f(x, k^2)}{\partial x} = K \otimes f - \frac{81}{16k^2 R^2}\alpha_s^2(k^2)[xg(x, k^2)]^2 \qquad (3.74)$$

where g is given by (3.71). The additional term, quadratic in g, in (3.74) is the leading order shadowing approximation; the negative sign leading to a suppression in the growth of the gluon density with decreasing x. The crucial parameter is R, where πR^2 specifies the transverse area in which the gluons are concentrated within the proton.

For illustration we take $R = 5$ GeV^{-1} (corresponding to gluons uniformly spread across the proton) and $R = 2$ GeV^{-1} (assuming the gluons are concentrated in "hot-spots" within the proton). The dashed curves in Figs. 3.16 - 3.19 show the effect of these two shadowing scenarios respectively on the $k_a^2 = 1$ GeV^2 prediction. We note that the shadowing effects are now slightly stronger than in the case [35] when the region of small k'^2 was entirely neglected. However shadowing is still rather a weak effect in the HERA regime and sets in

117

very gradually, unless compact "hot-spots" of gluons occur. In particular we are far from the saturation limit.

We have found [39] that $F_2^{[LL]}$ behaves like $Cx^{-\lambda}$ for $x \lesssim 10^{-3}$ where the predicted value of λ is relatively insensitive to the uncertainties associated with the infrared region. The inclusion of shadowing means that λ is no longer constant but that its value decreases with decreasing x, as illustrated by the dashed curves. The predictions for $Q^2 = 15$ GeV^2 (and $k_a^2 = 1$ GeV^2) are shown in Fig. 3.20. Conventional shadowing ($R = 5$ GeV^{-1}) has relatively little impact on λ, and even if "hot-spots" were to exist λ remains significantly above the soft-pomeron expectation of 0.08.
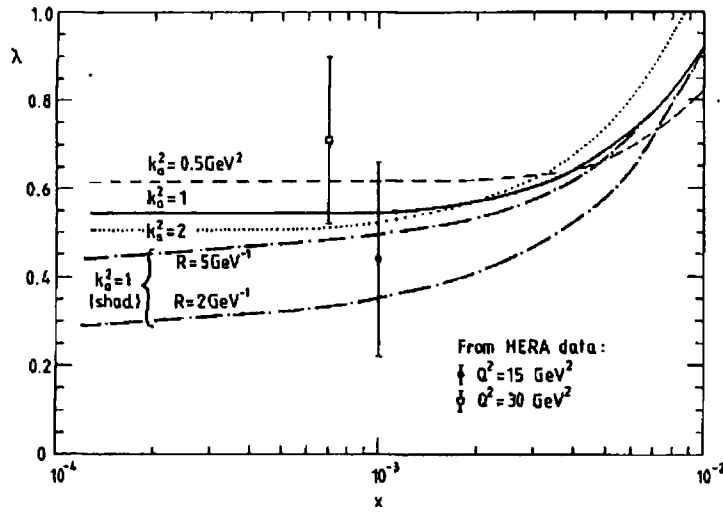
Figure 3.20: The effective slope λ, defined by $F_2 = F_2^{Bg} + Cx^{-\lambda}$ where F_2^{Bg} is given by (3.73), for various choices of the infrared parameter k_a^2. The lower two (dot-dashed) curves show the effect of the conventional ($R = 5$ GeV^{-1}) and "hot-spot" ($R = 2$ GeV^{-1}) shadowing on the $k_a^2 = 1$ GeV^2 predictions. The "data" points are calculated from the H1 and ZEUS data shown in Figs. 3.16 and 3.17.

We have checked that the large values of λ, which are essentially independent of x for $x \leq 10^{-3}$, remain true for other physically reasonable choices of the background $F_2^{Bg}(x, Q^2)$. Indeed the values of λ obtained in Fig. 3.20 are much larger than would result from any straightforward extrapolation of the fixed target F_2 data to small x. Consider for example the value of λ obtained from the extrapolation of the D_0' set of MRS partons [40] to small x. (The D_0 partons provide an excellent description of the fixed tar-

get data which only exist for $x > 10^{-2}$). The parton set D_0 develops, via Altarelli-Parisi evolution, a small x behaviour of the form

$$F_2 \sim \exp[2(\xi(Q_0^2, Q^2)\log(1/x))^{1/2}] \tag{3.75}$$

where the "evolution length"

$$\xi(Q_0^2, Q^2) = \int_{Q_0^2}^{Q^2} \frac{dQ'^2}{Q'^2} \frac{3\alpha_s(Q'^2)}{\pi} \tag{3.76}$$

The increase of F_2 with decreasing x can be translated into an effective $x^{-\lambda}$ behaviour in the HERA regime. In fact the value of λ is found to be about 0.11 at $Q^2 = 15$ GeV^2 and 0.15 at $Q^2 = 30$ GeV^2; slightly increasing with Q^2 on account of the increase in the evolution length $\xi(Q_0^2, Q^2)$. Note that these small values of λ rely on the choice of a sufficiently large value of Q_0^2, for instance MRS evolve from $Q_0^2 = 4$ GeV^2.

However GRV [16] have obtained partons by evolving from a valence like input at $Q_0^2 = 0.3$ GeV^2. The very low value of Q_0^2 corresponds to a relatively large evolution length $\xi(Q_0^2, Q^2)$ for Q^2 in the HERA region i.e. $Q^2 \sim 20$ GeV^2. In this way they obtain a steeper small x behaviour for F_2 (see (3.75) and (3.76)) compatible with the data. In fact this double leading log. behaviour mimics an $x^{-\lambda}$ form with $\lambda \sim 0.4$ in HERA regime. However we do not believe that this is an acceptable explanation of the data since the steepness is mainly generated in the very low Q^2 region where perturbative QCD is invalid (see, for example, [18] and subsection 1.2.2).

In order to obtain the steep $x^{-\lambda}$ type behaviour with $\lambda \sim 0.5$ within the Altarelli-Parisi formalism (and when the evolution starts at moderately large value of $Q_0^2 \sim 5$ GeV^2) one has to impose this steep behaviour in the parametrisation of the starting gluon and sea-quark distributions at the reference scale Q_0^2 as it is done for instance in the case of the D_- set of MRS partons [11, 40]. In this procedure however one does not use the BFKL equation, that is the singular behaviour is not generated explicitly by QCD dynamics.

3.5.5: Discussion.

The recent measurements [42, 43] of the deep inelastic structure function F_2 at HERA explore the small x regime for the first time. The data show that F_2 increases as x

decreases from 10^{-2} to a few $\times 10^{-4}$, and do not follow a straightforward extrapolation of the fixed target measurements [30, 31] that exist above $x \sim 10^{-2}$. This novel behaviour is in line with the growth anticipated from perturbative QCD via the k_T-factorization formula, symbolically of the form

$$F_2 = f \otimes F_2^{(0)}, \tag{3.77}$$

which links the small x behaviour of F_2 with that of the universal unintegrated gluon distribution f via the quark box contribution $F_2^{(0)}$ to photon-gluon fusion. The growth of F_2 with decreasing x is thus associated with the BFKL leading $\log(1/x)$ summation of soft gluon emissions which yields the small x behaviour $f(x, k^2)) \sim x^{-\lambda}$ with $\lambda \sim 0.5$.

However the contribution from the infrared (low transverse momentum) region, which occurs in the convolution of (3.77), leads to a sizeable uncertainty in the predictions. Motivated by the apparent agreement between the data and the expectations of perturbative QCD, we have attempted to improve the treatment of the low k^2 regime. In particular, rather than imposing a low k^2 cut-off, we employ a physically motivated infrared form for $f(x, k^2)$ which allows us to extrapolate right down to $k^2 = 0$. This reduces the uncertainty in the predictions for F_2, although the normalisation still depends significantly on the choice of the value of an infrared (form factor) parameter k_a^2. However the effective slope λ which specifies the $x^{-\lambda}$ shape is much less sensitive to the ambiguities at low k^2. In Section 3.3 we gathered together general arguments which suggested that the slope might be relatively immune from infrared effects and in this section we have performed explicit numerical tests to verify the result.

In Figs. 3.16 and 3.17 we compared the perturbative QCD calculations for F_2 with the recent HERA data. The dramatic growth with decreasing x is apparent in both the data and the QCD predictions. The various curves show the sensitivity of the QCD determination to the variation of the infrared cut-off and to shadowing effects. Fig. 3.20 translates these results into a comparison for λ [where λ is defined by the the $x^{-\lambda}$ growth of the BFKL component of $F_2(x, Q^2)$]. We see that QCD indeed predicts an approximate $x^{-0.5}$ behaviour at small x (or in the extreme case of "hot-spot" shadowing an $x^{-0.3}$ type growth with decreasing x).

120

The results from HERA are very encouraging and suggest that H1 and ZEUS may have seen the first evidence for the BFKL growth arising from the leading $\log(1/x)$ soft gluon resummation. Figs. 3.16, 3.17 and 3.20 should be regarded as an indication of what may be learnt when much higher statistics data become available and allow a detailed comparison. At the moment it is only possible to make predictions in the leading $\log(1/x)$ approximation. Much effort is being devoted to obtaining the next-to-leading contributions and, when available, these should be incorporated. Inspection of Fig. 3.20 suggests that, from a study of the x dependence of λ for $x \leq 10^{-3}$, we may then be able to quantify the effects of shadowing.

3.6: Scaling violations.

The first measurements of the proton structure function $F_2(x, Q^2)$ at small x have been made by the H1[44] and ZEUS[45] collaborations at HERA. A striking increase of F_2 with decreasing x is observed which is consistent with the expectations of perturbative QCD at small x as embodied in the BFKL equation. This equation effectively performs a leading $\alpha_s \log(1/x)$ resummation of soft gluon emissions, which results in a small x behaviour $F_2 \sim x^{-\lambda}$ with $\lambda \sim 0.5$.

The data at $Q^2 = 15$ and 30 GeV^2 are shown in figure 3.21 together with a representative set of predictions and extrapolations, whose distinguishing features we elucidate below. These curves fall into two general categories. The first, category (A), is phenomenological and is based on parametric forms extrapolated to small x with Q^2 behaviour governed by the next-to-leading order Altarelli-Parisi equations. The parameters are determined by global fits to data at larger x (examples are the curves in figure 3.21 labelled MRS(D$'_-$)[40], MRS(H)[46] and, to some extent, also GRV[16], but see below). The second approach, denoted (B), is, in principle, more fundamental. Here perturbative QCD is used in the form of the BFKL equation to evolve to small x from known behaviour at larger x (e.g. AKMS[35]). In other words in approach (A) the small x behaviour is input in the parametric forms used for the parton distributions at some scale $Q^2 = Q_0^2$, whereas in (B) an $x^{-\lambda}$ behaviour at small x is generated dynamically with a determined value of λ. Of course in the phenomenological approach, (A), it is possible to input a BFKL-motivated small x behaviour into the starting distributions (e.g. MRS(D$'_-$) and MRS(H) have $xg, xq_{\text{sea}} \sim x^{-\lambda}$ with $\lambda = 0.5$ and 0.3 respectively). Since the $x^{-\lambda}$ behaviour, for these values of λ, is stable to evolution in Q^2 we may anticipate that it will be difficult to distinguish approaches (A) and (B). However the Q^2 behaviour (or scaling violations) of F_2 is, in principle, different in the two approaches.
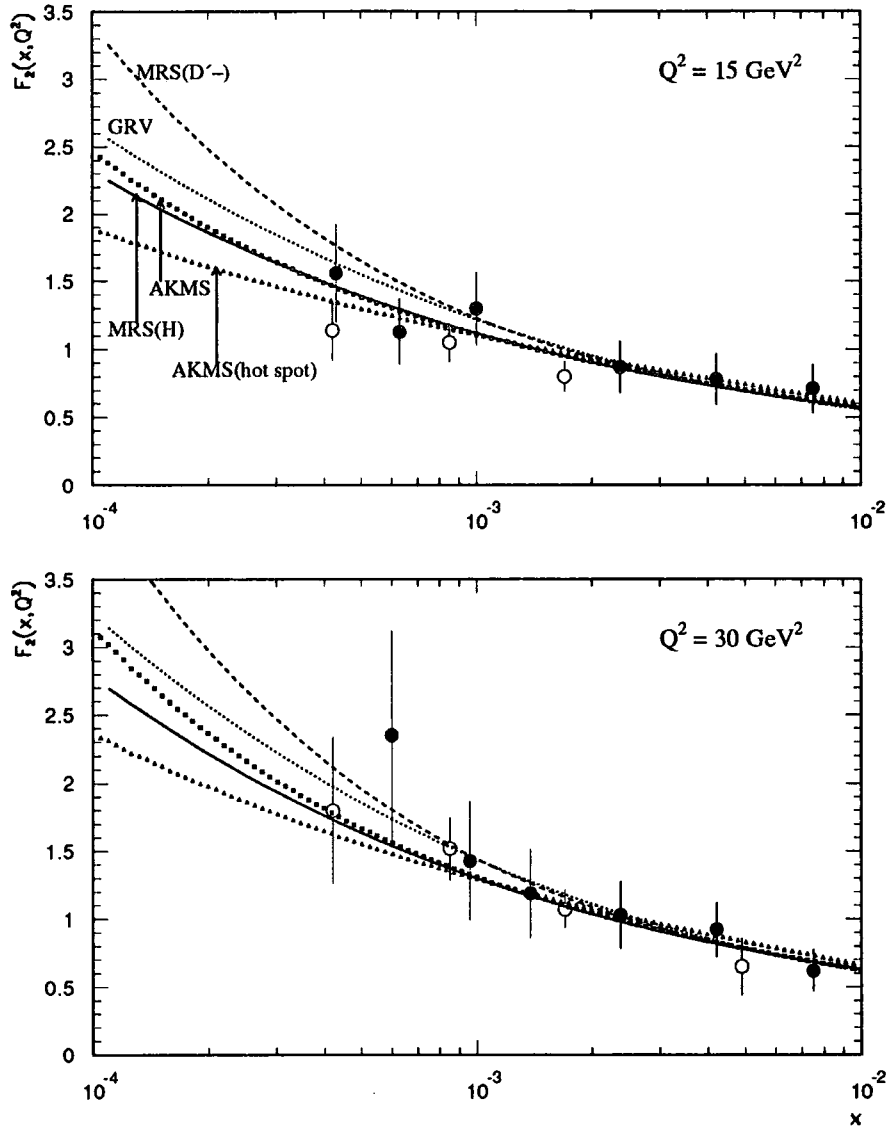
Figure 3.21: The measurements of $F_2(x, Q^2)$ at $Q^2 = 15$ and 30 GeV^2 by the H1[44] and ZEUS[45] collaborations shown by closed and open data points respectively, with the statistical and systematic errors added in quadrature; the H1 and ZEUS data have a global normalization uncertainty of $\pm 8\%$ and $\pm 7\%$ respectively. The continuous, dotted and dashed curves respectively correspond to the values of F_2 obtained from MRS(H)[46], GRV[16] and MRS(D$'_-$)[40] partons. The curves that are shown as a sequence of small squares (triangles) correspond to the unshadowed (strong or "hot-spot" shadowing) AKMS predictions obtained by computing $F_2 = f \otimes F_2^{(0)} + F_2$(background) as in ref.[39] and as described in the text.

The Altarelli-Parisi Q^2 evolution is controlled by the anomalous dimensions of the splitting functions (and by the coefficient functions) which have been computed perturbatively up to next-to-leading order. On the other hand the BFKL approach, at small x, corresponds to an infinite order resummation of these quantities, keeping only leading $\log(1/x)$ terms. Summing the leading $\log(1/x)$ terms, besides generating an $x^{-\lambda}$ behaviour, gives its own characteristic Q^2 dependence. One of our main purposes is to study whether or not the BFKL behaviour, which may be more theoretically valid at small x, can be distinguished from the approximate Altarelli-Parisi parametric forms which neglect the $\log(1/x)$ resummation.

If we were to assume that Altarelli-Parisi evolution is valid at small x then

$$\frac{\partial F_2(x, Q^2)}{\partial \log Q^2} \simeq 2 \sum_q e_q^2 \frac{\alpha_s(Q^2)}{2\pi} \int_x^1 \frac{dy}{y} \frac{x}{y} P_{qg}\left(\frac{x}{y}\right) yg(y, Q^2) + \ldots , \qquad (3.78)$$

and hence the Q^2 behaviour of F_2 can be varied by simply exploiting the freedom in the gluon distribution at small x. However the situation is much more constrained when the BFKL equation is used to determine the (unintegrated) gluon distribution $f(x, k^2)$. Then F_2 may be calculated[35] using the k_T-factorization theorem[13]

$$F_2(x, Q^2) = \int_x^1 \frac{dx'}{x'} \int \frac{dk^2}{k^4} f\left(\frac{x}{x'}, k^2\right) F_2^{(0)}(x', k^2, Q^2) \qquad (3.79)$$

where x/x' and k are the longitudinal momentum fraction and transverse momentum that are carried by the gluon which dissociates into the $q\bar{q}$ pair, see figure 3.22. $F_2^{(0)}$ is the quark box (and crossed box) amplitude for gluon-virtual photon fusion[35].
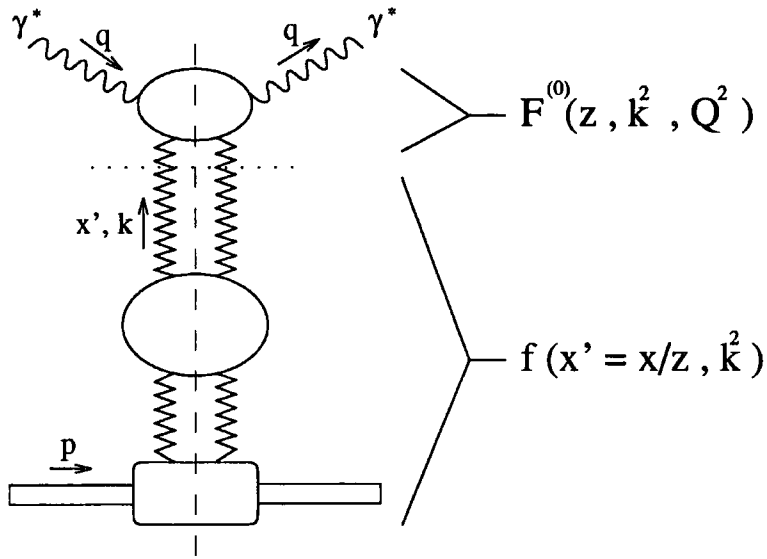
Figure 3.22: Diagrammatic display of the k_T-factorization formula (3.79), which is symbolically of the form $F_2 = f \otimes F_2^{(0)}$, where f denotes the gluon ladder and $F_2^{(0)}$ the quark box (and crossed box) amplitude.

In order to gain insight into the different possible Q^2 dependences of F_2 it is useful to introduce the moment function of the (unintegrated) gluon distribution

$$f(n, k^2) = \int_0^1 dx\, x^{n-2} f(x, k^2). \tag{3.80}$$

The evolution of the moment function is given by the renormalization group equation

$$f(n, k^2) = f(n, k_0^2) \exp\left[\int_{k_0^2}^{k^2} \frac{dk'^2}{k'^2} \gamma(n, \alpha_s(k'^2))\right] \tag{3.81}$$

where the anomalous dimension $\gamma(n, \alpha_s)$ is known. From eq.(3.81) we see that the behaviour at small x is controlled by the leading singularity of $f(n, k^2)$ in the n plane. In the leading $\log(1/x)$ approximation $\gamma(n, \alpha_s)$ is just a function of the single variable

$\alpha_s(k^2)/(n-1)$ and is determined by the BFKL kernel. Its value is such that[47]

$$1 - \frac{3\alpha_s(k^2)}{\pi(n-1)}\tilde{K}(\gamma) = 0 \tag{3.82}$$

is satisfied, with

$$\tilde{K}(\gamma) = 2\Psi(1) - \Psi(\gamma) - \Psi(1-\gamma), \tag{3.83}$$

where Ψ is the logarithmic derivative of the Euler gamma function.

For fixed α_s the leading singularity of $f(n, k^2)$ is a square root branch point at $n = 1 + \lambda_L$ where $\lambda_L = 3\alpha_s\tilde{K}(\frac{1}{2})/\pi = 12\alpha_s\log 2/\pi$. Comparing with eq.(3.82) we find that $\gamma(1 + \lambda_L, \alpha_s) = \frac{1}{2}$. Thus, from eq.(3.81), it directly follows that

$$f(x, k^2) \sim (k^2)^{\frac{1}{2}}x^{-\lambda_L}. \tag{3.84}$$

Since $F_2^{(0)}/k^2$ in eq.(3.79) is simply a function of k^2/Q^2, this leading behaviour feeds through into F_2 to give

$$F_2(x, Q^2) \sim (Q^2)^{\frac{1}{2}}x^{-\lambda_L}, \tag{3.85}$$

where in (3.84) and (3.85) we have omitted slowly varying logarithmic factors.

Formula (3.81) is valid for running α_s, provided n remains to the right of the branch point throughout the region of integration, that is provided $n > 1 + 12\alpha_s(k_0^2)\log 2/\pi$. (For smaller values of n the k^2 dependence of $f(n, k^2)$ is more involved[48].) For running α_s the small x behaviour of $f(x, k^2)$ is controlled by the leading *pole* singularity of $f(n, k^2)$ which occurs at $n = 1 + \bar{\lambda}$, where now $\bar{\lambda}$ has to be calculated numerically[12]. A value of $\bar{\lambda} \approx 0.5$ is found, with rather little sensitivity to the treatment of the infrared region of the BFKL equation[39]. The k^2 dependence of f (and hence the Q^2 dependence of F_2) is determined by the residue β of this pole. Using eq.(3.81) we have

$$f \sim \beta(k^2)x^{-\bar{\lambda}} \tag{3.86}$$

where

$$\beta(k^2) \sim \exp\left[\int_{k_0^2}^{k^2} \frac{dk'^2}{k'^2}\gamma(1 + \bar{\lambda}, \alpha_s(k'^2))\right]. \tag{3.87}$$

From the above discussion we see that this form is valid provided $k^2 \geq k_0^2 \geq \kappa^2(\bar{\lambda})$, where $\kappa^2(\bar{\lambda})$ satisfies the implicit equation $\bar{\lambda} = 12\alpha_s(\kappa^2(\bar{\lambda}))\log 2/\pi$. Similarly, provided

that $Q^2 \geq \kappa^2(\bar{\lambda})$, we have

$$F_2(x, Q^2) \sim \beta(Q^2) x^{-\bar{\lambda}}, \tag{3.88}$$

up to slight modifications which result from known Q^2 effects embedded in $F_2^{(0)}$. Note that for $Q^2 \gtrsim \kappa^2(\bar{\lambda})$ we should again get an approximate $(Q^2)^{\frac{1}{2}}$ behaviour of $F_2(x, Q^2)$, although it may (at moderately small values of x) be modified by the non-leading contributions. Here we are also interested in $Q^2 < \kappa^2(\bar{\lambda})$ and then the form of β is more involved[48].

In the leading $\log(1/x)$ approximation the anomalous dimension, $\gamma(n, \alpha_s)$, is a power series in $\alpha_s/(n-1)$. For the BFKL approach $\gamma(n, \alpha_s)$ contains the sum of all these terms. If only the first term were retained then the Q^2 behaviour would correspond to Altarelli-Parisi evolution from a singular $x^{-\bar{\lambda}}$ gluon starting distribution with only $g \to gg$ transitions included and with the splitting function $P_{gg}(z)$ approximated by its singular $1/z$ term.

It is useful to compare the Q^2 dependence of F_2 which results from the theoretically motivated BFKL approach, (B), with that of the Altarelli-Parisi Q^2 evolution of approach (A). For Altarelli-Parisi evolution the Q^2 behaviour of F_2 depends on the small x behaviour of the parton starting distributions. If we assume that the starting distributions are non-singular at small x (i.e. $xg(x, Q_0^2)$ and $xq_{\text{sea}}(x, Q_0^2)$ approach a constant limit for $x \to 0$), then the leading term, which drives both the Q^2 and x dependence at small x, is of the double logarithmic form

$$F_2(x, Q^2) \sim \exp\left[2\{\xi(Q_0^2, Q^2)\log(1/x)\}^{\frac{1}{2}}\right], \tag{3.89}$$

where

$$\xi(Q_0^2, Q^2) = \int_{Q_0^2}^{Q^2} \frac{dq^2}{q^2} \frac{3\alpha_s(q^2)}{\pi}. \tag{3.90}$$

From (3.89) we see that, as x decreases, F_2 increases faster than any power of $\log(1/x)$ but slower than any power of x.

If, on the other hand, the starting gluon and sea quark distributions are assumed to have singular behaviour in the small x limit i.e.

$$xg(x, Q_0^2), xq_{\text{sea}}(x, Q_0^2) \sim x^{-\lambda} \tag{3.91}$$

127

with $\lambda > 0$, then the structure function $F_2(x, Q^2)$ behaves as

$$F_2(x, Q^2) \sim x^{-\lambda} h(Q^2) \tag{3.92}$$

where the function $h(Q^2)$ is determined by the corresponding anomalous dimensions of the moments of the (singlet) parton distributions at $n = 1 + \lambda$, as well as by the coefficient functions.

We emphasize again that, in contrast to the BFKL approach, for (next-to-leading order) Altarelli-Parisi evolution the relevant quantities which determine $h(Q^2)$ are computed from the first (two) terms in the perturbative expansion in α_s. Thus terms are neglected which may in principle be important at small x, corresponding to the infinite sum of powers of $\alpha_s/(n-1)$ in γ (and in the coefficient function).

Note that in both cases (i.e. eqs.(3.89) and (3.92)) Altarelli-Parisi evolution gives a slope of the structure function, $\partial F_2(x, Q^2)/\partial \log(Q^2)$, which increases with decreasing x. The MRS(D$'_-$)[40] and MRS(H)[46] extrapolations are examples of (3.92), with $\lambda = 0.5$ and 0.3 respectively. On the other hand, the behaviour of F_2 obtained from the GRV[16] partons is an example of (3.89). In the GRV model the partons are generated from a valence-like input at a very low scale, $Q_0^2 = 0.3 \text{GeV}^2$ (and then the valence is matched to MRS at much higher Q^2). Due to the long evolution length, $\xi(Q_0^2, Q^2)$, in reaching the Q^2 values corresponding to the small x HERA data the GRV prediction tends to the double logarithmic form of (3.89). The GRV model is probably best regarded as a phenomenological way of obtaining steep distributions at a conventional input scale, say 4GeV^2, since the steepness is mainly generated in the very low Q^2 region where perturbative QCD is unreliable[18]. Note, however, that the steepness is specified by the evolution and is not a free parameter. In fact, in the region of the HERA data, the GRV form mimics an $x^{-\lambda}$ behaviour with $\lambda \sim 0.4$, although for smaller x it is less steep.

To summarize, we have discussed four different ways of generating a steep x behaviour of $F_2(x, Q^2)$ at small x, each with its own characteristic Q^2 dependence: the BFKL fixed and running α_s forms, (3.85) and (3.88), the Altarelli-Parisi double leading logarithmic form with a long Q^2 evolution, (3.89), and finally Altarelli-Parisi evolution from a steep $x^{-\lambda}$ input, (3.92). Examples of such forms are, respectively, the fixed and running α_s AKMS predictions[35,39], and the GRV[16] and MRS(H)[46] extrapolations. Their Q^2

128

dependences are compared with each other in figure 3.23 at given values of small x in the HERA regime. For reference the MRS(D'_-)[40] extrapolation is also shown.
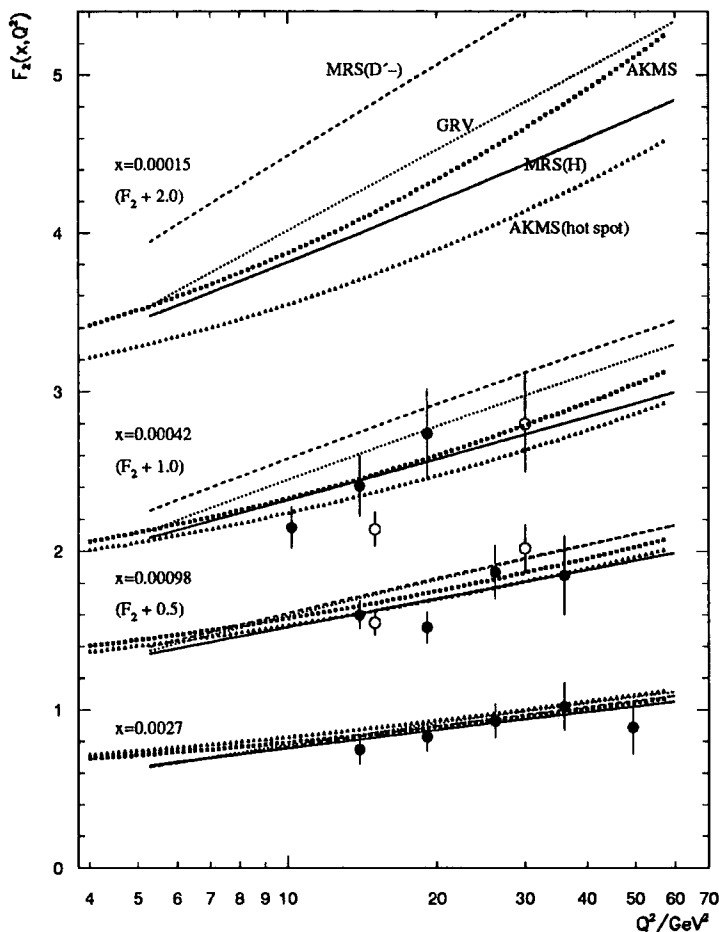
Figure 3.23: The Q^2 dependence of $F_2(x, Q^2)$ at small x (note the shifts of scale between the plots at the different x values, which have been introduced for clarity). The curves are as in figure 3.21. Also shown are the measurements of the 1992 HERA run obtained by the ZEUS collaboration[45] (open points) and, by the H1 collaboration[49] using their "electron" analysis (closed points). Only statistical errors of the data are shown. The ZEUS points shown on the $x=0.00098$ curves are measured at an average $x=0.00085$. A challenge for future experiments is to distinguish between curves like AKMS and MRS(H), both of which give a satisfactory description of the existing data.

The theoretical curves are calculated either from eq.(3.79) (where f is the complete numerical solution of the BFKL equation obtained as described in the previous sections 3.4 and 3.5), or from the full next-to-leading order Altarelli-Parisi evolution. We also show,

in Fig. 3.23, H1[49] and ZEUS[45] measurements of F_2 made during the 1992 HERA run, corresponding to an integrated luminosity of 25nb^{-1}. Only the statistical errors of the data are shown. Measurements will be made with much higher luminosity, and at smaller x values, in the future.

Several features of this plot are noteworthy. First, if we compare the data with the "$x^{-\lambda}$ dependences" of the Altarelli-Parisi forms of MRS(D$'_-$), GRV and MRS(H) (which have respectively λ =0.5, "$\approx$0.4", and 0.3), then we see that MRS(D$'_-$) and GRV are disfavoured. So we are left with MRS(H), which, in fact, was devised simply to reproduce[1] the HERA data of refs. [44,45].

Second, we see that the AKMS prediction (which pre-dated the HERA data) is, like MRS(H), in good agreement with the x and Q^2 dependence of the data. In principle, it is an absolute perturbative QCD prediction of $F_2(x, Q^2)$ at small x in terms of the known behaviour at larger x, but, in practice, the overall normalization depends on the treatment of the infrared region of the BFKL equation[35,39]. We can therefore normalise the BFKL-based predictions so as to approximately describe the data at $x = 0.0027$ by adjusting a parameter which is introduced[39] in the description of the infrared region. For the running α_s AKMS calculation, this is achieved if the infrared parameter $k_a^2 \approx 2\text{GeV}^2$ (with $k_c^2 = 1\text{GeV}^2$), in the notation of section 3.5. Strictly speaking, within the genuine leading $\log(1/x)$ approximation the coupling α_s should be kept fixed[2] . We therefore also solved the BFKL equation with fixed α_s, choosing a value α_s=0.25 so as to have a satisfactory normalization. The resulting Q^2 dependence of $F_2(x, Q^2)$ turned out to be almost identical to that calculated from the solution of the BFKL equation with running α_s. For clarity, we therefore have omitted the fixed α_s curve from figure 3.23. Also a background (or non-BFKL) contribution to F_2 has to be included in the AKMS calculation[3] ; this explains why MRS(H), with λ=0.3, and AKMS, with $\bar{\lambda} \approx 0.5$, both give equally good descriptions

---

[1] See also the partons of the CTEQ collaboration which have λ=0.27[50].

[2] The use of running α_s has the advantage that then the BFKL equation reduces to the Altarelli-Parisi equation in the double leading logarithm approximation when the transverse momenta of the gluons become strongly ordered.

[3] To be precise, we take $F_2(\text{background}) = F_2(x_0 = 0.1, Q^2)(x/x_0)^{-0.08}$ [39]; a form which is motivated by "soft" Pomeron Regge behaviour[41]. Other reasonable choices of the background do not change our conclusions.

of the HERA data.

A third feature of figure 3.23 is the stronger Q^2 dependence of the AKMS predictions as compared with the MRS and GRV extrapolations which are based on Altarelli-Parisi evolution. This we had anticipated, with a growth approaching $(Q^2)^{\frac{1}{2}}$ for BFKL as compared with the approximately linear $\log Q^2$ behaviour characteristic of Altarelli-Parisi evolution. In reality, at the smallest x value shown we find that the AKMS growth is reduced to about $(Q^2)^{\frac{1}{3}}$, due to the fact that F_2(background) is still significant. Although we see that the BFKL and Altarelli-Parisi Q^2 behaviours are quite distinctive, to actually distinguish between them will clearly be an experimental challenge, particularly since $Q^2 \lesssim 15\text{GeV}^2$ is the kinematic reach of HERA at the lowest x value shown. Recall that the BFKL and Altarelli-Parisi equations effectively resum the leading $\log(1/x)$ and $\log(Q^2)$ contributions respectively. Thus the BFKL equation is appropriate in the small x region where $\alpha_s \log(1/x) \sim 1$ yet $\alpha_s \log(Q^2/Q_0^2) \ll 1$, where Q_0^2 is some (sufficiently large) reference scale. If the latter were also ~ 1 then both $\log(1/x)$ and $\log(Q^2/Q_0^2)$ have to be treated on an equal footing [6], as is done, for instance, in the unified equation proposed by Marchesini et al.[9]. For this reason we restrict our study of small x via the BFKL equation to the region $5 \lesssim Q^2 \lesssim 50\text{GeV}^2$. As it happens, the very small x HERA data lie well within this limited Q^2 interval.

So far we have neglected the effects of parton shadowing. If, as is conventionally expected, the gluons are spread reasonably uniformly across the proton then we anticipate that the effects will be small in the HERA regime[39]. For illustration we have therefore shown the effects of (speculative) "hot-spot" shadowing, corresponding to concentrations of gluons in small hot-spots of transverse area πR^2 inside the proton with, say, $R = 2\text{GeV}^{-1}$. In this case, to normalise the predictions at x=0.0027, we need to take the infrared parameter $k_a^2 \approx 1.5\text{GeV}^2$. With decreasing x, we see from figure 3.23, that this shadowed AKMS prediction increases more slowly than the unshadowed one, but that it keeps the characteristic "BFKL Q^2 curvature".

To conclude, we have performed a detailed analysis of the Q^2 dependence of the structure function $F_2(x, Q^2)$ in the small x region which is being probed at HERA. We have found that the theoretically-motivated BFKL-based predictions do indeed lead, in the HERA small x regime, to a more pronounced curvature of $F_2(x, Q^2)$ than those based on next-to-leading order Altarelli-Parisi evolution. The difference is illustrated in figure 3.23

by the comparison of the AKMS curve with that for MRS(H). From the figure we see that data at the smallest possible x values will be the most revealing. The measurements shown are from the 1992 run, but data with much higher luminosity, and at smaller x, will become available in the near future.

3.7: Conclusions.

In the previous sections we have made explicit calculations for the structure functions as $x \to 0$ on the basis of the BFKL formalism. Here we gather together the lessons learnt from this analysis and summarise the main results.

Our starting point was the assertion that, at small x, we expected the gluon distribution to rise dramatically as a result of soft gluon radiation. These effects were modelled by applying the BFKL equation to the gluon distribution, which determines how $f(x, \vec{k})$ changes as we change the amount of phase space — that is, $\log(1/x)$ — available for parton decays. Infrared effects play a role in this equation and rob the formalism of its absolute predictability; but we expect that there will be some contribution from the purely perturbative domain in which all transverse momenta $\vec{k}^2 > 1 - 2$ GeV^2. To focus on this region we invoke a cutoff on the transverse momentum integrations.

Owing to the large gluon density, a large fraction of the $\gamma^* p$ cross section will originate from the virtual photon striking a quark which has been radiated perturbatively from a gluon. Consequently, once the gluon distribution is 'known' (from the BFKL equation) then convoluting this with a suitable $\gamma^* g$ interaction will give a large contribution to the cross section. We calculated the appropriate 'impact factor' for photon gluon fusion to lowest order and performed the numerical analysis necessary to determine the contribution of this process to F_2. We found that, indeed, this process can give a large contribution to the structure functions. However our analysis showed that the normalisation of the BFKL contribution is sensitive to the infrared region, and that the contribution to the structure functions from the 'non-perturbative' domain of small $\vec{k}^2$ must be large. As a model for this contribution we assumed that it should have the characteristics of 'soft pomeron' exchange, and so be fairly independent of x and Q^2. This seems fairly reasonable, since the dominant mechanism driving both the x and Q^2 dependence here is the soft gluon radiation which is accounted for by the BFKL equation. In fact, the results from HERA

do indicate that there is a significant contribution to F_2 owing to diffractive events [51], for which the emission of a 'soft pomeron' by the proton and subsequent γ^*P interaction is a viable model [52]. The observed overall normalisation of this component, however, seems smaller than that of our 'background'.

In an attempt to find some effect of the BFKL formalism which is less dependent on the model for the infrared region, we focussed attention away from the absolute normalisation of the structure function and towards its x-dependence. We studied the effective slope λ of the perturbative component of the structure functions, where $F_2 = F_2^{np} + Cx^{-\lambda}$. Our analytic formulae showed that we could expect this to have less dependence on the infra red region, and our numerical calculations bore out this expectation. We found that the BFKL formalism suggested a slope $\lambda \sim 0.5$, compatible with the data provided that the background, nonperturbative component is accounted for.

With a suitable normalisation, fixed by tuning the treatment of the infra red region, the resulting structure functions from our model are in good agreement with the observed x and Q^2 dependence of the data from HERA. A similar agreement can be obtained through conventional methods based on the next to leading order DGLAP equations provided we start evolving from an input distribution at $Q^2 = 4$ GeV^2 which contains a steep $x^{-\lambda}$ growth. The x-behaviour in this approach can be varied at will, but the Q^2 behaviour is fixed in terms of the DGLAP equations. In order to compare the two formalisms then, we compared the scaling violations of the structure functions. Our results showed that the structure functions based on the BFKL formalism showed a stronger scaling violation than those coming from standard NLO analyses, but that the effect is not really very strong in the HERA region. Given the theoretical uncertainties in the BFKL approach, notably the 'background' component of F_2, an unambiguous test of the BFKL resummation based on structure function analysis does not seem to be possible in the domain probed by HERA.

References.

[1] E.A. Kuraev, L.N. Lipatov and V. Fadin, Zh. Eksp. Teor. Fiz. **72** (1977) 373; Sov. Phys. JETP **45** (1977) 199

[2] Ya.Ya. Balitskij and L.N. Lipatov, Yad. Fiz. **28** (1978) 1597; Sov. J. Nucl. Phys. **28** (1978) 822.

[3] L.N. Lipatov, in "Perturbative QCD", ed. A.H. Mueller (World Scientific, Singapore, 1989) p. 411

[4] J.B. Bronzan and R.L. Sugar, Phys. Rev. **D17** (1978) 585

[5] T. Jaroszewicz, Acta Phys. Polon. **B11** (1980) 965

[6] L.V. Gribov, E.M. Levin and M.G. Ryskin, Phys. Rep. **100** (1983) 1

[7] M. Ciafaloni, Nucl. Phys. **296** (1988) 49

[8] S. Catani, F. Fiorani and G. Marchesini, Phys. Lett. **B234** (1990) 339; Nucl. Phys. **B336** (1990) 18

[9] G. Marchesini, Proc. of Workshop "QCD at 200 TeV", Erice, Italy, June 1990, eds. L. Cifarelli and Yu.L. Dokshitzer, Plenum Press, New York 1992, p. 183

[10] E.M. Levin, Orsay lectures, LPTPE preprint 91/02 (1991)

[11] A.D. Martin, R.G. Roberts and W.J. Stirling, Phys. Rev. **D47** (1993) 867

[12] J. Kwiecinski, A.D. Martin and P.J. Sutton, Phys. Lett. **B264** 199 (1991) ; Phys. Rev. **D44** 2640 (1991).

[13] S. Catani, M. Ciafaloni and F. Hautmann, Phys. Lett. **B242** (1990) 91; Nucl. Phys. **B366** (1991) 135; S. Catani, M. Ciafaloni and F. Hautmann, Proc. of the Workshop "Physics at HERA", DESY, Hamburg, Germany, October 1992, eds. W. Buchmüller and G. Ingelman, Vol. 2 (1992) p690; S. Catani, CERN preprint CERN-TH-6524/92.

[14] J.C. Collins and R.K. Ellis, Nucl. Phys. **B360** (1991) 3

[15] J. Kwiecinski, A.D. Martin and P.J. Sutton, Phys. Rev. D46 (1992) 921; J. Kwiecinski, A.D. Martin and P.J. Sutton, Phys. Lett. B287 (1992) 254; A.D. Martin, J. Kwiecinski and P.J. Sutton, Nucl. Phys. B (Proc. Suppl.) **29A** (1992) 67

[16] M. Glück, R.M. Godbole and E. Reya, Z. Phys. C **41** 667 (1989); M. Glück, E. Reya and A. Vogt, Z. Phys. C48 475 (1990); Z. Phys. C53 127 (1992); Dortmund Univ. preprint DO-TH-92-19.

[17] V. Barone et al., Int. J. Mod. Phys. **A8** ,2779 (1993); Phys. Lett. **B292** ,181 (1992)

[18] J.R. Forshaw, Phys. Lett. **B314** (1993) 425

[19] L.N. Lipatov and G.V. Frolov, Sov. J. Nucl. Phys. **13**, 333 (1971)

[20] J. Bartels, M. Loewe and A. De Roeck, Z. Phys. C54 (1992) 635; A. De Roeck, Nucl. Phys. B (Proc. Suppl.) 29A (1992) 61

[21] E.M. Levin and M.G. Ryskin, Yad. Fiz. 53, 1052 (1991)

[22] J. Bartels and H. Lotter, Phys. Lett. B309 (1993) 400

[23] J.C. Collins and P.V. Landshoff, Phys. Lett. B276 (1992) 196

[24] A.H. Mueller, J. Phys. G17 (1991) 1443

[25] J. Bartels, M. Besancon, A. De Roeck and J. Kurzhoefer, "Measurements of Hot Spots at HERA", Proc. of the Workshop "Physics at HERA", DESY, Hamburg, Germany, October 1992, eds. W. Buchmüller and G. Ingelman

[26] W.K. Tang, Phys. Lett. B278 (1992) 363

[27] S. Catani and F. Hautmann, Nucl. Phys. B427 (1994) 475

[28] J. Kwieciński and A.D. Martin, Durham preprint DTP/95/34, April 1995.

[29] R.G. Roberts, private communication

[30] NMC collaboration: P. Amaudruz et al., Phys. Lett. B295 (1992) 159

[31] BCDMS collaboration: A.C. Benvenuti et al., Phys. Lett. B223 (1989) 485

[32] J. Kwieciński, A.D. Martin, R.G. Roberts and W.J. Stirling, Phys. Rev. D42, 3645 (1990)

[33] B.R. Webber, Proceedings of the 17th Workshop "QCD at 200 TeV", Erice, June 1990; ed. L. Cifarelli and Y. Dokshitzer, Plenum Press, New York, 1992; B.R. Webber, p. 285, vol. 1 of ref. HERA. G. Marchesini and B.R. Webber, Nucl. Phys. B386, 215 (1992)

[34] E.M. Levin, M.G. Ryskin, V.T. Kim, Yu.M. Shabelski and A.G. Shuvaev, Sov. J. Nucl. Phys. 54, 867 (1991)

[35] A.J. Askew, J. Kwieciński, A.D. Martin and P.J. Sutton, Phys. Rev D47 (1993) 3775

[36] R.E. Hancock and D.A. Ross, Nucl. Phys. B383 (1992) 575

[37] J.R. Forshaw and P.N. Harriman, Phys. Rev. D46 1992) 3778

[38] A.D. Martin, J. Phys. G19 (1993) 1603

[39] A.J. Askew, J. Kwieciński, A.D. Martin and P.J. Sutton, Mod. Phys. Lett. **A8** (1993) 3813; Phys. Rev. **D49**, 4402 (1994)

[40] A.D. Martin, R.G. Roberts and W.J. Stirling, Phys. Lett. **B306** (1993) 145

[41] P.V. Landshoff, Proc. XXVII Rencontre de Moriond (Editions Frontieres, 1992, ed. J. Tran Thanh Van); A. Donnachie and P.V. Landshoff, Phys. Lett. **B296** (1992) 227; Z. Phys. **C61** (1994) 139

[42] H1 collaboration, preliminary data July 1994, courtesy of A. De Roeck.

[43] ZEUS collaboration: Z. Phys. **C65**, 379 (1995)

[44] H1 collaboration: I. Abt et al., Nucl. Phys. **B407** (1993) 515

[45] ZEUS collaboration: M. Derrick et al., Phys. Lett. **B316** (1993) 412

[46] A.D. Martin, W.J. Stirling and R.G. Roberts, preprint RAL-93-077 (1993)

[47] T. Jaroszewicz, Phys. Lett. **B116** (1982) 291

[48] J. Kwieciński, Z.Phys. **C29** (1985) 561; J.C. Collins and J. Kwieciński, Nucl. Phys. **B316** (1989) 307

[49] H1 collaboration: I. Abt et al., Phys. Lett. **B321** (1994) 161

[50] CTEQ collaboration: J. Botts et al., preprint MSU-HEP 93/18 (1993)

[51] ZEUS collaboration, Phys. Lett. **B332**, 228 (1994);
H1 collaboration, Nucl. Phys. **B429**,477 (1994) and Phys. Lett. **B348**, 681 (1995)

[52] K. Golec-Biernat and J. Kwieciński, INP report No. 1670/PH, April 1995

4

Dijet production at HERA as a probe of BFKL dynamics.

*Loneliness and the feeling of being unwanted is the most terrible poverty.*

Mother Teresa

4.1: Introduction.

The production of dijets at the HERA electron-proton collider offers an excellent opportunity to study the properties of the gluon distribution of the proton at small x. At lowest order, dijets[1] are produced by the emission of a "hard" gluon from the initial or final state of the struck quark (the QCD Compton process $\gamma q \to gq$) or by photon-gluon fusion ($\gamma g \to q\bar{q}$). The dijet events of particular interest are those in which the two jets tend to go in the virtual photon direction (in the γp centre-of-mass frame) but separated by a rapidity interval which is small relative to their large individual rapidities. In this configuration the proton-gluon fusion process dominates and small values of x_g are sampled. Here x_g is the longitudinal fraction of the proton's momentum carried by the interacting gluon. The process is shown diagrammatically in figure 4.1, where the dominant structure of the interacting gluon at small x_g is exposed. We also show the transverse momenta p_{1T}, p_{2T} and k_T of the outgoing (quark, antiquark) jets and the incoming gluon.

---

[1] As is customary, we use the term "dijet" to refer to two jets produced in addition to the jet formed by the remnants of the proton.

137
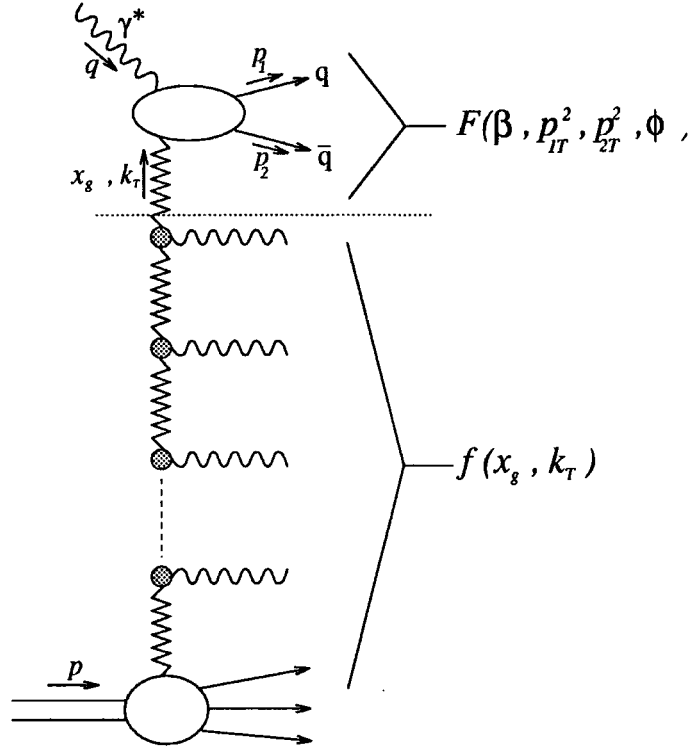
Figure 4.1: A diagrammatic representation of dijet production by photon gluon fusion, $\gamma g \rightarrow q\bar{q}$, at small x_g. The function f is the (unintegrated) gluon distribution of the proton. The cross section is given by the k_T-factorization formula (4.8), which has the symbolic form $\sigma = f \otimes \mathcal{F}$. $\mathcal{F}$ denotes the quark box (and crossed box) contribution.

Dijets can be produced at HERA via direct photons either by photoproduction ($Q^2 \approx 0$) [1,2] or by deep-inelastic electroproduction (Q^2 of $O(10 \text{ GeV}^2)$). In the former case it is much more difficult to extract the direct photon events from the events in which the photon is resolved into its constituent partons [3]. In fact it appears likely that a larger "clean" dijet event sample will be obtained for electroproduction, and so we study this process. We are especially interested in the properties of the gluon at small x_g. However the values of x_g that are sampled in any deep inelastic study exposing the final state are always greater than the Bjorken x. In our case $x_g \approx (1 + \hat{s}/Q^2)x$, where $\sqrt{\hat{s}}$ is the c.m. energy of the produced dijet system. So the lower the values of p_T, for which the jets can be clearly identified, the better.

138

4.2: Dijet production in the BFKL formalism.

In principle, the calculation of the dijet production cross section requires integration over the complete phase space of the transverse momenta k_T of the gluon. In the conventional approach we

(i) restrict the integration over k_T^2 to the region $k_T^2 \ll p_{iT}^2$ and

(ii) let $k_T^2 = 0$ in the calculation of the subprocess cross section $\hat{\sigma}(\gamma g \rightarrow q\bar{q})$, i.e. we evaluate $\hat{\sigma}$ with the gluon on-mass-shell.

As a result we get the familiar factorization formula, which symbolically is of the form

$$x_g g(x_g, \mu^2) \otimes \hat{\sigma}(\gamma g \rightarrow q\bar{q}, \mu^2) \tag{4.1}$$

where the scale $\mu^2 \sim p_{iT}^2$. In this way we can probe the conventional gluon distribution, g, of the proton. However, at small x_g, the strong-ordering approximation is no longer applicable – we must keep the full k_T^2 dependence of $\hat{\sigma}$ and integrate over the full k_T^2 phase space. As a consequence we must work in terms of the gluon distribution $f(x_g, k_T^2, \mu^2)$ unintegrated over k_T^2 [4,5,6], that is

$$x_g g(x_g, \mu^2) = \int^{\mu^2} \frac{dk_T^2}{k_T^2} f(x_g, k_T^2, \mu^2). \tag{4.2}$$

At small x_g the function f satisfies the BFKL equation [7],

$$\frac{\partial f(x_g, k_T^2)}{\partial \log(1/x_g)} = \frac{3\alpha_s}{\pi} k_T^2 \int \frac{dk_T'^2}{k_T'^2} \left[\frac{f(x_g, k_T'^2) - f(x_g, k_T^2)}{|k_T'^2 - k_T^2|} + \frac{f(x_g, k_T^2)}{(4k_T'^4 + k_T^4)^{\frac{1}{2}}} \right], \tag{4.3}$$

which effectively resums the large leading $\log(1/x_g)$ contributions which arise from the sum of the gluon emission diagrams of the type shown in figure 4.1 together with the virtual corrections. Note that, at small x_g, the gluon distribution f becomes independent of the scale μ^2. Two characteristic features of the solution of the BFKL equation are

(i) the leading small x_g behaviour of the form

$$f(x_g, k_T^2) \sim x_g^{-\lambda} \tag{4.4}$$

where $\lambda \approx 0.5$, and

(ii) a "diffusion" in k_T with decreasing x_g which arises from the "random-walk" in the k_T of the gluons as we proceed along the gluon chain [8, 9].

The first property gives rise to a growth in dijet production with decreasing x_g. However this behaviour can be mimicked by eq. (4.1) with a conventional gluon which evolves from a singular distribution at some starting scale, that is $x_g g \sim x_g^{-\lambda}$. The singular small x_g behaviour is stable to the evolution. The second property is more unique to BFKL dynamics. The diffusion in k_T manifests itself in a weakening of the back-to-back azimuthal correlation of the two outgoing jets of transverse momenta p_{1T} and p_{2T}. As x (and hence x_g) decrease, larger k_T's are sampled and broader azimuthal distributions are expected. On the other hand the strong-ordering of the transverse momenta of conventional dijet production leads to a narrow distribution about the back-to-back jet configuration. Thus, in principle, a measurement of the azimuthal distribution offers a direct determination of the k_T dependence of the gluon distribution $f(x_g, k_T^2)$. In practice the situation is not so clear. The azimuthal distribution will also be broadened by higher-order conventional QCD effects. To see whether these will mask the BFKL signal we therefore also compute the azimuthal distribution resulting from the emission of a third "hard" QCD jet.

We begin by using BFKL dynamics at small x_g to calculate the differential dijet cross section as a function of ϕ, the azimuthal angle between the transverse momenta p_{1T} and p_{2T} of the two jets. That is we evaluate

$$\frac{d\sigma}{dx dQ^2 d\phi} = \frac{4\pi\alpha^2}{Q^4 x}\left[(1-y+\frac{y^2}{2})\frac{dF_T(x,Q^2,\phi)}{d\phi} + (1-y)\frac{dF_L(x,Q^2,\phi)}{d\phi}\right] \quad (4.5)$$

where, as usual, the deep inelastic variables $Q^2 = -q^2$, $x = Q^2/2p.q$ and $y = p.q/p.p_e$ where p_e, p and q are the four momenta of the incident electron, proton and virtual photon respectively, see figure 4.1. The differential structure functions $dF_i/d\phi$ can be computed from the k_T-factorization formula, which is shown symbolically in figure 4.1. It is convenient to express the jet four-momenta in terms of Sudakov variables

$$
\begin{aligned}
p_1 &= (1-\beta)q' + \alpha_1 p + \mathbf{p_{1T}} \\
p_2 &= \beta q' + \alpha_2 p + \mathbf{p_{2T}}
\end{aligned}
\quad (4.6)
$$

where $q' = q + xp$ and p are basic lightlike momenta. Thus, since the jets are on-mass-shell,

140

we have

$$\alpha_1 = \left(\frac{p_{1T}^2 + m_q^2}{(1-\beta)Q^2}\right)x, \qquad \alpha_2 = \left(\frac{p_{2T}^2 + m_q^2}{\beta Q^2}\right)x \qquad (4.7)$$

where m_q is the mass of the quark. The Bjorken variable $x \approx Q^2/2p.q'$. The factorization formula for the differential structure functions is

$$\frac{dF_i(x, Q^2, \phi)}{d\phi} = \sum_q \int_0^1 d\beta \int \frac{dp_{1T}^2 dp_{2T}^2}{k_T^4} f(x_g, k_T^2) \mathcal{F}_i^q(\beta, p_{1T}^2, p_{2T}^2, \phi) \qquad (4.8)$$

with $i = T, L$ and where the "factorization" variables

$$\begin{aligned}
x_g &= x + \alpha_1 + \alpha_2 \quad (\gtrsim [1 + 4p_{iT}^2/Q^2]x) \\
k_T^2 &= p_{1T}^2 + p_{2T}^2 + 2p_{1T}p_{2T}\cos\phi.
\end{aligned} \qquad (4.9)$$

The functions $\mathcal{F}_i^q$ which describe virtual photon-virtual gluon fusion, $\gamma g \to q\bar{q}$, at small x_g are [10]

$$\begin{aligned}
\mathcal{F}_T^q(\beta, p_{1T}^2, p_{2T}^2, \phi) &= e_q^2 \frac{Q^2}{8\pi^2}\alpha_s[\beta^2 + (1-\beta)^2]\left\{\frac{p_{1T}^2}{D_1^2} + \frac{p_{2T}^2}{D_2^2} + 2\frac{p_{1T}p_{2T}\cos\phi}{D_1 D_2}\right\} \\
&\quad + e_q^2 \frac{Q^2}{8\pi^2}\alpha_s m_q^2 \left\{\frac{1}{D_1^2} + \frac{1}{D_2^2} - \frac{2}{D_1 D_2}\right\}
\end{aligned} \qquad (4.10)$$

$$\mathcal{F}_L^q(\beta, p_{1T}^2, p_{2T}^2, \phi) = e_q^2 \frac{Q^4}{2\pi^2}\alpha_s\beta^2(1-\beta)^2\left\{\frac{1}{D_1^2} + \frac{1}{D_2^2} - \frac{2}{D_1 D_2}\right\} \qquad (4.11)$$

where e_q is the charge of the quark q and where the denominators

$$D_i = p_{iT}^2 + m_q^2 + \beta(1-\beta)Q^2. \qquad (4.12)$$

The first two terms in $\{\dots\}$ in (4.10) and (4.11) correspond to quark box contributions with p_1 being first a quark and then an antiquark jet, whereas the third term is the "crossed-box" interference term. Note that the apparent divergence of the integral in (4.8) at $k_T^2 = 0$ (that is at $\phi = \pi$) is cancelled by the zeros of the functions f and $\mathcal{F}_{T,L}$, see (4.10) and (4.11).

141

The only unknown in the determination of the differential cross section for deep-inelastic dijet production, $d\sigma/dxdQ^2d\phi$, is the gluon distribution $f(x_g, k_T^2)$ that enters in (4.8). We calculate f by solving the differential form of the BFKL equation, (4.3), using knowledge of the gluon at $x_g = 10^{-2}$, as described in the previous chapter. The normalisation (though not the x_g behaviour) of f is dependent on the treatment of the infrared k_T region. However, the gluon distribution f can also be used to predict the behaviour of the structure function F_2 itself, via the inclusive form of the k_T-factorization formula (4.8), see ref. [9]. Thus we can fix the infrared parameter in the determination of f so as to reproduce the low x measurements of F_2 at HERA[11]. The result is shown by continuous curves in figure 4.2, and corresponds to the choice $k_a^2 = 2$ GeV^2. We see that an excellent description of F_2 is obtained. Now that f has been fully specified in this way, we should be able to predict the azimuthal distribution reliably, provided, of course, that we sample sufficiently small values of x_g for the BFKL solution to be appropriate.
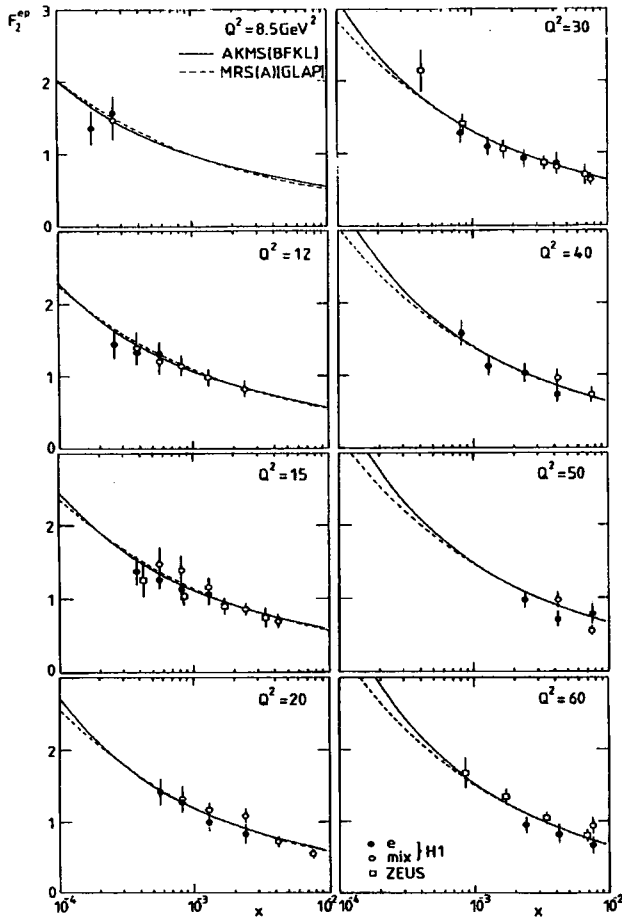
Figure 4.2:

The measurements of F_2 at HERA (preliminary data from the 1993 run[11]) shown together with the BFKL description[9] (continuous curves) and the MRS(A) parton analysis fit[12] (dashed curves). The measurements of the H1 collaboration at $Q^2 = 65$ GeV^2 are shown on the $Q^2 = 60$ GeV^2 plot.

4.3: Results.

In figure 4.3a we show $dF_T/d\phi$ calculated from the k_T-factorization formula, (4.8), for deep-inelastic dijet events with $Q^2 = 10$ GeV^2 for three different values of x. Each jet is required to have transverse energy squared, E_T^2, greater than 10 GeV^2. We notice a rapid increase in the dijet rate with decreasing x, and a weakening of the azimuthal back-to-back correlation. This last observation is more evident from figure 4.3b which shows the same distributions normalized to a common maximum value at $\phi = \pi$. The broadening with decreasing x is a manifestation of the diffusion in k_T which is characteristic of BFKL dynamics. The detailed shape in the region of $\phi \approx \pi$ will not be reliable, since it corresponds to small values of the transverse momentum k_T, of the gluon (see figure 4.1). Moreover hadronization effects will influence the distribution in this region. Rather we should study the normalised distribution, $dF_T/d\phi$, away from $\phi = \pi$, say outside the interval 180 ± 20 degrees.

The characteristic BFKL behaviour of the solution $f(x, k_T^2)$ of (4.3) only has a chance to set in for $x \lesssim 10^{-3}$. The precocious onset of this leading $\log(1/x)$ behaviour does indeed appear compatible with the striking rise of F_2 with decreasing x that has been observed at HERA, see figure 4.2. However this is not conclusive evidence of BFKL dynamics. The F_2 data can equally well be described by Altarelli-Parisi (or GLAP) evolution. For example the dashed curves in figure 4.2 are the description obtained from a recent global structure function analysis based on (next-to-leading order) GLAP evolution from "singular" parton distributions at $Q^2 = 4$ GeV^2[12]. To distinguish BFKL dynamics from conventional QCD we must look into properties of the final state at small x, such as the weakening of the back-to-back correlations in the dijet events. However there is a price to pay. The BFKL dynamics is sampled at larger "x" for final state processes than is the case for the inclusive F_2 measurement. In our example of dijets with E_T^2(jet) > 10 GeV^2 and $Q^2 = 10$ GeV^2, we see from (4.9) that we sample values of $x_g \gtrsim 5x$. Thus if $f(x_g, k_T^2)$ assumes a characteristic BFKL behaviour for $x_g \lesssim 10^{-3}$, then we anticipate that the broadening of the ϕ distribution, with decreasing x, will only be relevant in the region $x \lesssim$ few $\times 10^{-4}$. This is near the limit of the region which is at present accessible at HERA. In figure 4.4 we therefore compare the dijet azimuthal distribution for $x = 2 \times 10^{-4}$ with that for $x = 10^{-3}$, that is two values of x which are appropriate for HERA.

143
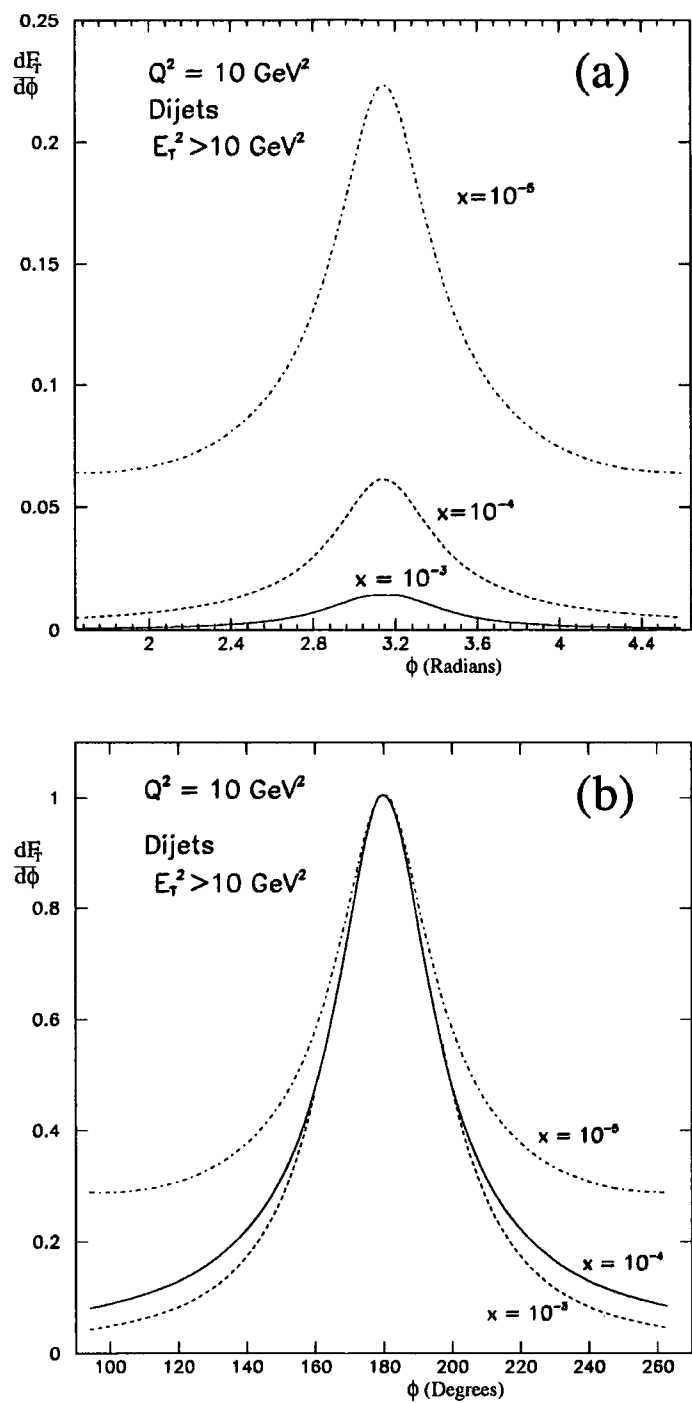
Figure 4.3: (a) The distribution $dF_T/d\phi$ predicted by the BFKL k_T-factorization formula, (4.8), for deep-inelastic dijet events with $Q^2 = 10$ GeV^2 and E_T^2(jet) > 10 GeV^2.

(b) The distributions normalized to a common maximum.

As mentioned above, the weakening of the back-to-back azimuthal correlations can also be obtained in a more conventional way from fixed-order QCD effects, in particular from 3+1 jet production. As usual the +1 refers to the jet associated with the remnants of the proton. Part of the 3+1 jet production is, of course, already included in the calculation based on BFKL dynamics, since the absence of strong-ordering in k_T means that the gluonic ladder contains additional (gluon) jets. Before drawing final conclusions we must therefore compare our BFKL dijet predictions with the azimuthal distribution coming from conventional 3+1 jet production. To calculate the latter we use the PROJET Monte Carlo [13]. We require two of the jets to have $E_T^2(\text{jet } 1, 2) > 10$ GeV^2 and the third to have $E_T^2(\text{jet } 3) < 10$ GeV^2, chosen so that two jets are "visible" and the third (which may be either a gluon or a quark) is relatively "soft". The results are shown by the histograms superimposed on figure 4.4. We have checked that the PROJET predictions in the region $|\phi - \pi| \gtrsim 20^0$ are not sensitive to a reasonable variation of the cut-off, $y_{ij} \equiv s_{ij}/W^2 > y_0$, that is used to regulate the infrared singularities.

We see from figure 4.4 that the appearance of dijet events in the "tails" of the azimuthal distribution, that is at angles such that $|\phi - \pi| \gtrsim 45^0$, at the predicted rate, will be a distinctive signal for BFKL dynamics. Nearer the back-to-back configuration the fixed-order QCD processes swamp the BFKL effect. Of course, since we work at the parton level and ignore the experimental problems of jet identification, only the BFKL signal can contribute for $|\phi - \pi| > 60^0$. If the cut, $E_T^2(\text{jet } 3) < 10$ GeV^2, on the third jet is removed and the azimuthal distribution is plotted as a function of the angle, ϕ, between the two jets with the largest E_T's then the PROJET prediction is essentially unchanged for $|\phi - \pi| \approx 20^0$, but is enhanced at larger angles with a steeper fall off towards the limiting angle $|\phi - \pi| = 60^0$.
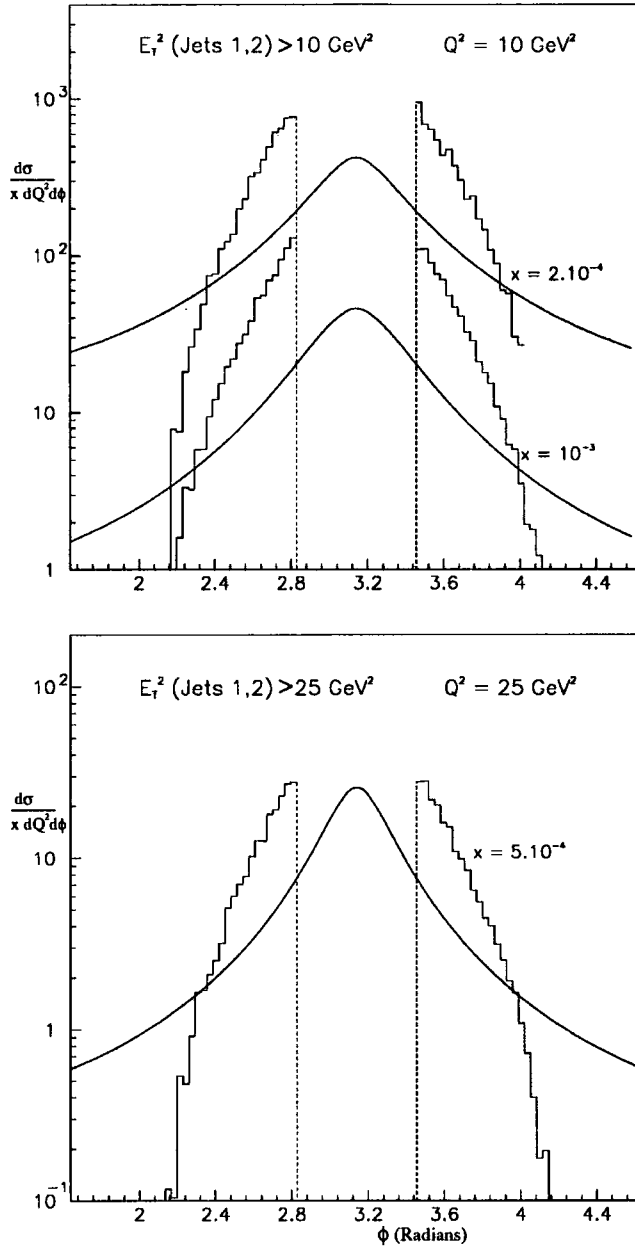
Figure 4.4: The curves are the differential cross section for dijet production predicted by BFKL dynamics, (4.5)-(4.12), whereas the histograms correspond to 3+1 jet production as determined by the PROJET Monte Carlo using MRS(A) partons [12]. In the first case, the broadening of the azimuthal distribution arises from the k_T dependence of the gluon distribution $f(x_g, k_T^2)$ found by solving the BFKL equation, (4.3). For 3+1 jet production we assume that the third jet has $E_T^2 < 10(25)$ GeV^2 in the upper (lower) plot.

The deep inelastic variables (x, Q^2) and jet cuts $(E_T > E_{0T})$ have been chosen in an attempt to optimize both the event rate and the BFKL signal at HERA. Clearly if we were able to go to smaller x (or, to be precise, smaller x_g) then the BFKL effect would be more pronounced, see figure 4.3. Now the observable deep inelastic region at HERA lies in the domain $Q^2/x \lesssim 10^5$ GeV^2. On the other hand, we see from (4.9) that $x_g \gtrsim x + 4(x/Q^2)E_{0T}^2$, when two jets with $E_T > E_{0T}$ are recorded. A higher jet threshold, E_{0T}, has the advantage that the fixed-order QCD contribution is suppressed relative to the BFKL signal, but (since Q^2/x is bounded) then a higher x_g is sampled. The lower plot in figure 4.4 shows the results for $Q^2 = E_{0T}^2 = 25$ GeV^2 and $x = 5 \times 10^{-4}$, for which x_g is increased by a factor of 2.5 in comparison to that sampled for $Q^2 = E_{0T}^2 = 10$ GeV^2 and $x = 2 \times 10^{-4}$.

4.4: Conclusions.

To sum up, the main aim of this chapter is to quantify the observation that BFKL dynamics weakens the azimuthal correlation of the $q, \bar{q}$ jets produced in small x deep-inelastic scattering via the photon-gluon fusion mechanism. We are able to obtain an absolute prediction since the parameter which specifies the infrared contribution to the BFKL equation is chosen such that the measurements of F_2 at HERA are reproduced. (That a physically reasonable choice of a single infrared parameter suffices to describe the observed small x behaviour of F_2 is a far from trivial test of BFKL dynamics.) For the dijet events we find a substantial broadening of the azimuthal distribution and an increase of this broadening with decreasing x. However, at HERA energies, we find that the fixed-order QCD contribution from 3+1 jet production exceeds the BFKL signal near the back-to-back configuration. Nevertheless at sufficiently large values of $|\phi - \pi|$ BFKL dynamics dominates and give rise to a distinctive "tail" to the azimuthal distribution at an observable rate. In this way dijet production at HERA offers an opportunity to study the k_T dependence of the gluon distribution of the proton.

References.

[1] M. Derrick et al., Phys. Lett. **B322** (1994) 287

[2] J.R. Forshaw and R.G. Roberts, Phys. Lett. **B335** (1994) 494

[3] A. De Roeck, private communication

[4] S. Catani, F. Fiorani and G. Marchesini, Phys. Lett. **B234** (1990) 339; Nucl. Phys. **B336** (1990) 18

[5] S. Catani, M. Ciafaloni and F. Hautmann, Phys. Lett. **B242** (1990) 190; Nucl. Phys. **B366** (1991) 135

[6] J.C. Collins and R.K. Ellis, Nucl. Phys. **B360** (1991) 3

[7] E.A. Kuraev, L.N. Lipatov and V. Fadin, Phys. Lett. **60B** (1975) 50, Zh. Eksp. Teor. Fiz. **72** (1977) 373 [Sov. Phys. JETP **45** (1977) 199]; Ya.Ya. Balitskij and L.N. Lipatov, Yad. Fiz. **28** (1978) 1597 [Sov. J. Nucl. Phys. **28** (1978) 822]; L.N. Lipatov, in "Perturbative QCD", edited by A.H. Mueller, World Scientific, Singapore, 1989, p. 411; J.B. Bronzan and R.L. Sugar, Phys. Rev. **D17** (1978) 585; T. Jaroszewicz, Acta Polon. **B11** (1980) 965

[8] J. Bartels and A. Lotter, Phys. Letts. **B309** (1993) 400

[9] A.J. Askew, J. Kwiecinski, A.D. Martin and P.J. Sutton, Phys. Rev. **D49** (1994) 4402

[10] A.J. Askew, J. Kwiecinski, A.D. Martin and P.J. Sutton, Phys. Rev. **D47** (1993) 3775

[11] H1 collaboration: I. Abt et al., Nucl. Phys. **B407** (1993) 515; K. Müller, Proc. of 29th Rencontre de Moriond, March 1994
ZEUS collaboration: M. Derrick et al., Phys. Lett. **B316** (1993) 412; G. Wolf, Proc. of International Workshop on Deep Inelastic Scattering, Eilat, Israel, Feb. 1994; M. Roco, Proc. of 29th Rencontre de Moriond, March 1994

[12] A.D. Martin, W.J. Stirling and R.G. Roberts, Phys. Rev. **D50**, 6734 (1994)

[13] D. Graudenz, PROJET: Jet cross sections in deep inelastic electron-proton scattering, version 3.6, to be published.

5

Summary and conclusions.

Fortunately, in her kindness and patience, Nature has never put the fatal question as to the meaning of their lives into the mouths of most people. And where no one asks, no one needs to answer.

Carl Jung

5.1: Small-x Physics: the theoretical framework.

The small-x limit of deep inelastic scattering represents one of the most interesting problems in QCD. As the intermediate region between the standard (intermediate-x) region of DIS, which is in principle well understood, and the asymptotic Regge domain, it provides a new window through which to view the 'pomeron' in QCD. While soft hadronic interactions, such as $2 \rightarrow 2$ scattering, elastically or with quantum number exchange, can be well described through Regge theory, the exact relationship of these models to the microscopic theory of QCD is still not clearly understood. In DIS at small-x the hope is that, due to the presence of the virtual photon, some progress can be made through perturbative methods. In a genuinely soft process, with no hard scale at all, it is not clear that the partonic language in which a perturbative analysis is phrased is at all appropriate. In DIS however, at least one side of the process is to be described perturbatively; hence there is the likelihood that the effects of perturbative resummation of leading logarithmic terms will become manifest.

Quite apart from these theoretical considerations, the small-x domain is of crucial importance phenomenologically. In the next generation of hadron colliders, typical events will probe the region $x \sim p_T^2/s \ll 1$. In order to undertake a reliable analysis of these events we

certainly need, as a preliminary step, to understand the somewhat simpler process of deep inelastic scattering in this region. In particular it is necessary to understand the relevance of higher order corrections, which are logarithmically enhanced in this kinematical region and so can be important.

In this thesis we have looked at the small-x limit of DIS as a possible probe of perturbative Regge asymptotics. Our analysis is based on the results of a resummation of leading logarithmic terms of the perturbation series, $\sim \alpha_s^n \log^n(1/x)$. The results of this resummation are most easily represented, for the phenomenological purposes here, in terms of the old fashioned language of Regge theory and Reggeon Field Theory. We find that the leading logarithmic results can be summarised as,

- Gluon exchange in the t-channel is replaced by a negative signature Reggeon with trajectory $\alpha(t) = 1 + \omega(t)$, with $\omega(t)$ calculable from perturbation theory,

- The 'pomeron' in this approach, that is the amplitude with vacuum quantum numbers in the t channel, is not a fundamental input to the RFT but arises later as the exchange of two or more Reggeons in the t channel. To leading log accuracy, only two-Reggeon exchange is important. There are large corrections (ie. leading log corrections) due to the interaction of these two Reggeons with each other. The effect of these interactions can be formulated in terms of an integral equation for the partial wave amplitude, the BFKL equation.

The main outcome of this analysis is that the 'BFKL pomeron' in this approximation is 'supercritical', that is it corresponds to a singularity in the j-plane which is to the right of unity, at $j = 1 + \lambda$, and thus leads to a power growth of total cross sections. The Froissart bound must be maintained by the inclusion of nonleading logarithmic corrections, though it is not fully clear which approach to take in this regard. Prior to these corrections becoming important, we would expect the original power growth to be reflected in the behaviour of structure functions for $x \to 0$; hence we performed numerical analysis to investigate this possibility.

5.2: Structure functions at small-x.

With the BFKL formalism as our starting point, we have put forward a set of structure functions for HERA which account for the leading logarithmic contributions. Our investi-

gations show that the perturbative generation of quark distributions from gluons via the $g \rightarrow q\bar{q}$ process can lead to a large contribution to the structure functions in the region $x \lesssim 10^{-3}, Q^2 \sim 10$ GeV^2 which is currently the focus of attention at the HERA collider. However, there are significant problems in applying the BFKL formalism to structure functions owing to the fact that nonperturbative effects are not explicitly factored out, unlike the case of the DGLAP formulation. Consequently some model for the nonperturbative contribution to the structure functions is required, which rather detracts from the merits of the formalism.

These nonperturbative effects however should have a small role in determining the Q^2 dependence of F_2, which ought to be driven by a perturbative mechanism. Furthermore, experience with soft hadronic processes would suggest that soft physics generates approximately energy independent cross sections; the most singular behaviour of a soft total cross section which has been observed rises no more rapidly than $\sigma_T \sim s^{0.08}$. This would translate through to a contribution to structure functions rising as $x^{-0.08}$. To obtain agreement with the HERA results we do invoke a 'background' contribution to the structure functions with these properties of being roughly independent of x and Q^2; this is unpleasant but mandatory. Later authors have encountered this same requirement for nonperturbative contributions [1].

In the light of these difficulties, it would seem that unambiguous tests of the BFKL resummation from structure functions alone are not really possible. Nevertheless, it is surprising to see how closely the resulting model is able to match the HERA data. It would certainly seem reasonable to say that the sharp growth which is observed owes its physical basis to multiple soft gluon bremsstrahlung; though we would have doubts about the reliability of quantitatively predicting the magnitude of these effects, owing to nonperturbative effects. For serious, quantitative phenomenology in the future it seems essential to factor out the nonperturbative region as one does in the DGLAP formalism. Some theoretical progress along these lines has been made in [2, 3], and an indication of the phenomenological necessity of understanding the role of higher order corrections is shown by the analysis of references [4,5].

References.

[1] N.N. Nikolaev and B.G. Zakharov, Phys. Lett. **B327**, 149 (1994) and references therein

[2] S. Catani and F. Hautmann, Nucl. Phys. B**427** (1994) 475

[3] J.C. Collins and R.K. Ellis, Nucl. Phys. B**360** (1991) 3

[4] R.K. Ellis, F. Hautmann and B.R. Webber, Phys. Lett. **B348**, 582 (1995)

[5] R.K. Ellis, Z. Kunszt and E.M. Levin, Nucl. Phys. **B420**, 517 (1994) Erratum - ibid. **B433**, 498 (1995)

Appendix A : Eigenvalues of the BFKL kernel.

Here we will compute explicitly the eigenvalues $\widetilde{\mathcal{K}}(\omega)$ of the BFKL equation, defined in equation (3.34a) as

$$\widetilde{\mathcal{K}}(\omega) = \int_0^\infty \frac{du}{u} u^{-\omega} \widetilde{\mathcal{K}}(u) \tag{A.1a}$$

$$= \int_0^\infty \frac{dv}{v} \left[\frac{v^\omega - 1}{|v-1|} + \frac{1}{(4v^2+1)^{\frac{1}{2}}} \right] \tag{A.1b}$$

where we have used (3.30a, 3.30b) and the change of variable $u \to 1/v$.

We can define $\widetilde{\mathcal{K}} = \widetilde{\mathcal{K}}_1 + \widetilde{\mathcal{K}}_2$ where

$$\widetilde{\mathcal{K}}_1(\omega) = \int_1^\infty \frac{dv}{v} \frac{v^\omega - 1}{v-1} \quad \text{and}$$

$$\widetilde{\mathcal{K}}_2(\omega) = \lim_{\epsilon,\delta \to 0^+} \left[\int_0^1 \frac{dv}{v^{1-\epsilon}} \frac{v^\omega}{(1-v)^{1-\delta}} - \int_0^1 \frac{dv}{v^{1-\epsilon}} \frac{1}{(1-v)^{1-\delta}} + \int_0^\infty \frac{dv}{v^{1-\epsilon}} \frac{1}{(4v^2+1)^{\frac{1}{2}}} \right].$$

(Here, we have introduced ϵ, δ in $\widetilde{\mathcal{K}}_2$ to regulate any divergence of the integrals for $x \to 0, 1$ so as to be able to integrate each part of the integrand seperately in terms of simple β functions.) On changing the integration variable in $\widetilde{\mathcal{K}}_1$ to $u = 1/v$ one gets*

$$\widetilde{\mathcal{K}}_1(\omega) = \int_0^1 du \frac{u^{-\omega} - 1}{1-u} = -\gamma_E - \psi(1-\omega).$$

The three integrals in $\widetilde{\mathcal{K}}_2$ can all be done in terms of β functions, using the relations[†]:

$$\int_0^1 dt \, t^{x-1}(1-t)^{y-1} = \beta(x,y) \quad \text{for } \mathcal{R}e\, x > 0, \mathcal{R}e\, y > 0, \text{ and}$$

$$2 \int_0^\infty dt \frac{t^{2x-1}}{(1+t^2)^{x+y}} = \beta(x,y) \quad \text{for } \mathcal{R}e\, x > 0, \mathcal{R}e\, y > 0$$

---

* See, eg. Gradshteyn and Ryzhik, "Table of integrals, series and products", fourth edition, section 8.36 for this integral representation of the ψ function.

[†] Gradshteyn and Ryzhik, section 8.380

from which we see that

$$\widetilde{\mathcal{K}}_2(\omega) = \lim_{\epsilon,\delta\to 0^+} \frac{2^{-\epsilon}}{2}\beta(\frac{\epsilon}{2},\frac{1}{2}-\frac{\epsilon}{2}) + \beta(\omega+\epsilon,\delta) - \beta(\epsilon,\delta).$$

Now, using the fundamental relations

$$\beta(x,y) = \frac{\Gamma(x)\Gamma(y)}{\Gamma(x+y)} \text{ and } \Gamma(x) = \frac{\Gamma(x+1)}{x}$$

(where the second transformation is advantageous in that it makes explicit the poles for ϵ and $\delta \to 0$) then K_2 can be rewritten as

$$\widetilde{\mathcal{K}}_2(\omega) = \lim_{\epsilon,\delta\to 0^+} 2^{-\epsilon}\frac{\Gamma(1+\frac{\epsilon}{2})\Gamma(\frac{1}{2}-\frac{\epsilon}{2})}{\Gamma(\frac{1}{2})}\times\frac{1}{\epsilon} + \frac{\Gamma(\omega+\epsilon)\Gamma(1+\delta)}{\Gamma(\omega+\epsilon+\delta)}\times\frac{1}{\delta} - \frac{\Gamma(1+\epsilon)\Gamma(1+\delta)}{\Gamma(1+\epsilon+\delta)}\times\frac{\epsilon+\delta}{\epsilon\delta}$$

We can now take the limit $\epsilon \to 0^+$ through using the expansion, $\Gamma(1+z) = 1 - \gamma_E z + O(z^2)$, when we get (just writing down the first and third terms above)

$$\lim_{\epsilon\to 0^+}\frac{1}{\epsilon}\Bigg[(1-\epsilon\log 2\cdots)(1-\gamma_E\frac{\epsilon}{2}\cdots)(1-\psi(\frac{1}{2})\frac{\epsilon}{2}\cdots)$$

$$-(1-\gamma_E\epsilon\cdots)(1-\psi(1+\delta)\epsilon\cdots)(1+\frac{\epsilon}{\delta})\Bigg]$$

$$= \Bigg[-\log 2 - \frac{\gamma_E}{2} - \frac{\psi(\frac{1}{2})}{2} + \gamma_E + \psi(1+\delta) + \frac{1}{\delta}\Bigg] = \gamma_E + \psi(1+\delta) + \frac{1}{\delta}.$$

(This uses $\psi(1/2) = -\gamma_E - 2\log 2$). We can now take the $\delta \to 0^+$ limit in the same way[†],

$$\widetilde{\mathcal{K}}_2(\omega) = \lim_{\delta\to 0^+}\frac{1}{\delta}\Bigg[\frac{\Gamma(\omega)\Gamma(1+\delta)}{\Gamma(\omega+\delta)} - 1\Bigg] \tag{A.2}$$

$$= \lim_{\delta\to 0^+}\frac{1}{\delta}\Bigg[(\Gamma(1)+\psi(1)\delta\cdots)(1-\psi(\omega)\delta\cdots) - 1\Bigg] \tag{A.3}$$

$$= \psi(1) - \psi(\omega) \tag{A.4}$$

So, by adding $\widetilde{\mathcal{K}}_1 + \widetilde{\mathcal{K}}_2$, we arrive at the following analytic form for the eigenvalues of the BFKL kernel:

$$\widetilde{\mathcal{K}}(\omega) = 2\psi(1) - \psi(\omega) - \psi(1-\omega).$$

[†] $\psi(1) = -\gamma_E$